

STUDY TO EVALUATE THE ECONOMIC FEASIBILITY OF REPLACING A
PRESSURE REDUCING VALVE WITH A PRESSURE REDUCING TURBINE
FOR A SPECIFIC CASE STUDY

Francis Joseph Nadaraju

A Research Report submitted to the Faculty of Engineering and the Built Environment, University of the Witwatersrand, in partial fulfilment of the requirements for the Master of Science in Engineering.

Johannesburg, 2011

TABLE OF CONTENTS

DECLARATION	i
ABSTRACT	ii
ACKNOWLEDGEMENTS	iii
LIST OF FIGURES	iv
LIST OF TABLES	vi
LIST OF SYMBOLS	vii
1 INTRODUCTION	1
1.1 Energy recovery	4
1.2 Plan of development	7
2 LITERATURE REVIEW	9
2.1 Energy recovery in mining applications	9
2.2 Pumps as turbines	15
2.3 Applications of pump-turbine systems	16
2.4 Conclusion	19
3 THEORETICAL BACKGROUND	20
3.1 First law of thermodynamics	20
3.2 Flow processes	21
3.3 Second law of thermodynamics	23
3.3.1 Heat engines.....	24
3.3.2 Entropy	27
3.4 Property relationships	29
3.4.1 Internal energy and enthalpy.....	29
3.4.2 Enthalpy and entropy	29
3.4.3 Specific volume.....	31
3.4.4 Joule-Thomson effect	31
3.5 Turbine expansion process	32
3.6 Mechanical energy balance	35
3.7 Frictional losses	36
3.7.1 Pipe friction.....	36
3.7.2 Other frictional losses	38
3.8 System characteristic	39

3.9	Electrical generators	40
3.9.1	Electrical drives	41
3.9.2	Operating speed	43
3.10	Conclusion	44
4	DISCUSSION	45
4.1	Anglogold Ashanti Mponeng mine (du Toit, 2009)	45
4.2	Design criteria	48
4.2.1	Water flow and pressure data	48
4.2.2	Regression of water flow and pressure data	49
4.2.3	Water temperature	54
4.2.4	Heat capacity	55
4.2.5	Specific volume and density	56
4.2.6	Viscosity	57
4.2.7	Joule-Thomson coefficient	58
4.2.8	Summary of design criteria	59
4.3	System modelling	59
4.3.1	System curve	59
4.3.2	Pump-turbine model	61
4.3.3	System alternatives: variable and constant speed operation	64
4.3.4	Energy recovery and discharge water temperature	73
4.3.5	Electrical design	74
4.3.6	System operation and control	79
4.4	Capital expenditure	83
4.5	Financial analysis	83
4.5.1	Net present value and internal rate of return	86
4.5.2	Payback period	87
4.6	Project management	88
4.7	Conclusion	88
5	CONCLUSION AND RECOMMENDATIONS	89
5.1	Summary of the project	89
5.2	Recommendations for further work	90
5.3	Closure	90
	REFERENCES	91
	BIBLIOGRAPHY	96

APPENDIX A	RAW DATA	98
APPENDIX B	REGRESSION OF WATER FLOW DATA.....	114
APPENDIX C	MANUFACTURER'S DATA	116
APPENDIX D	SAMPLE CALCULATIONS.....	118
APPENDIX E	ESKOM TARIFFS	129
APPENDIX F	CAPITAL EXPENDITURE.....	132
APPENDIX G	FINANCIAL CALCULATIONS	133
APPENDIX H	PROJECT SCHEDULE	135

DECLARATION

I declare that this research report is my own unaided work. It is being submitted to the Degree of Master of Science to the University of the Witwatersrand, Johannesburg. It has not been submitted before for any degree or examination to any other degree.

.....

..... day of year

ABSTRACT

The technical and economic feasibility of energy recovery, using of a reverse-running pump, has been carried out. Water flow and pressure data for an underground pressure-reducing station, at AngloGold Ashanti Mponeng mine, was used. A statistical analysis resulted in a design flow and pressure.

Turbine curves for a HPH 28-1S pump were provided by Sulzer and regression models were used to predict system performance. Variable and constant speed systems were proposed. The expected energy recovered would be 318.5 kW and 319.1 kW for the variable and constant speed systems, respectively. The discharge water temperature for both systems would be 10.32 °C.

The constant speed system was preferred since the capital cost (R 3 776 900) and payback period was lower (2.3 years), while the NPV (R 11 645 000) and IRR (42.9 %) was higher. The system should be constructed to confirm the design calculations and predicted results.

ACKNOWLEDGEMENTS

There are several people who assisted me in my quest for knowledge.

I would like to express my gratitude to the following people for the supply of data, technical information and assistance: Mr Andrew Robbins at AngloGold Ashanti Mponeng mine; Mr Alexander Bergh at Sulzer and Mr Alastair Gerrard at Zest Energy.

I would also like to thank the staff at Bluhm Burton Engineering. I received technical assistance and encouragement from Dr Steven Bluhm and Mr Ross Wilson. To Mr Avinash Andhee, Mr Itumeleng Monnahela and Mr Duran Durieux, I am grateful for the editorial assistance (and reminding me that English is my first language!). I am also grateful to Mr Philip Venter and Mr Evert Zwarts for assistance with the engineering drawings. In particular, I am indebted to Mr Russell Ramsden for sharing his knowledge and wisdom, and providing much needed encouragement to complete this study.

To my supervisor Professor Huw Phillips, whose guidance proved useful in maintaining a focused study, with achievement of the outlined objectives.

In closing, I would like to express my heartfelt gratitude to my parents, Dean and Anne Nadaraju, for their unwavering support and encouragement; especially during this study.

LIST OF FIGURES

Figure 1.1 Typical layout of a water reticulation and ice system for a deep mine (Funnell et. al., 2006).....	3
Figure 1.2 Pelton wheel turbine (Douglas et. al., 1995).....	5
Figure 1.3 Reaction turbine (radial flow): Francis turbine (Douglas et. al., 1995) .	6
Figure 1.4 Reaction turbine (axial flow): Kaplan turbine (Douglas et. al., 1995) ...	6
Figure 1.5 Standard pump in normal operation (a) and reverse operation (b) (after Douglas et. al., 1995).....	7
Figure 2.1 Francis turbine installed at a three-stage spray chamber (Ferguson and Bluhm, 1984)	11
Figure 2.2 Three-pipe chamber feeder system (Hoffman, 1994).....	13
Figure 2.3 Operating sequence of the 3 CPF (Walters and Pretorius, 1994).....	14
Figure 2.4 Schematic of Hydrotreating process (Gopalakrishnan, 1986).....	17
Figure 2.5 Schematic of Gas scrubbing process (Gopalakrishnan, 1986).....	17
Figure 3.1 A flow process (after Smith et. al., 2001).....	21
Figure 3.2 PV diagram showing the Carnot cycle for an ideal gas (Smith et. al., 2001)	25
Figure 3.3 A reversible cyclic process (Smith et. al., 2001)	28
Figure 3.4 Expansion process of a fluid (after Smith et. al., 2001)	34
Figure 3.5 Friction factor chart (Perry and Green, 1997).....	37
Figure 3.6 System curve and turbine curve.....	40
Figure 3.7 Electromechanical converter system.....	40
Figure 3.8 Cross-section through an electrical drive	41
Figure 3.9 Operating modes of an induction machine (after Gray, 1989)	42
Figure 4.1 Mponeng water reticulation system (du Toit, 2009).....	46
Figure 4.2 84 Level Ice dam (after du Toit, 2009).....	48
Figure 4.3 Average water flow through 104 Level PRV station (19 to 26 March 2010)	51
Figure 4.4 Average discharge pressure downstream of 104 Level PRV station (19 to 26 March 2010)	51
Figure 4.5 Average water flow through 104 Level PRV station (typical)	52
Figure 4.6 Average discharge pressure downstream of 104 Level PRV station (typical).....	53
Figure 4.7 Air and water temperatures measured at Mponeng (du Toit, 2010)...	54
Figure 4.8 System curve and pump-turbine curve.....	61

Figure 4.9 Pump-turbine head curve regression	63
Figure 4.10 Pump-turbine efficiency curve regression	64
Figure 4.11 Schematic layout of a variable turbine speed pressure reducing system (van Antwerpen and Greyvenstein, 2005).....	65
Figure 4.12 System and pump-turbine curves (variable speed)	65
Figure 4.13 Pump-turbine efficiency curve (variable speed).....	66
Figure 4.14 System and pump-turbine curves (constant speed)	68
Figure 4.15 Pump-turbine efficiency curve (constant speed).....	69
Figure 4.16 System efficiency for variable and constant speed alternatives.....	71
Figure 4.17 Process flow diagram (FN-PT-10-001).....	72
Figure 4.18 General arrangement of pump-turbine & generator – variable speed (FN-PT-10-004)	75
Figure 4.19 General arrangement of pump-turbine & generator – constant speed (FN-PT-10-005)	76
Figure 4.20 Single line diagram – variable speed (FN-PT-10-006).....	77
Figure 4.21 Single line diagram – constant speed (FN-PT-10-007).....	77
Figure 4.22 Power profile for a typical week (variable speed alternative)	78
Figure 4.23 Power profile for a typical week (constant speed alternative)	78
Figure 4.24 Piping and instrumentation diagram – variable speed (FN-PT-10-002)	80
Figure 4.25 Piping and instrumentation diagram – constant speed (FN-PT-10-003)	82
Figure 4.26 Power generated and Eskom tariffs for a Friday at constant speed.	84
Figure 4.27 Projected cash inflows and outflows for the pump-turbine system (variable speed).....	85
Figure 4.28 Projected cash inflows and outflows for the pump-turbine system (constant speed).....	86
Figure B1 Histogram for water flow through the 104 Level station	115
Figure C1 500 kW induction generator for variable speed alternative	117
Figure C2 400 kW induction generator for constant speed alternative	117
Figure E1 Eskom’s defined time of use periods (Conradie, 2010).....	129
Figure E2 Transmission zones and applicable percentages (Conradie, 2010) .	130
Figure E3 Nominal Megaflex tariff for a weekday.....	131
Figure E4 Nominal Megaflex tariff for a Saturday.....	131

LIST OF TABLES

Table 3.1 Friction losses for pipe components (after Massey, 1970).....	39
Table 4.1 Mining level depths	45
Table 4.2 Average water flow and pressure for 104 Level PRV station.....	50
Table 4.3 Variation of heat capacity with temperature.....	55
Table 4.4 Variation of specific volume and density with temperature	56
Table 4.5 Variation of viscosity with temperature	57
Table 4.6 Variation of volume expansivity and Joule-Thomson coefficient with temperature	58
Table 4.7 Modes of operation for the pump-turbine system at variable speed....	67
Table 4.8 Modes of operation for the pump-turbine system at constant speed...	70
Table 4.9 Eskom Megaflex tariffs (2012).....	83
Table 4.10 Electrical power income for a week in 2012.....	85
Table 4.11 Net present values and Internal rates of return.....	87
Table B1 Statistical analysis of water flow data.....	115
Table D2: Eskom Megaflex tariffs (2012)	125
Table D3 Power generated during Eskom defined periods	126
Table D4 Energy generated during Eskom defined periods	126
Table D5 Electrical power income for a week (2012)	127
Table D6 Summary of present value costs.....	128

LIST OF SYMBOLS

a	Pump-turbine head/speed/flow modelling constant
A	Area
C_P	Molar or specific heat capacity, constant pressure
C_V	Molar or specific heat capacity, constant volume
D	Pipe inside diameter
f	Friction factor
g	Local acceleration of gravity
h	Pump head
h_{con}	Head loss, abrupt contraction
h_{ex}	Head loss, abrupt enlargement
h_f	Head loss, pipe friction
h_L	Head loss, other pipe fittings (bend, tee, valve, etc.)
H	Molar or specific enthalpy, $\equiv U + PV$
(ΔH_S)	Molar or specific enthalpy change, constant entropy
$(\Delta H'_S)$	Molar or specific enthalpy change, equivalent, constant entropy
K_L	Head loss coefficient
L	Characteristic length
m	Mass
\dot{m}	Mass flow rate
N	Steady state shaft speed
N_S	Steady state synchronous shaft speed
P	Absolute pressure
ΔP_f	Absolute pressure change, pipe friction
$\Delta P'$	Absolute pressure change, equivalent
PRV	Pressure-reducing valve
q	Volumetric flow rate
Q	Heat
R	Universal gas constant
Re	Reynolds number, $\equiv Lu\rho/\mu_F$
s	Number of pump stages
S	Molar or specific entropy
T	Absolute temperature, kelvins

T	Shaft torque
u	Velocity
U	Molar or specific internal energy
V	Molar or specific volume
W	Work
\dot{W}	Work rate (power)
W_s	Shaft work for flow process
\dot{W}_s	Shaft power for flow process
$(W_s)_s$	Shaft work for flow process, constant entropy
y	Efficiency modelling constant
z	Elevation above a datum level
NPV	Net present value
IRR	Internal rate of return
PV	Principle or present value
FV	Total of principle and accumulated interest at time n
i	Interest rate based on length of one interest period
n	Number of time units or interest periods
Greek letters	
β	Volume expansivity
ε	Pipe roughness
η	Efficiency
κ	Isothermal compressibility
μ_F	Fluid viscosity
μ_H	Joule-Thomson coefficient, constant enthalpy
μ_S	Joule-Thomson coefficient, constant entropy
ρ	Molar or specific density, $\equiv 1/V$
ϕ	Flow coefficient, $\equiv q/N$
Subscripts	
SYS	Reference to the system

1 INTRODUCTION

Mining activity is an essential component of the South African economy, contributing 8 % to gross domestic product and providing approximately 500 000 jobs (Marais, 2010). Increased activity and/or better returns on the capital employed in this sector of the economy would certainly prove favourable for South Africa's wealth. Consequently, mining of available mineral resources and undertaking exploration activity (to seek new mineral resources) would be fruitful.

AngloGold Ashanti's Mponeng mine has progressed to a depth of 3 955 metres below surface and is the deepest gold mine in South Africa. The life-of-mine could be extended by further 20 years if mining goes to an estimated depth of 4 100 metres below surface (O'Donnell, 2010). Another expansion project is currently taking place at Gold Fields' South Deep mine. Gold production will increase to between 750 000 and 850 000 ounces per year by the end of 2014. This will be achieved by extension of the mine, which is currently 2 693 metres below surface to depths between 2 500 and 3 500 metres below surface (Creamer, 2010).

At these greater depths, higher virgin rock temperatures will be observed and auto-compression effects¹ will result in higher air temperatures. It therefore becomes necessary to provide both adequate ventilation and cooling for the mine. Prudence must be exercised during the design and implementation phases of the mine ventilation system, as costs can escalate dramatically.

The ventilation system in South African mines normally consists of main fans installed on surface, in an exhaust arrangement, on the ventilation shaft. The air will be induced to flow down the main shaft, through the underground tunnels and workings and out of the mine via the ventilation shaft. Up to a depth of about 2 000 metres below surface, the air alone can provide adequate cooling for acceptable working conditions. Below this depth, there will be diminished cooling potential of the air along with an unacceptable working environment underground

¹ The pressure of the air increases at greater depths due to the increase in the weight of the air (in the shaft). This is defined as "auto-compression" and results in an increase in the air temperature.

(Bluhm et.al., 2003). When mining has progressed beyond this point, the air must be cooled to once again achieve acceptable working conditions.

Air cooling is carried out in heat exchangers using chilled water from refrigeration machines. The refrigeration machines and heat exchangers are installed on surface and cooled air is sent down the intake shaft. Once again, at a critical depth the cold air loses its cooling potential and provision of more surface cooling and refrigeration is ineffective in providing an acceptable working environment underground.

When this point has been reached, the mine cooling system has to be modified. Since the “auto-compression” effect for water is strictly zero, compared to dry air at typical mine temperature and pressure ($9.75 + 0.022 \text{ }^\circ\text{C per km}$); chilled water is fed underground rather than more cooled air (Ramsden, 1983). The chilled water is fed to underground heat exchangers to achieve bulk cooling of the air and spot cooling close to the workings.

Deep-level mines, such as Mponeng and South Deep, have complex ventilation and cooling systems – this includes various combinations of surface and underground refrigeration machines and heat exchangers. A typical water reticulation and ice system is shown in Figure 1.1.

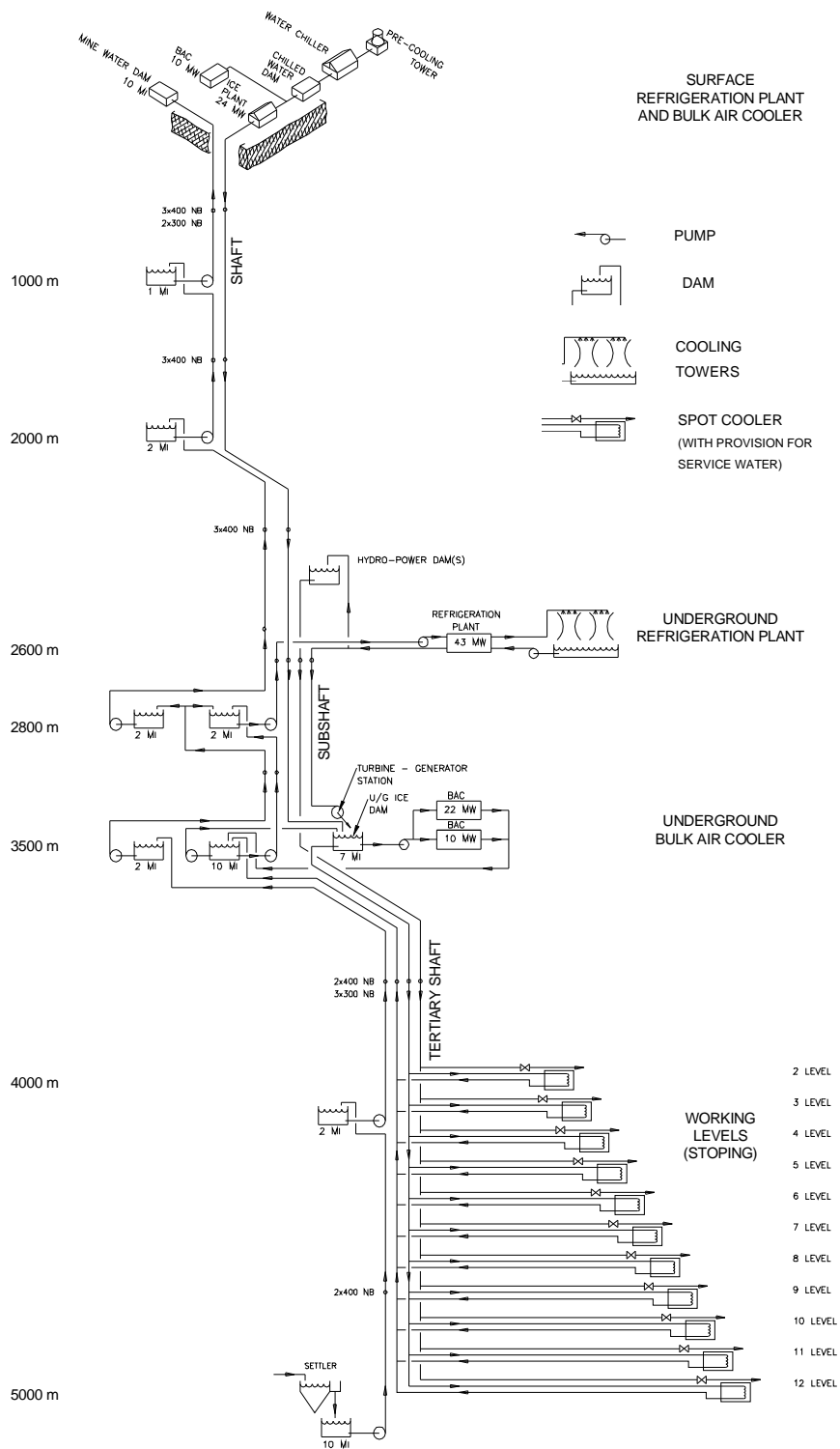


Figure 1.1 Typical layout of a water reticulation and ice system for a deep mine (Funnell et. al., 2006)

1.1 Energy recovery

A typical water reticulation system would include the distribution of water between surface and underground. Refrigeration machines located on surface will chill mine water for bulk cooling of air and will be fed underground. The water flowing down a mine shaft to a level underground (in a closed pipe), will increase in potential energy as greater depths are reached. This energy is manifested as an increase in water pressure. On a level underground, the water pressure is reduced by control valves, before the water is distributed. This pressure drop is the dissipation of the potential energy via friction. This frictional loss takes place at constant enthalpy and results in an increase in the temperature of the water. This process is referred to as the Joule-Thomson effect.

As mentioned previously, the chilled water is used in bulk air cooling and spot cooling close to the working areas. An elevated water temperature (downstream of the pressure-reducing valve) has the consequence of reducing cooling potential. The water will therefore reach the working areas at a higher temperature. It is possible to minimise the water temperature rise, through the employment of energy recovery devices. One such device, a turbine, is in use at South African mining operations.

A turbine is a mechanical device that converts potential and/or kinetic energy from a fluid into useful work. It typically consists of rotating blades mounted on a hub; onto which a shaft is mounted. The fluid will cause the blades to turn, resulting in the rotation of the shaft. The turbine can be used to drive other mechanical devices such as pumps or fans; or to generate electricity when coupled to a generator. Turbines can be classified as impulse and reaction type devices. Reaction turbines are further classified as radial and axial flow types.

In an impulse turbine, the direction of the working fluid is changed by directing it onto the turbine blades. The kinetic energy of the fluid results in the rotation of the turbine blades. The discharge pressure of the fluid will drop to the local barometric pressure. Typically, nozzles are used to accelerate the fluid prior to striking the turbine blades or buckets. Pelton wheels (Figure 1.2) are impulse turbines commonly used and are suitable for heads in the range of about 150-2 000 m head.

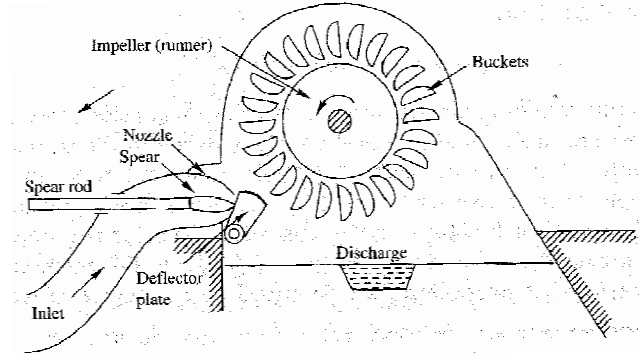


Figure 1.2 Pelton wheel turbine (Douglas et. al., 1995)

A radial flow reaction turbine that finds use in a variety of head and flow applications is the Francis turbine (Figure 1.3). The pressure of the fluid induces a torque on the turbine blades; causing it to rotate. Water will enter the volute; pass through a set of fixed guide vanes followed by adjustable guide vanes. The water then passes through the rotor blades and exits through the draft tube at 90° to the inlet water. The volute exit diameter is smaller than the inlet diameter. The pressure drop will take place as the fluid moves through the turbine. Guide vanes direct the fluid onto the rotor blades. A Francis turbine would typically operate at heads of between 30 and 500 m.

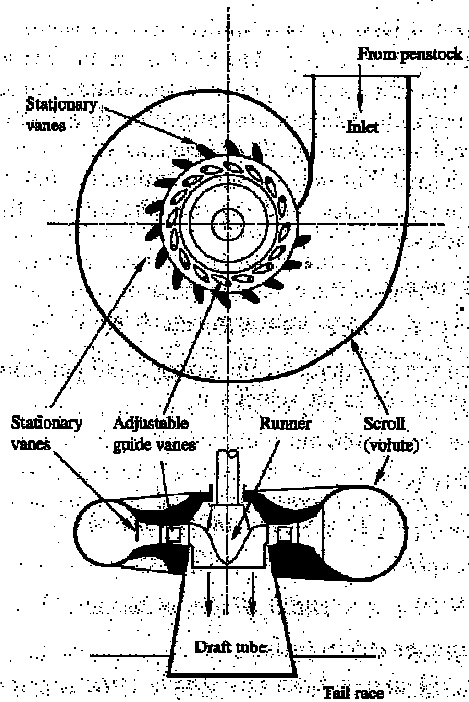


Figure 1.3 Reaction turbine (radial flow): Francis turbine (Douglas et. al., 1995)

Another type of reaction turbine is the Kaplan turbine (Figure 1.4). Water will flow axially over the runner blades since the fixed guide vanes will force the fluid to move at 90°. This is fluid motion takes place since the guide vanes are positioned at a plane higher than the runner blades. Typical applications are high flow rates and low heads and high torques are produced.

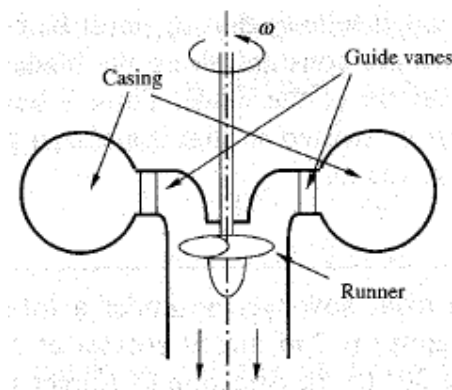


Figure 1.4 Reaction turbine (axial flow): Kaplan turbine (Douglas et. al., 1995)

A standard pump can also operate as a turbine. The normal operation of a pump is to move a fluid from one point to another by increasing the pressure of the fluid. The fluid will normally enter the suction end of the pump; and leave at a higher pressure at the discharge end of the pump. When a fluid at a high pressure enters the pump at the discharge end, the pump impeller will rotate and the fluid will leave the suction end of the pump at a lower pressure.

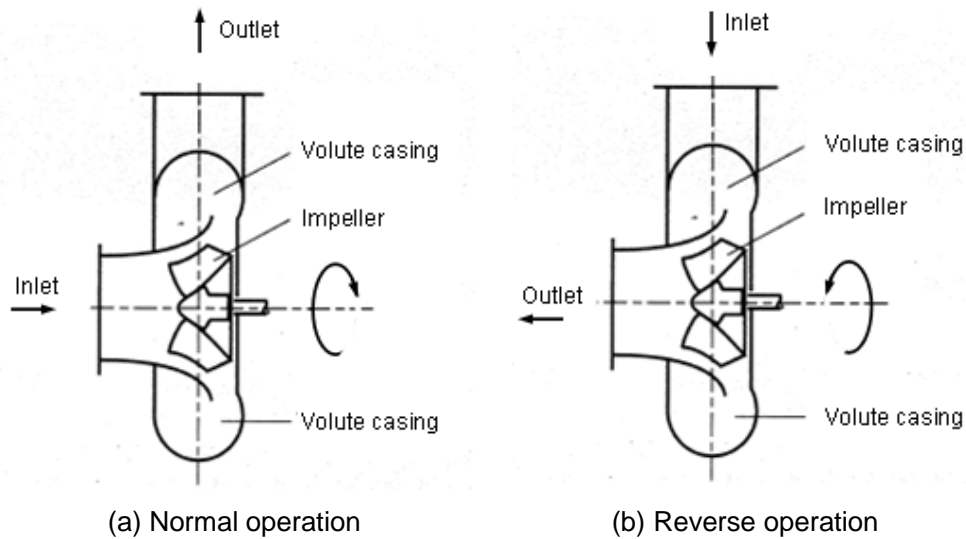


Figure 1.5 Standard pump in normal operation (a) and reverse operation (b) (after Douglas et. al., 1995)

1.2 Plan of development

At present, a pressure-reducing valve station is installed underground on 104 Level at Mponeng mine (3 160 m below surface). The water originates from a dam located on 84 Level (2 560 m below surface). The water enters the valve station at a pressure of 52 bar and discharges at a pressure of 10.5 bar due to frictional losses. It will therefore be possible to recover some of this potential energy through the employment of a turbine. It is envisaged to use a standard centrifugal pump operating in reverse to recover this energy.

A detailed design of the pump-turbine system will be undertaken. It is envisaged to replace a pressure reducing valve station with this system, should a business case arise from potential cost and energy savings.

This Project Report commences with a review of energy recovery in a mining context, followed by applications that make use of pumps as turbines (Chapter 2).

The theory governing the pump-turbine system will be described Chapter 3. The thermodynamics and fluid mechanics governing the system will be derived from first principles.

The pump-turbine system design will be based on data recorded at Mponeng mine (Chapter 4). Design criteria will be extracted from the data and from physical property databanks; and this will form the basis of the design. The system design will be based on models proposed by van Antwerpen and Greyvenstein (2005). The economic feasibility will be ascertained using financial models (net present value, internal rate of return and payback period).

The conclusions will be presented in Chapter 5 and recommendations will also be included.

2 LITERATURE REVIEW

A study by Whillier (1977) has shown that the temperature of water flowing down a mine shaft will increase by 2.33 °C per kilometre of depth. This temperature increase is attributed to the dissipation of the potential energy by friction. A turbine can be installed to recover part of the potential energy and reduce the water temperature rise. The study also illustrated that the installation of a turbine with an efficiency of 70 % increased the cooling potential of the water by 11.6 %. For a similar turbine having an efficiency of 60 %, the value of energy recovered would be approximately R 70 500 per annum (at a rate of R 60 per annum per kW recovered). The expected value of energy recovered in 2011 would be R 9 232 500 at a rate of R 7 900 per annum per kW². The benefit of energy recovery using turbines is therefore justified.

The subject of energy recovery will be examined in further detail in this chapter. This will include past work undertaken within the mining sector, followed by a general overview of pumps operating as turbines. The chapter concludes with applications of pump-turbines.

2.1 Energy recovery in mining applications

Pressure-reducing valves installed in chilled water systems negatively impact on the system efficiency. The temperature of chilled water downstream of the pressure-reducing valve will increase. The water then reaches the air coolers at an elevated temperature resulting in cooling duties which are lower than predicted. It has been shown that a total loss of 2 MW can be incurred at ten pressure-reducing stations dissipating 200 m of static head at a flow of 100 l/s. The loss in available cooling amounts to in excess of R 2 million per year (R 7.6 million in 2011), for each valve. A recommendation from the study was that small turbines should be used to effect pressure regulation (Bluhm et.al, 2000).

² The “escalation” of the values from 1977 to present day values (in 2011) are illustrated in APPENDIX D, Section D.9).

The pelton wheel turbine, coupled to a generator, is an established technology and finds use in many deep-level mines. The water discharge pressure drops to the local atmospheric pressure, which can be a disadvantage. To avoid this problem, the turbine can be used to drive a pump for distribution of the chilled water to the working areas. It should be borne in mind that such a pump can increase the water temperature, if it does not operate at the best efficiency point. In general, pumps operating at higher heads tend to be considerably inefficient, and the “wasted” energy is transferred to the pumped medium. Thus, the use of a pump having a high flow and low head can allow for better efficiencies being observed (Gopal and Harper, 1999).

A pelton wheel turbine system has been installed at Buffelsfontein gold mine in Klerksdorp. The turbine-generator system was installed 1 525 m below surface and the turbine was designed to handle a water flow of 300 l/s and a net head of 1 435 m. An induction generator with an output power of 3 900 kW and a voltage of 6 600 kV was selected. An average saving of 1 746 MWh per month has been reported and the power generated has been estimated at 3 MW, with an availability of 84 %. The saving from this system amounts to R 45 000 per month (van der Merwe, 1986). The saving in 2011 would be R 1.7 million per month.

Torbin (1989) has described an energy recovery system installed at the Lucky Friday mine located in Mullan, Idaho. Four alternatives were considered, namely, a turbine coupled to a generator; a turbine used to drive a pump; a turbine used to drive a pump-motor; and a turbine used to drive a compressor. The turbine alternatives included the Pelton wheel (reaction-type), Francis turbine (impulse-type) and standard reverse-running pump. The energy recovery system selected was the turbine-generator set, with the turbine being the Pelton wheel. The preference was attributed to the Pelton wheel being able to maintain high efficiency over a wide water flow range and therefore sustain high electrical output during most shifts in the mining operation. The turbine was designed to generate 210 kW of power at a design water flow of 31.5 l/s and inlet head of 840 m. The rated efficiency is 87 %. After a year of operation, the system produced

1 460 MWh of electricity with an annual power saving of \$ 38 000 (R 99 770)³. The expected saving in 2011 would be R 2 534 500 per annum.

The water that discharges from a Francis turbine has residual pressure. Ramsden and Bluhm (1985) have exploited this concept in a two-stage spray chamber having a design duty of 2 000 kW. Water at a pressure of 1 000 kPa was fed to the turbine and the discharge water, at a pressure of 300 kPa, was sprayed into the first stage of the heat exchanger. The power recovered in the turbine from the potential energy was used to drive the restage pumps. The water pressure downstream of the pump was also 300 kPa. The overall system efficiency was 43 %.

Ferguson and Bluhm (1984) have extended the above system to a three-stage spray chamber. The system is illustrated in Figure 2.1.

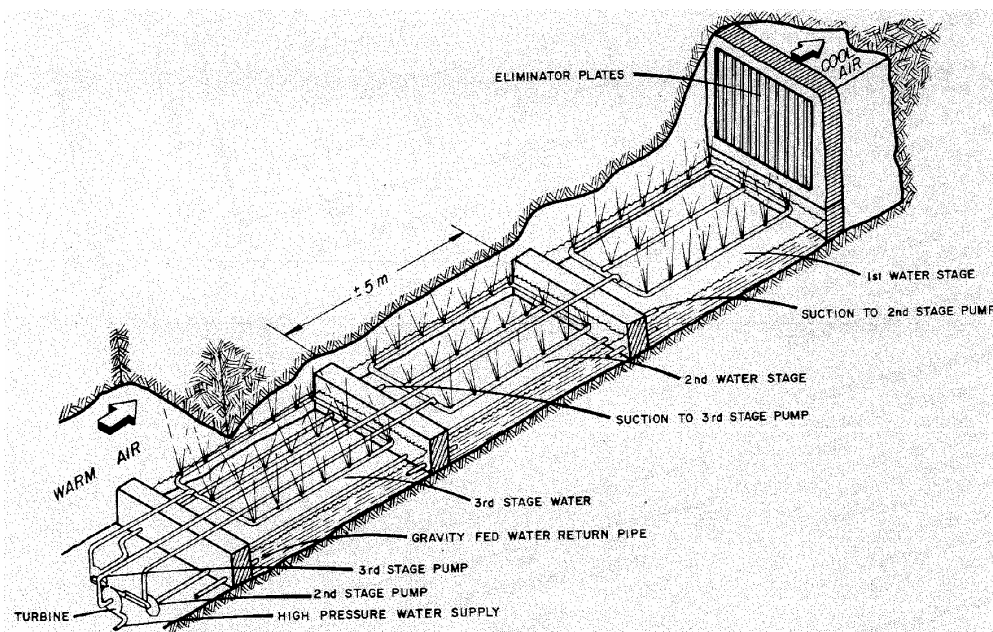


Figure 2.1 Francis turbine installed at a three-stage spray chamber (Ferguson and Bluhm, 1984)

³ The average annual exchange rate in 1989 was R 2.60 per US \$ (South African Reserve Bank, 2011).

The turbine was selected for an inlet pressure of 1 000 kPa and a discharge pressure of 175 kPa. The turbine was coupled to the restage pumps via a v-belt. The pumps resprayed the water into the second and third stages of the spray chamber. The spray chamber had a design cooling duty of 750 kW, air flow of 36 kg/s (at a density of 1.2 kg/s) and an inlet air temperature of 29.0 °C (wet-bulb). The design water flow was 15 l/s per stage, with the water entering the first stage at 13.5 °C. The outlet air temperature was 29.0 °C (wet-bulb) while the water leaving the third stage was 25.5 °C. The turbine efficiency was reported at 54 % and observed to operate as per specification. The overall combined efficiency of the pump-turbine arrangement was 42 %. The factor-of-merit for the spray chamber was 0.75 while a water efficiency of 80 % was noted. A financial evaluation showed that for a 10 kW Francis turbine, the payback period is less than a year (R 200 per kW in 1984 or R 11 300 per kW in 2011). Also, the cost of electric motors (for the pumps) was saved.

Another study showed a Francis-type turbine being used to drive a 610 mm axial fan. Such fans are typically installed at air coolers positioned close to the working areas. The water flow and pressure entering the turbine were varied to ascertain the performance of this system. It was concluded that the overall efficiency is likely to be 40 %. This shows the versatility of a turbine in driving mechanical equipment (Ramsden and Bluhm, 1985).

Another existing energy recovery system in deep-level mining described by Gopal and Harper (1999) is the three-pipe chamber feeder (3 CPF). The system is based on the U-tube principle: the flow of cold water down the shaft is balanced by the flow of warm water out of the mine. A booster pump is located on surface to overcome pipe friction, while pumps are used to feed cold and warm water through the system (Figure 2.2). The operation is described in Figure 2.3.

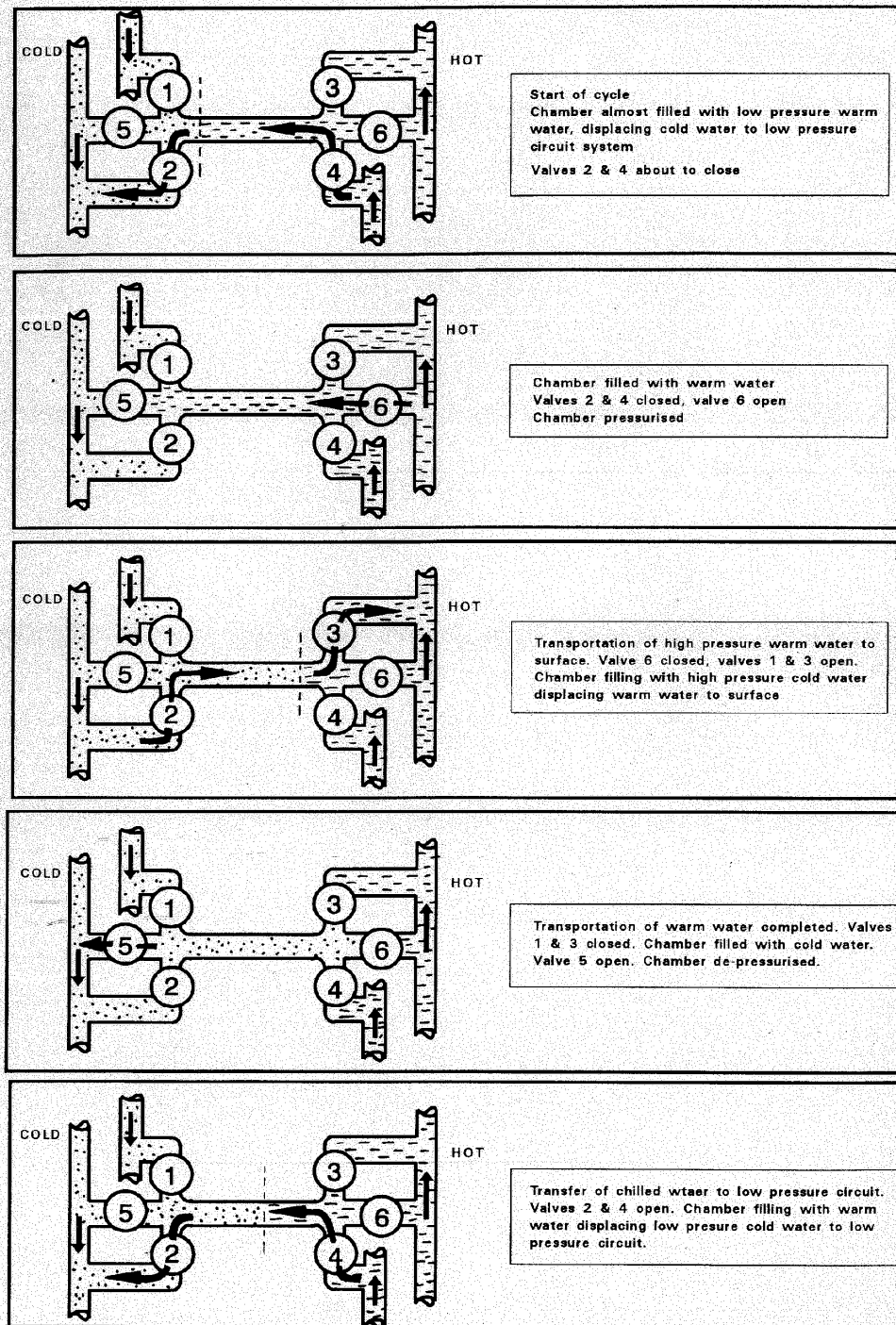


Figure 2.2 Three-pipe chamber feeder system (Hoffman, 1994)

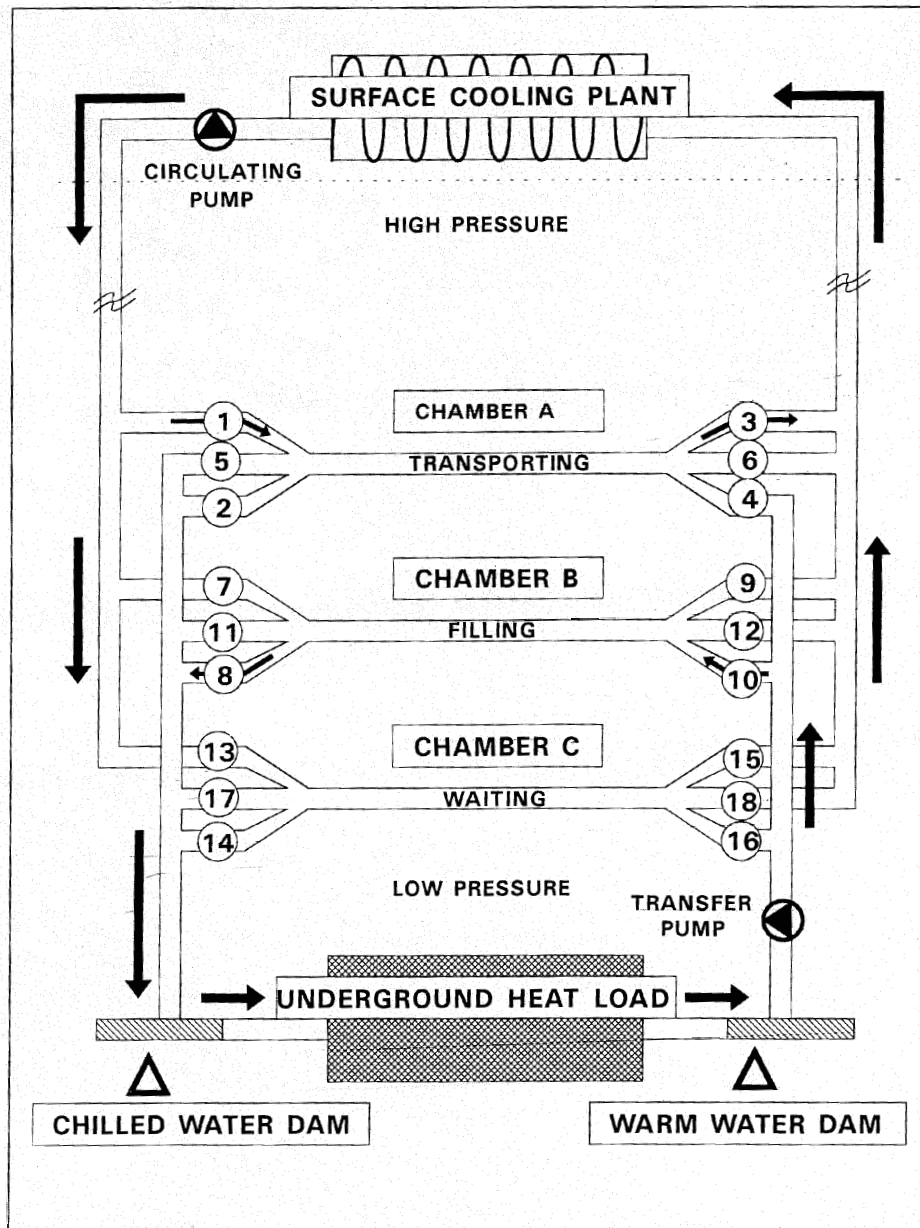


Figure 2.3 Operating sequence of the 3 CPF (Walters and Pretorius, 1994)

Several disadvantages of the 3 CPF are highlighted. The system requires high capital expenditure, has limited flexibility and requires several pumps to operate. Also, down-times tend to have negative financial implications. However, the 3 CPF has low operating costs; has a high efficiency and reliability (Gopal and Harper, 1999).

Hoffman (1994) suggests that the installation of the 3 CPF would impact on the design of the water reticulation circuit. Larger hot water dams would be required underground for flexibility and pumping should be done during periods of maximum demand. It is also recommended to achieve dam level control and pump operation using sophisticated control systems.

2.2 Pumps as turbines

The benefits of operating a standard water pump as a turbine include low manufacturing cost, short delivery times, low runaway speeds as well as large output range. The disadvantages to be borne in mind include lower best efficiency point, lower efficiency at part load and higher losses associated with regulating the water flow rate (Laux, 1982). Pump manufacturers (such as KSB) are focussing on the benefits of pumps operating in reverse and are investing resources into development of this technology (Orchard and Klos, 2009).

Pump-turbines are used in several applications including chemical and petrochemical processes; reverse-osmosis operations, and water supply systems (Laux, 1982). Isolated rural communities typically employ pump-turbine systems in micro-hydro schemes to generate electricity (Ramos and Borga, 2000).

Depending on the application and specified duty, Buse (1981) has provided a methodology on how to select the pump for reverse operation. Most pump manufacturers do not provide the equivalent turbine curves for a given pump, and mathematical relations are provided to select a pump for turbine operation; and to predict the performance of the pump in turbine mode.

A recent study was carried out by Derakshan and Nourbakhsh (2008) to predict the operation of a pump in reverse. Dimensionless pump parameters at the best efficiency point, for the pump in reverse mode, were determined theoretically from pump characteristics in normal mode. A computational fluid dynamics (CFD) analysis was also carried out for the pump in normal and reverse operation. This allowed for the generation of pump-turbine curves. A test-rig was constructed to verify the theoretical and CFD analyses. The experimental results showed that, at the best efficiency point for the pump in reverse mode, the discharge number, head number, power number and efficiency were 1.1 %, 1.1 %, 1.1 % and 1.1 % respectively.

4.7 %, 5.25 % and 2.1 % higher than the theoretical predictions, respectively. The CFD model showed that the discharge number, head number and power number were 1.1 %, 22.9 % and 16.4 % lower than the experimental data, respectively. The efficiency of the pump in reverse mode was 5.5 % higher than the value predicted by the CFD model. The reason attributed to this observation was the flow path of the water being different; when in normal and reverse modes.

2.3 Applications of pump-turbine systems

The purification of seawater via reverse-osmosis makes use of high pressures ranging between 5.5 and 7.0 MPa. Part of this energy is recovered in the clean water, while the balance is “wasted” in the brine solution. It is possible to recover up to 80 % of the “wasted” energy using a low cost pump-turbine (Raja and Paizza, 1981). More recently, Sulzer have developed a compact pump-turbine system that enables the recovery of energy from the brine. The system comprises a multi-stage pump coupled to a pelton wheel on a common shaft. It is however possible to replace this system with a reverse-running pump (Scholl, 2000).

Gopalakrishnan (1986) describes three processes that make use of pumps as turbines. In the hydrocarbon industry, hydrogen is used to increase the purity of liquid olefins. This usually takes place at high temperature and pressure. A typical arrangement for the pump-turbine system is shown in Figure 2.4. The high pressure stream leaving the reactor can be used to drive the pump-turbine and provide part of the load for the motor. The clutch ensures that the turbine does not overload the motor.

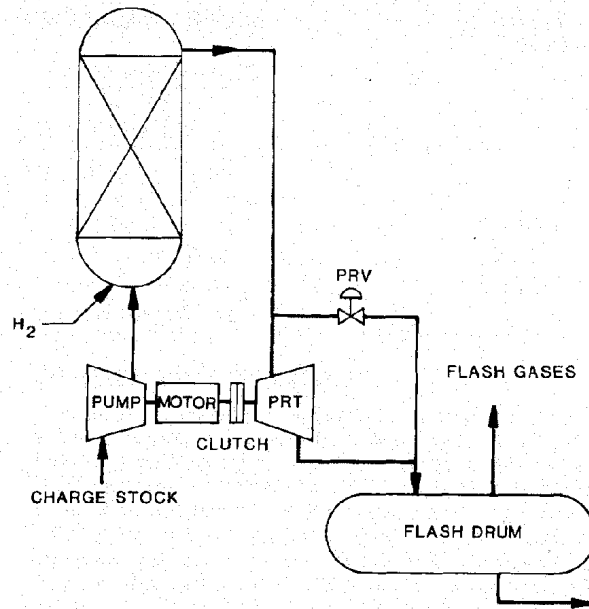


Figure 2.4 Schematic of Hydrotreating process (Gopalakrishnan, 1986)

The second application would be scrubbing of natural gas by a liquid, such as monoethanolamine or diethanolamine. The reactor exit stream would drive the pump-turbine as shown in Figure 2.5. The manufacture of synthetic ammonia would be the third application and is similar to the scrubbing process.

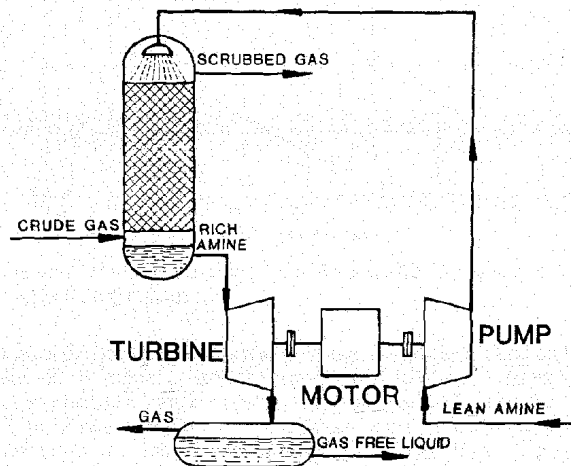


Figure 2.5 Schematic of Gas scrubbing process (Gopalakrishnan, 1986)

Pump-turbines are also suitable for use in micro hydro-power systems. Pumps operating in reverse are preferred for generating electricity in rural areas due their

practicality and low cost. Mankbadi and Mikhail (1984) describe the methodology for design of the low-head hydropower pump-turbine system. The governing equations are presented, which include static and dynamic system losses.

Williams (1996) describes two areas where the system has been constructed. In 1991, the pump-turbine system was installed at a remote farm in North England and has been operating successfully. The system has resulted in savings of up to \$ 1 500 (R 6 440)⁴ per year in fuel and maintenance. The savings in 2011 is expected to amount to R 50 100 per year. The second pump-turbine system was installed in Indonesia. The overall system efficiency was reported at 48 % from a head of 19 m and water flow of 50 l/s.

A pump-turbine hydropower system has been designed for Lao People's Democratic Republic in South East Asia. Several options were considered for generating power, which included solar energy. The pump as turbine system was selected as the best alternative, when compared to propeller and cross-flow turbines. The projected installation time is expected to be three weeks after all electrical and mechanical equipment is delivered to the site. However, construction has been placed on hold due to the unavailability of funds. The pump as turbine system for low head applications is still considered a viable technical and economical alternative (Arriaga, 2010).

Van Antwerpen and Greyvenstein (2005) have proposed a concept design for a pump operating in reverse. Two alternatives for the concept have been provided, namely, constant and variable pump-turbine speed. Theoretical models have been derived from first principles for the head and efficiency, as a function of flow and speed. These mathematical models were data-fitted to manufacturer supplied data. The concept was developed to recover the energy from water flowing down a mine shaft. The two alternatives were evaluated technically, and it was concluded that the constant speed system was the better option. The constant speed system was preferred due to its simplicity and that it maintains an

⁴ The average annual exchange rate in 1996 was R 4.30 per US \$ (South African Reserve Bank, 2011).

acceptable level of efficiency, over a wide flow range. Moreover, the system can be constructed from off-the-shelf components.

2.4 Conclusion

The economic benefit of employing energy recovery systems has been shown in the previous sections. In a mining context, energy recovery systems have made use of Pelton wheels, Francis turbines and three-chamber pipe feeders. Other industries have also made use of these technologies, including standard pumps operating in reverse.

The type of system in a particular industry will depend on the prevailing process conditions. Consequently, the energy recovery system must be carefully designed to maximise the system efficiency at minimum cost.

When considering the standard pump, it is primarily designed for moving fluid from one point to another. However, reversing the operation of the pump makes this machine quite versatile: in reverse mode it can behave as an energy recovery turbine. Furthermore, the low manufacturing cost, short delivery times and low runaway speeds encourage the use of reverse-running pumps as turbines.

3 THEORETICAL BACKGROUND

The examination of the pump-turbine system will invoke the laws of thermodynamics which will indicate the energy changes that will take place in the system. In order to understand how the system will be influenced by the thermodynamics, it is necessary to examine these laws in detail.

3.1 First law of thermodynamics

The law of conservation of energy states that the total quantity of energy will remain constant: when the energy disappears in one form it simultaneously appears in other forms. This postulate can be examined by considering two distinct parts, the *system* and its *surroundings*. To distinguish the parts, a process occurs within the boundary of the system; while anything with which the system interacts is the surroundings. A mathematical statement for the conservation of energy is

$$\Delta(\text{energy of the system}) + \Delta(\text{energy of the surroundings}) = 0 \quad (3.1)$$

This equation states that any change (Δ) in energy of the system will affect the energy of the surroundings. Defining a closed system as a boundary across which mass may not pass while energy is allowed to pass; this energy will appear as heat (Q) and work (W). Adopting the sign convention that the energy leaving the system is negative,

$$\Delta(\text{energy of the surroundings}) = -Q - W \quad (3.2)$$

Substituting into equation (3.1),

$$\Delta(\text{energy of the system}) = Q + W \quad (3.3)$$

This means that an energy change within a closed system is the energy transferred to it as heat and work. Also, the only energy change that typically occurs within a closed system, results in a change in the internal energy only.

This is expressed as

$$\Delta U = Q + W \quad (3.4)$$

This describes finite changes in internal energy of the system. For infinitesimal changes,

$$dU = dQ + dW \quad (3.5)$$

Equations (3.4) and (3.5) are mathematical expressions for the first law of thermodynamics.

3.2 Flow processes

When considering flow processes, the concept of an open system must be adopted. The open system allows both mass and energy to cross the system boundary. In an open system, the laws of thermodynamics still apply, along with the principles of fluid mechanics. The study of fluid mechanics is based on Newton's second law and results from pressure gradients present within the fluid. Furthermore, the fluid may exhibit temperature, velocity and concentration gradients. Therefore, the combination of thermodynamics and fluid mechanics will allow for the determination of the state of the system including the rate at which the process would occur.

Considering an open system (Figure 3.1) with flowing streams across the system boundary, the mass flow rate \dot{m} , is related to the volumetric flow rate q and the fluid density ρ . Also the fluid velocity u is dependent on the volumetric flow through the cross-sectional area A .

$$\dot{m} = q \rho \quad \text{and} \quad q = u A \quad (3.6a)$$

therefore,
$$\dot{m} = u A \rho \quad (3.6b)$$

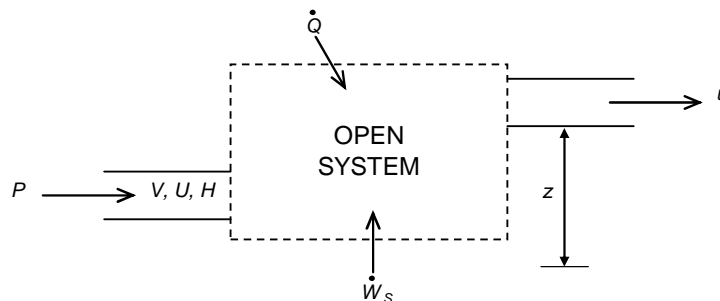


Figure 3.1 A flow process (after Smith et. al., 2001)

The conservation of mass for the system is stated as:

rate of mass entering the system – rate of mass leaving the system + rate of
change of mass in the system = 0

or mathematically,

$$dm/dt + \Delta(\dot{m}) = 0 \quad (3.7a)$$

$$dm/dt + \Delta(u A \rho) = 0 \quad (3.7b)$$

Equation (3.7a) is the general mass balance and is often called the continuity equation. The 'Δ' in this equation is the difference between the inlet and outlet flows to the system. When the mass within the system remains constant with respect to time, the system is characterised as 'steady-state' and

$$\Delta(u A \rho) = 0 \quad (3.8)$$

The special case of a system having a single inlet and single outlet, and a process that is at steady-state, equation (3.8) becomes

$$u_{in} A_{in} \rho_{in} - u_{out} A_{out} \rho_{out} = 0 \quad (3.9a)$$

and,
$$\dot{m} = u_{in} A_{in} \rho_{in} = u_{out} A_{out} \rho_{out} = \text{constant} \quad (3.9b)$$

Now considering the conservation of energy, the rate of change of energy in the system would be the same as the net rate of transfer of energy into the system. The streams entering and leaving the system will have energy associated with them, which will result in an energy change in the system. The total energy of each stream will be $U + \frac{1}{2}u^2 + gz$, where u is the average velocity of the stream, z is the elevation with respect to a datum level and g is the local acceleration due to gravity⁵. The energy balance is now written as

$$d(mU)/dt + \Delta[(U + \frac{1}{2} u^2 + g z) \dot{m}] = \dot{Q} + \text{work rate} \quad (3.10)$$

The 'work rate' would include moving the fluid through the entrances and exits of the system, and arises from Newton's second law. This term can be described by $(PV) \dot{m}$ and is work done on the system. The work rate would also include

⁵ The value for g in the Witwatersrand region is taken as 9.79 m/s² (Whillier, 1977).

work done on the system by stirring, as well as the work done by the system in the form of expansion or contraction – this term is the shaft work, \dot{W}_S

$$d(mU)/dt + \Delta [(U + \frac{1}{2} u^2 + g z) \dot{m}] + \Delta [(P V) \dot{m}] = \dot{Q} + \dot{W}_S \quad (3.11)$$

Introducing the definition of enthalpy $H = U + P V$, and rearranging results in

$$d(mU)/dt + \Delta [(H + \frac{1}{2} u^2 + g z) \dot{m}] = \dot{Q} + \dot{W}_S \quad (3.12)$$

The energy balance for an open system at steady-state, having a single entrance and exit, results in

$$(\Delta H + \frac{1}{2} \Delta u^2 + g \Delta z) \dot{m} = \dot{Q} + \dot{W}_S \quad (3.13)$$

The ‘ Δ ’ would once again refer to the inlet minus the outlet. Dividing by the mass flow rate yields

$$\Delta H + \frac{1}{2} \Delta u^2 + g \Delta z = Q + W_S \quad (3.14)$$

3.3 Second law of thermodynamics

The first law shows that energy can be transformed from one form into another. However, there are limitations on the transformation. In the energy balance, the work and heat terms are included as additive terms. This has the underlying simplification that one joule of heat is equivalent to one joule of work. Mathematically this may be true, but this is not the case when actual processes are considered.

Considering the conversion of potential energy of an object into kinetic energy by acceleration, or into electrical energy by operating a generator. This indicates that work can be completely transformed into other forms of energy. This conversion can approach an efficiency of 100 % by the elimination of friction and other dissipative influences. However, the conversion of heat into other forms of energy or work is not very efficient. Also, there are restrictions imposed on the conversion of heat into other useful forms of energy. This leads to the development of the second law of thermodynamics. Two statements can summarise the restriction:

1. It is not possible for a system to undergo a process that results solely in the conversion heat absorbed completely into work done by the system; and
2. Heat transfer can not take place from a lower temperature to a higher temperature.

Statement one means that when heat is absorbed by the system, work will be done by the system on the surroundings and

$$\Delta(\text{energy of the system}) = Q - W \quad (3.15)$$

Therefore, from equation (3.1),

$$\Delta(\text{energy of the surroundings}) = -Q + W \quad (3.16)$$

To combat the change in the surroundings, heat must be absorbed by the surroundings and work must be done by the surroundings on the system. This cyclic process returns the system to its original state, with no net work being produced. This proves the first statement.

3.3.1 Heat engines

The second law can be understood from a macroscopic perspective, by considering heat engines. These are mechanical devices that absorb heat in a cyclic process and produce work. The process involves the absorption of heat by the system at a high temperature and rejection of heat to the surroundings at a lower temperature; along with the production of work. The operation of a heat engine can be described by considering the concept of a heat reservoir, a body that can absorb an infinite amount of heat without causing a change in its temperature. The first law of thermodynamics can be written for a heat engine that absorbs heat $|Q_H|$ from a hot reservoir, produces work $|W|$, and rejects heat $|Q_C|$ to a cold reservoir and returns to its original state. Absolute values are used so that to make the equations independent of sign convention.

$$|W| = |Q_H| + |Q_C| \quad (3.17)$$

The thermal efficiency is defined as

$$\eta = \text{net work output} / \text{heat absorbed}$$

Introducing equation (3.17),

$$\eta = |W| / |Q_H| = (|Q_H| + |Q_C|) / |Q_H| \quad (3.18a)$$

$$\eta = 1 - |Q_C| / |Q_H| \quad (3.18b)$$

The heat engine will be 100 % efficient ($\eta = 1$) when the $|Q_C|$ is zero. It should be noted that no engine has been built that is 100 % efficient, which further emphasizes Statement 1 of the second law of thermodynamics. The upper limit for the efficiency of a heat engine is determined by the Carnot engine, a reversible heat engine. The Carnot cycle for an ideal gas is described in four steps and is shown in Figure 3.2.

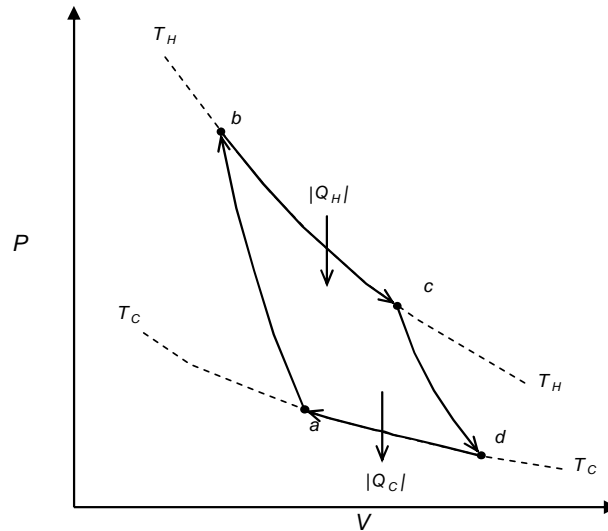


Figure 3.2 *PV* diagram showing the Carnot cycle for an ideal gas (Smith et. al., 2001)

The cycle proceeds in the following order:

- a-b The system at a temperature T_C undergoes a reversible adiabatic process causing the temperature to increase to T_H .
- b-c Heat $|Q_H|$ is absorbed by the system from the hot reservoir and the system undergoes a reversible isothermal process.
- c-d A reversible adiabatic process results in the temperature of the system returning to T_C .
- d-a The system rejects heat $|Q_C|$ to the cold reservoir during a reversible isothermal process.

The ideal Carnot engine absorbs heat at the temperature of the hot reservoir and rejects heat at the temperature of the cold reservoir. For a real heat engine, a temperature difference exists between the system and the heat reservoirs making the process irreversible.

The concept of the irreversible heat engine and the reversible Carnot engine results in the development of Carnot's equations. The equation of state for an ideal gas is

$$PV = RT \quad (3.19)$$

The ideal gas is considered to exhibit no molecular interactions, with the conclusion that the internal energy is dependent only on the temperature⁶. By definition the heat capacity at constant volume C_V is

$$C_V = (\partial U / \partial T)_V \quad (3.20)$$

The first law for an ideal gas undergoing a reversible process is

$$C_V dT = dQ + dW \quad (3.21)$$

and noting that $dW = -P dV$ and $P = RT / V$,

$$dQ = C_V dT + RT dV / V \quad (3.22)$$

For the isothermal steps ($dT = 0$), b-c and d-a, equation (3.22) is rearranged and integrated to yield

$$|Q_H| = RT_H \ln (V_C / V_b) \quad (3.23a)$$

$$|Q_C| = RT_C \ln (V_d / V_a) \quad (3.23b)$$

and

$$|Q_H| / |Q_C| = (T_H / T_C) [\ln (V_C / V_b) / \ln (V_d / V_a)] \quad (3.24)$$

Now considering the adiabatic steps ($dQ = 0$), a-b and c-d, rewriting equation (3.22) will result in

$$-(C_V / R) dT / T = dV / V \quad (3.25)$$

⁶ These simplifying assumptions can not be used to describe the behaviour of real gases, however, the ideal gas is a useful model to compare the behaviour of real gases.

Integrating from T_C to T_H yields

$$\int (C_V / R) dT / T = \ln (V_a / V_b) \quad (3.26a)$$

$$\int (C_V / R) dT / T = \ln (V_d / V_C) \quad (3.26b)$$

Since the left side of these equations (3.26a) and (3.26b) are identical

$$\ln (V_a / V_b) = \ln (V_d / V_C) \quad (3.27a)$$

or,
$$\ln (V_C / V_b) = \ln (V_d / V_a) \quad (3.27b)$$

and equation (3.24) becomes

$$|Q_H| / |Q_C| = T_H / T_C \quad (3.28)$$

Combining this result with the definition of the thermal efficiency

$$\eta = |W| / |Q_H| = 1 - T_C / T_H \quad (3.29)$$

Equations (3.28) and (3.29) are known as Carnot's equations. The efficiency will approach unity when the value of $|Q_C|$ is zero, corresponding with absolute zero for T_C , and $|Q_H|$ approaching infinity. None of these conditions are attainable resulting in the conclusion that real engines operate at values less than unity.

3.3.2 Entropy

The Carnot equations can be rewritten by considering an engine absorbing heat Q_H and the rejecting heat Q_C to the surroundings. Equation (3.28) then becomes

$$Q_H / T_H = - Q_C / T_C \quad (3.30a)$$

or
$$Q_H / T_H + Q_C / T_C = 0 \quad (3.30b)$$

This means that when an engine undergoes a reversible cyclic process of absorbing and rejecting heat, the engine returns to its original state. All properties associated with the engine including temperature, pressure and internal energy return to their initial values. Equation (3.30b) shows that a property exists, represented by Q / T , that will restore the system to its original state after traversing a cyclic process.

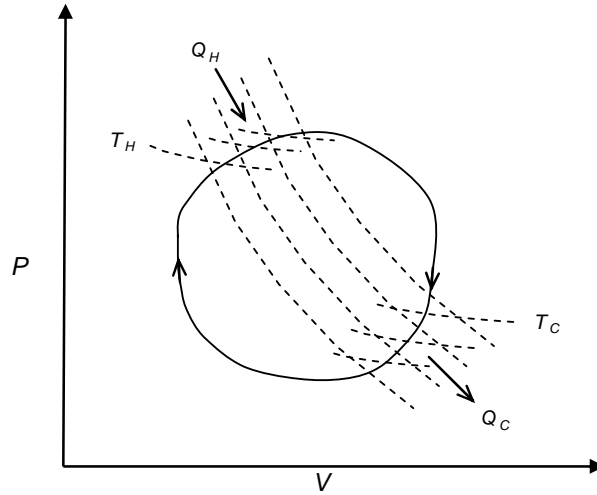


Figure 3.3 A reversible cyclic process (Smith et. al., 2001)

For each Carnot cycle shown in Figure 3.3, isotherms (T_C and T_H) and adiabats (Q_H and Q_C) are drawn for different Carnot cycles. When the adiabatic curves become closely spaced to give infinitesimal isothermal steps, the heat quantities become differential and

$$dQ_H / T_H + dQ_C / T_C = 0 \quad (3.31)$$

When the working fluid of the engine undergoes the cyclic process, it will attain temperatures T_H and T_C . Also, these temperatures are the absolute temperatures of the working fluid. Summation of all the terms in equation (3.30b) leads to the integral

$$\oint dQ / T = 0 \quad (3.32)$$

This equation applied to a heat engine undergoing an arbitrary cyclic that is reversible. This indicates the presence of a property that will sum to zero when traversing such a process. The definition of entropy (S) is defined as

$$dS = dQ / T \quad (3.33a)$$

or
$$dQ = T dS \quad (3.33b)$$

When a process is reversible and adiabatic, $dQ = 0$ and by equation (3.33a) $dS = 0$. This process will take place at constant entropy or is said to be isentropic.

3.4 Property relationships

3.4.1 Internal energy and enthalpy

The first law can be expressed as

$$dU = dQ + dW \quad (3.5)$$

The work done by the system for a reversible process is given by

$$dW = -P dV \quad (3.34)$$

where P is the pressure of the fluid.

Combining equations (3.5), (3.33a) and (3.34) yields

$$dU = T dS - P dV \quad (3.35)$$

Equation (3.35) has combined the first and second laws for the special case of a reversible process. It can be seen that there are state properties on the right-hand side of the equation, which implies that they are path independent. It is therefore possible to apply this equation to any process that undergoes differential change from one state to another, with the restriction that the mass remains constant.

Enthalpy, H , is defined as

$$H = U + PV \quad (3.36)$$

Differentiation of the enthalpy, equation (3.36), gives

$$dH = dU + P dV + V dP \quad (3.37)$$

Substitution of equation (3.35) into (3.37) yields

$$dH = T dS + V dP \quad (3.38)$$

Equations (3.35) and (3.38) are fundamental property relations for internal energy and enthalpy. These relations can be applied to fluid that is homogenous and of constant composition.

3.4.2 Enthalpy and entropy

It is quite useful to express enthalpy and entropy of a homogeneous phase as a function of temperature and pressure. This can be stated as

$$H = H(T, P) \quad (3.39a)$$

$$S = S(T, P) \quad (3.39b)$$

and in terms of partial derivatives

$$dH = (\partial H / \partial T)_P dT + (\partial H / \partial P)_T dP \quad (3.40a)$$

$$dS = (\partial S / \partial T)_P dT + (\partial S / \partial P)_T dP \quad (3.40b)$$

By definition, the heat capacity at constant pressure C_P is given by

$$C_P = (\partial H / \partial T)_P \quad (3.41)$$

At constant pressure, dividing equation (3.38) by dT gives

$$(\partial H / \partial T)_P = T(\partial S / \partial T)_P \quad (3.42)$$

Combining equations (3.41) and (3.42):

$$(\partial S / \partial T)_P = C_P / T \quad (3.43)$$

The Maxwell equation⁷ relates pressure derivative to volume:

$$(\partial S / \partial P)_T = -(\partial V / \partial T)_P \quad (3.44)$$

Dividing equation (3.38) by dP and restricting to constant temperature

$$(\partial H / \partial P)_T = T(\partial S / \partial P)_T + V \quad (3.45)$$

and substituting (3.44) gives

$$(\partial H / \partial P)_T = V - T(\partial V / \partial T)_P \quad (3.46)$$

Hence equation (3.40a) becomes

$$dH = C_P dT + [V - T(\partial V / \partial T)_P] dP \quad (3.47)$$

and

$$dS = (C_P / T) dT - (\partial V / \partial T)_P dP \quad (3.48)$$

⁷ These are the second derivatives of the thermodynamic fundamental property relations (Smith et. al., 2001).

By introducing volume expansivity β to eliminate the partial derivative,

$$\beta = (1/V) (\partial V / \partial T)_P \quad (3.53)$$

$$dH = C_p dT + (1 - \beta T) V dP \quad (3.49)$$

$$dS = (C_p / T) dT - \beta V dP \quad (3.50)$$

Equations (3.49) and (3.50) are general equations for enthalpy and entropy as a function of temperature and pressure.

3.4.3 Specific volume

The specific volume V , of a fluid may be expressed as a function of temperature and pressure. Following a similar procedure for the enthalpy and entropy,

$$V = V(T, P) \quad (3.51)$$

and in terms of partial derivatives

$$dV = (\partial V / \partial T)_P dT + (\partial V / \partial P)_T dP \quad (3.52)$$

For a liquid (in the single-phase region), two properties are defined, namely, volume expansivity β

$$\beta = (1/V) (\partial V / \partial T)_P \quad (3.53)$$

and isothermal compressibility, κ

$$\kappa = - (1/V) (\partial V / \partial P)_T \quad (3.54)$$

For liquids, β is positive (water between 0°C and 4°C is an exception) and κ is positive. At conditions not close to the critical point, β and κ are weak functions of temperature and pressure respectively. Thus little error is introduced when volume expansivity and isothermal compressibility are assumed constant. This is a better approximation than assuming the fluid is incompressible, which has the implication of specific volume being independent of temperature and pressure, and constant.

3.4.4 Joule-Thomson effect

When a fluid undergoes an isenthalpic process (constant enthalpy), without a significant change in kinetic or potential energy, the fluid pressure will change.

No shaft work would be produced and frictional losses can be considered negligible. If the process is also adiabatic ($Q = 0$) the energy balance, equation (3.14) (Section 3.2) reduces to

$$\Delta H = 0 \quad \text{or} \quad H_{in} = H_{out} \quad (3.55)$$

and results in the definition of the 'Joule-Thomson coefficient' μ_H which is defined as

$$\mu_H = (\partial T / \partial P)_H \quad (3.56)$$

Considering the enthalpy as a function of temperature and pressure in equation (3.49), an isenthalpic process will lead to

$$C_P dT = (\beta T - 1) V dP \quad (3.57)$$

Rearranging results in

$$\mu_H = (\partial T / \partial P)_H = (\beta T - 1) V / C_P \quad (3.58)$$

Similarly, for an isentropic process where $\Delta S = 0$, or $S_{in} = S_{out}$, the Joule-Thomson coefficient at constant entropy, μ_S can be defined as

$$\mu_S = (\partial T / \partial P)_S \quad (3.59)$$

At constant entropy, equation (3.50) becomes

$$(C_P / T) dT = \beta V dP \quad (3.60)$$

Rearranging and introducing μ_H from equation (3.56) results in

$$\mu_S = (\partial T / \partial P)_S = \beta V T / C_P \quad (3.61a)$$

or

$$\mu_S = \mu_H + V / C_P \quad (3.61b)$$

When high pressure water flows through a pressure-reducing valve, the pressure loss occurs at constant enthalpy (Whillier, 1977) and the temperature increase is described by the Joule-Thomson coefficient at constant enthalpy, μ_H .

3.5 Turbine expansion process

When a fluid at a high pressure flows through a turbine, the fluid will expand and result in a high velocity stream. This increases the kinetic energy of the fluid.

The kinetic energy is then converted into shaft work. This process is manifested by a fluid impinging on the blades of a turbine; and the subsequent rotation of the turbine shaft.

The energy balance, equation (3.13), can be written for the turbine. Assuming the inlet and outlet pipe sizes are the same ($u_1 = u_2$) and heat transfer into the system is negligible, the energy balance simplifies to

$$\dot{W}_S = (\Delta H + g \Delta z) \dot{m} \quad (3.62)$$

The potential energy term would be the difference in elevation between the centre-lines of the inlet and outlet and would be constant.

For an adiabatic, isentropic process the fundamental property relation

$dH = T dS + V dP$ becomes

$$dH = V dP \quad (3.63a)$$

and integrating yields

$$(\Delta H)_S = V \Delta P \quad (3.63b)$$

If a new term $\Delta H'$ is defined that combines the pressure and potential energy terms of equation (3.62), the equivalent form of the enthalpy difference would be

$$(\Delta H')_S = V \Delta P' \quad (3.64)$$

The $\Delta P'$ would be the “equivalent differential pressure” of the combined pressure and potential energy terms. This would only be valid under the assumption of a reversible adiabatic process (i.e. isentropic).

The expansion process of a turbine can be best understood by using an enthalpy-entropy plot, which is sometimes referred to as a Mollier diagram.

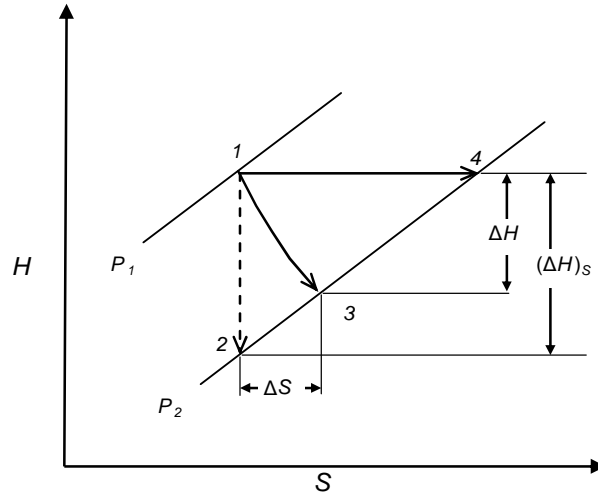


Figure 3.4 Expansion process of a fluid (after Smith et. al., 2001)

When a fluid at a high pressure undergoes an expansion process, the fluid will follow one of three paths, namely, isentropic, isenthalpic and a path lying between these two boundaries.

Isentropic expansion will occur when moving from point 1 to point 2 in Figure 3.4. This constant entropy process will result in the maximum shaft work being produced. It should be noted that this process is also adiabatic. The isentropic work done is

$$(W_s)_s = (\Delta H')_s \quad (3.65)$$

The temperature change for an isentropic process is given by equation (3.59) (pp 32). It should be noted that there will be a reduction in temperature (point 2).

An isenthalpic process will result an expansion that increases the kinetic energy, without any shaft work being produced. Instead, the kinetic energy will be converted into friction and increase the temperature of the fluid. In this case, there is no turbine present. This constant enthalpy process is commonly referred to as 'throttling' and will follow the path 1-4 (Figure 3.4). The Joule-Thomson coefficient (equation (3.56), pp 32) is used to determine the temperature of throttling process.

With a turbine present, a path moving from point 1 to 3 will be followed. This arises from the fact that no turbine is 100 % efficient. Consequently, the turbine efficiency η is defined as the ratio of the actual shaft work to the isentropic shaft work,

$$\eta = W_S / (W_S)_S \quad (3.66a)$$

and
$$\eta = \Delta H' / (\Delta H')_S \quad (3.66b)$$

The outlet temperature of the turbine, will be higher than the temperature of an isentropic expansion and lower than the temperature of a throttling process ($T_2 < T_3 < T_4$). It should be noted that the process will result in the same outlet pressure (only the path will be different). Therefore, the turbine outlet temperature can be determined from heat capacity data (C_P).

$$\Delta H' = C_P (T_4 - T_3) \quad (3.67a)$$

or
$$(\Delta H')_S - \Delta H' = C_P (T_3 - T_2) \quad (3.67b)$$

3.6 Mechanical energy balance

In deriving the energy balance for an open system (Section 3.2) the ideal case of frictionless flow was considered. This assumes that the fluid has zero viscosity. However, real fluids exhibit viscous effects and work is done to overcome friction. This energy is converted into thermal energy that increases the internal energy of the fluid. The net effect is an increase in fluid temperature and a decrease in the available energy for conversion into work. This loss can be expressed as $\Delta U - Q$. It is convenient to express this friction loss as the 'head loss' h_f . For a fluid of constant density,

$$g h_f = \Delta U - Q \quad (3.68)$$

Rewriting the energy balance for an open system at steady-state, equation (3.11) becomes

$$\Delta [(U + \frac{1}{2} u^2 + g z) \dot{m}] + \Delta [(P V) \dot{m}] = \dot{Q} + \dot{W}_S \quad (3.69)$$

Assuming no heat is added to the system but heat will originate from frictional losses, dividing by the mass flow rate and defining the entrance and exit as points 1 and 2

$$U_1 + \frac{1}{2} u_1^2 + g z_1 + P_1 V_1 = W_S - Q + U_2 + \frac{1}{2} u_2^2 + g z_2 + P_2 V_2 \quad (3.70)$$

Introducing the head loss and replacing V with density, ρ

$$P_1 / \rho_1 + \frac{1}{2} u_1^2 + g z_1 = P_2 / \rho_2 + \frac{1}{2} u_2^2 + g z_2 + W_s + g h_f \quad (3.71)$$

The above equation will apply to an incompressible fluid (constant fluid density). It should be noted that the increase in the temperature of the fluid due to friction is usually negligible. Equation (3.71) is commonly referred to as a mechanical energy balance. Mechanical energy can be described as work or a form that can be readily converted into work. The friction term $g h_f$ is the sum of all friction losses in the system.

3.7 Frictional losses

In a pipe system, some of the components would include valves, elbows and bends. The fluid flowing in the network would encounter frictional losses due to these components. The estimation of this energy dissipation is vital to ascertain the effect on the system.

3.7.1 Pipe friction

A fluid can exhibit two kinds of flow, namely, laminar and turbulent. At low velocities, the fluid will move in straight lines and is usually referred to as 'laminar' flow. Turbulent flow is characterised by disorderly fluid motion and is observed at higher velocities. A 'transitional' flow regime exists between laminar and turbulent flows. The flow regime for an incompressible fluid, can be determined by using the 'Reynolds' number (Re).

The Reynolds number relates the viscous and inertial forces a fluid flowing in a conduit, and is defined as

$$Re = Lu\rho / \mu_F \quad (3.72)$$

For fluid flowing in a circular pipe, the characteristic length L , can be replaced with the pipe inside diameter D . The upper limit for laminar flow occurs at $Re \approx 2\,100$, while turbulent flow will occur at approximately $Re > 5\,000$ (the transitional region will lie between these two values). Since the fluid motion is different in

each flow regime, the frictional loss of the fluid will be different for laminar, transitional and turbulent flows.

The frictional pressure loss in a pipe (ΔP_f), can be determined using the following relation (Perry and Green, 1997):

$$\Delta P_f = 4f(L/D)\rho u^2 / 2 \quad (3.73)$$

The friction factor f , is the drag force per unit wetted surface area, divided by the product of density and velocity head $\frac{1}{2}\rho u^2$. The friction factor is dependent on the Reynolds number Re , and the pipe roughness ε . The surface roughness will vary in size, shape and spacing, but an acceptable average value would suffice. In general, the relative roughness ε/D is used to estimate the friction factor.

Figure 3.5 shows a plot of friction factor as a function of Re and ε/D , for laminar and turbulent flow regimes.

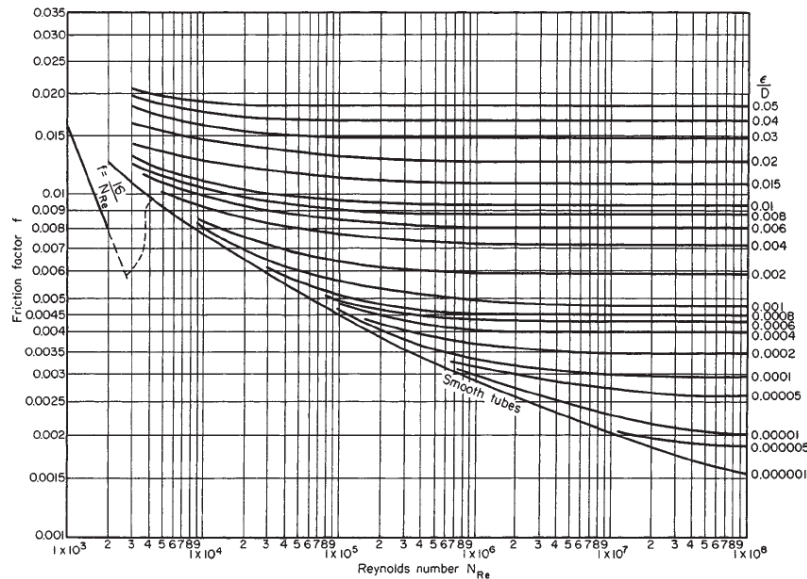


Figure 3.5 Friction factor chart (Perry and Green, 1997)

The use of a graph can introduce some error into the final solution. To try and reduce the error, equations are available to calculate f . For laminar flow

$$f = 16 / Re \quad (3.74)$$

and for turbulent flow, the Colebrook relation (Perry and Green, 1997) can be used for rough pipes:

$$1 / f^{1/2} = -4 \log [\epsilon / 3.7 D + 1.256 / (Re f^{1/2})] \quad (3.75)$$

For smooth pipes, the Blasius equation (Perry and Green, 1997) gives a good approximation over a wide range.

$$f = 0.079 / Re^{0.25} \quad (3.76)$$

3.7.2 Other frictional losses

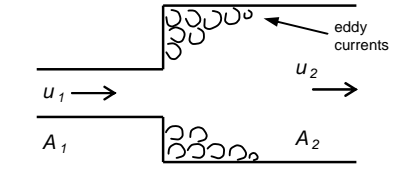
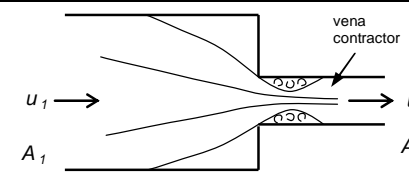
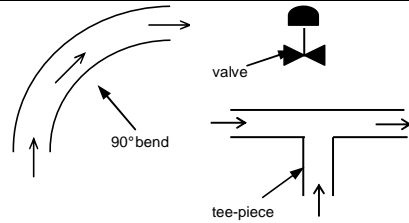
In a pipe network, the area can increase abruptly, resulting in turbulence and eddy currents. Assuming turbulent flow in both sections, the pressure loss can be evaluated using equations listed in Table 3.1. The geometric opposite, an abrupt contraction, also results in a pressure loss due to the formation of a vena contractor downstream of the junction. There is also eddy formation between the wall of the pipe and the vena contractor.

When fluid flows through a bend, the change in direction gives rise to turbulence and a subsequent loss in pressure. The magnitude of the loss is dependent on the curvature of the bend.

Pipe fittings such as valves and couplings also result in friction losses. The loss is proportional to the flow path through the fitting – a high pressure loss will occur through a tortuous flow path.

The pressure losses for the above components are proportional to the velocity head. Table 3.1 lists the equations for calculating the head losses. The pressure loss is obtained by multiplying the head loss by ρg . For pipe fittings, values for K_L are available in the literature (Perry and Green, 1997).

Table 3.1 Friction losses for pipe components (after Massey, 1970)

Abrupt enlargement		$h_{ex} = K_L(1 - A_1/A_2)u_1^2 / 2$
Abrupt contraction		$h_{con} = K_L(1 - A_2/A_1)u_2^2 / 2$
Other fittings (bends, tees, valves, etc.)		$h_L = K_L u^2 / 2$

3.8 System characteristic

The previous section showed that the friction losses arise from the presence of pipe fittings, and is dependent on the fluid velocity. It is convenient to examine the system at various flow rates and present this in graphical format (Figure 3.6). The system pressure is calculated from the mechanical energy balance (equation (3.71), pp 36) at varying flow rates.

The turbine performance curve is also plotted on the same set of axes. The turbine curve is typically provided by turbine manufacturers. The system operating point occurs at the intersection of the system and turbine curves.

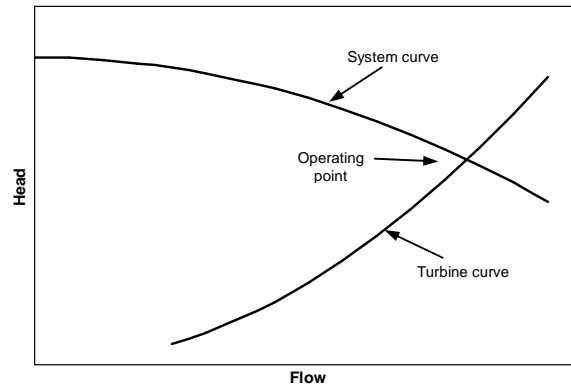


Figure 3.6 System curve and turbine curve

3.9 Electrical generators

There are several devices available that can convert electrical energy into mechanical energy and vice versa. Typically, the conversion takes place due to the presence of an electromagnetic field. The concept is explored by considering the conservation of energy, noting the restrictions imposed by the second law of thermodynamics on the inefficiency. There are three parts to the conversion system, namely, the electrical system, mechanical system and a coupling field to “link” these two systems (Figure 3.7).

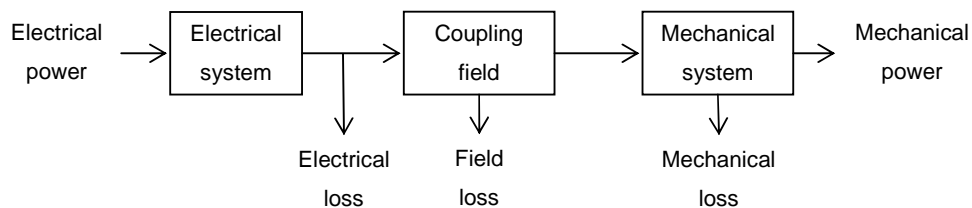


Figure 3.7 Electromechanical converter system

The electrical loss would be the windings loss (stator and rotor losses) present in the electrical drive, while the field loss would result from the variation in magnetic field within the drive. The mechanical losses would result due to moving parts and friction.

Figure 3.7 describes the conversion of electrical to mechanical energy: an electrical input is applied and a mechanical shaft would rotate. Traversing the path from right to left would describe the reverse operation.

3.9.1 Electrical drives

An electrical drive is a machine that achieves the electromagnetic conversion. It is composed of a rotor in the centre of the machine and a stator on the periphery of the machine, separated by an air-gap. The rotor is allowed to move while the stator is fixed to the machine. Magnetic pole-pairs (north and south) are fixed to the stator.

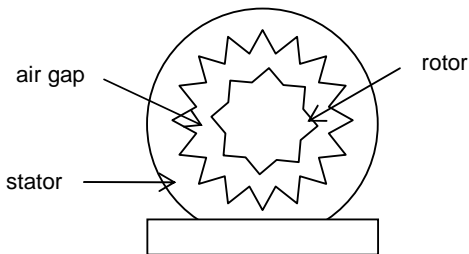


Figure 3.8 Cross-section through an electrical drive

Slots are cut into the outer part of the rotor and the inner part of the stator. Conductors are placed within these slots to form windings. When current flows through a winding, it is termed a field winding. An armature winding results when an induced voltage results across the given winding. The air gap is the physical boundary between the rotor and stator.

The electric machine construction would determine the operation of the drive. This would include the positions of the armature and field windings within the rotor and stator. Consequently, three types of electrical drives used for electromechanical conversion are available: direct current (dc), induction and synchronous machines.

The field windings of a dc machine are installed in the stator while the armature windings are present within the rotor. When operating as a generator a shaft coupled to the rotor, would cause the rotor to turn. Rotation within the stator magnetic field would induce a voltage and hence alternating current (ac) would flow through the armature windings. A commutator-brush system keeps the current in a single direction. The electromagnetic flux produced within the air gap, induces direct current within the field windings of the stator. The dc machine

can operate as a motor: when a dc current is applied to the stator windings, ac current is induced in the rotor windings causing the rotor to turn a shaft.

A synchronous machine has the field windings present within the rotor, while the armature windings are installed within the stator. The synchronous machine operates in reverse compared to the dc machine. The rotating shaft causes the rotor to turn and dc current is induced within the rotor windings. Electromagnetic flux induced in the air gap results in a voltage across the stator windings – ac current flows through the stator windings. When an ac current is applied to the stator windings, dc current would flow through the rotor windings. The rotor would then turn a shaft and the synchronous machine then operates as a motor.

In an induction machine, the stator windings would function both as armature and field windings. The rotor construction can be similar to the stator or composed of aluminium or copper bars in the rotor slots with rings attached to the ends. When the rotor turns due to a rotating shaft, electromagnetic flux generated within the air gap, induces current to flow within the rotor and stator windings. Ac current is produced in the stator windings. The induction machine can also operate as a motor when an ac current is applied to the stator windings. The modes of operation of an induction machine can be described in Figure 3.9.

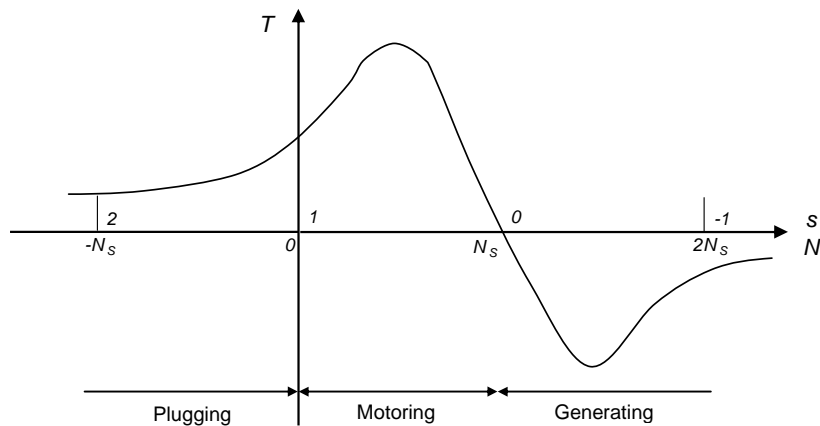


Figure 3.9 Operating modes of an induction machine (after Gray, 1989)

When an electrical supply is applied to the stator, the rotor will turn in the same direction as the stator rotating electromagnetic field. This is the “motoring” region indicated in the figure above and is the typical operation of the machine. The

steady-state speed, N is lower than the synchronous speed N_s . The torque T , will be in the same direction as the stator rotating magnetic field.

When the rotor speed increases above the synchronous speed, the machine will produce a torque opposite in direction to the stator rotating magnetic field. The flow of power will reverse and be fed back to the supply.

Plugging occurs when the rotor turns in the opposite direction to the stator magnetic field, but the torque produced will oppose rotor motion.

The slip s , is also shown in Figure 3.9 and is defined as the difference between the rotor speed N and synchronous speed N_s

$$s = (N_s - N) / N_s \quad (3.77)$$

During the normal operation of motoring, the slip would lie between zero and one; while the slip would be negative during power generation.

3.9.2 Operating speed

The electrical drive can be coupled to the turbine via a gearbox, or it can be direct-driven. The water flow through the turbine will determine the turbine shaft speed and hence the speed of the drive. If the water flow is not constant, the turbine shaft speed would impact on the design of the electrical system. Two strategies can be adopted for the design of the electrical system, namely, a constant speed system or a variable speed system.

A simple constant speed system would use an induction machine that is directly coupled to the turbine; and operates at the supply frequency. In South Africa, the supply frequency is 50 Hz and for a 2-pole electrical drive, this corresponds to a synchronous rotational speed of 3 000 rpm. This would then fix the turbine operating water flow to a single value. The consequence is the capture of energy at this water flow and head.

The variable speed system can also have the turbine and electrical drive directly coupled. The drive would use power electronics (typically inverters and rectifiers)

to convert the variable voltage and frequency into a constant voltage and frequency (Patel, 2006). A range of water flows is then allowed to flow through the turbine and therefore, it is possible to recover more energy.

3.10 Conclusion

The pump-turbine system will be subject to the laws of conservation of mass and conservation of energy. Consequently, mass and energy balances are required to ensure that the system obeys these laws.

The energy balance was derived from the first law of thermodynamics and simplifying assumptions to the proposed models have been made for the different components. It was necessary to incorporate the second law of thermodynamics to ensure that the models predicted actual rather than ideal behaviour.

The energy recovered by the pump-turbine was shown graphically on the Mollier diagram (Figure 3.4) and will be calculated using the method described in Section 3.5.

The system is also composed of pipes, pipe fittings and valves that are subject to frictional losses (described in Section 3.7). This will assist in the generation of a system curve (Figure 3.6) in combination with the mechanical energy balance (Section 3.6).

4 DISCUSSION

The system design is based on data received from the AngloGold Ashanti Mponeng mine. The data included water flow and discharge pressure of two pressure reducing stations, located on 99 and 104 Levels. A description of Mponeng mine will be provided, followed by a summary of the design criteria employed. The design methodology will, thereafter, be described with suitable justifications. The feasibility of the proposed energy recovery system will also be illustrated in this chapter.

4.1 AngloGold Ashanti Mponeng mine (du Toit, 2009)

The datum level on surface is taken at 1.5 m above the main shaft collar. The shaft collar is approximately 1 550 m above sea level. The elevations of the mine levels (metres below datum, m bd) can be summarised in the table below:

Table 4.1 Mining level depths

Mining level	Depth
45 Level	1 360 m bd
70 Level	2 134 m bd
84 Level	2 560 m bd
89 Level	2 712 m bd
94 Level	2 862 m bd
99 Level	3 012 m bd
104 Level	3 162 m bd
109 Level	3 312 m bd
110 Level	3 342 m bd
120 Level	3 647 m bd

The water reticulation system at Mponeng is illustrated in Figure 4.1.

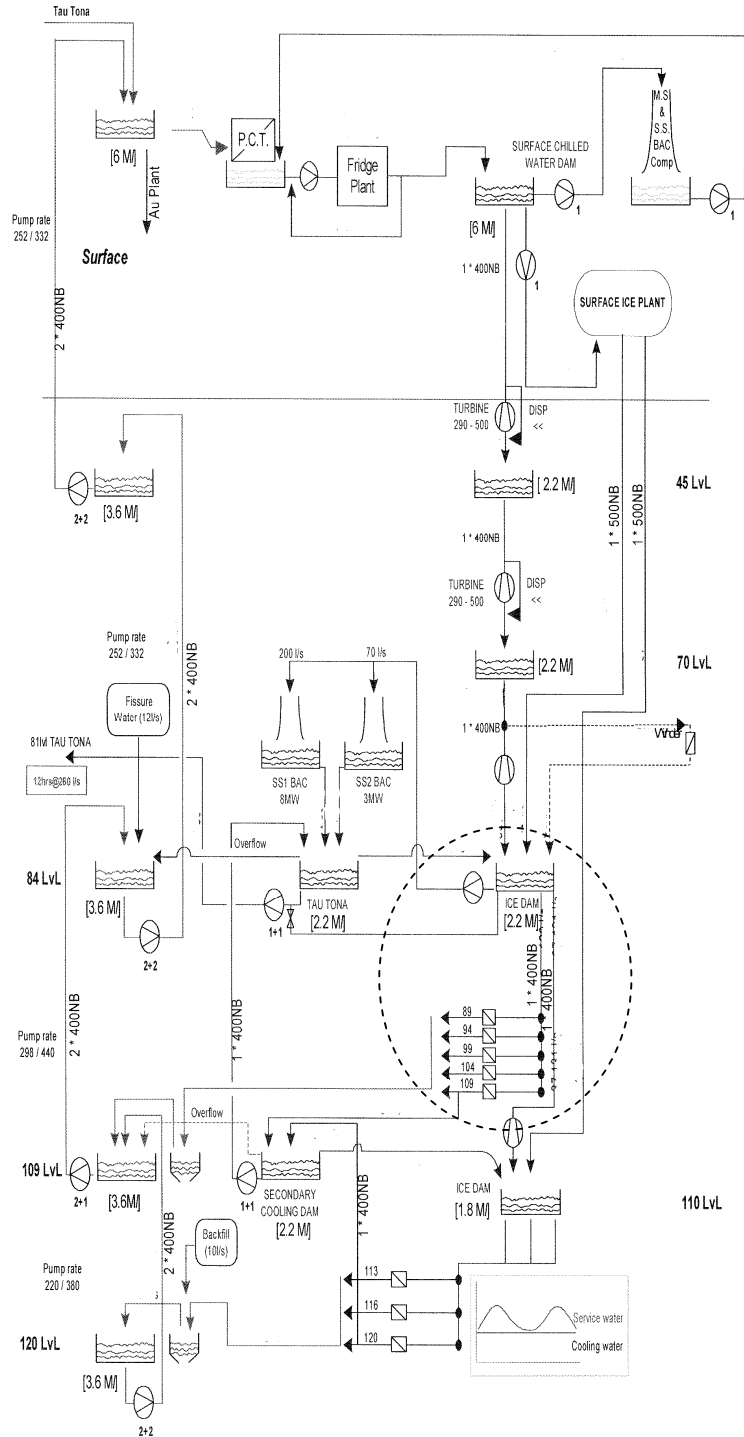


Figure 4.1 Mponeng water reticulation system (du Toit, 2009)

Refrigeration machines located on surface cool water and discharges the water into a holding dam on surface. Part of the water is pumped from this dam to a bulk air cooler located on surface to cool the downcast air. A small quantity of water is pumped to an ice-machine also located on surface. The balance of water from the holding dam is fed by gravity to dams located below surface on 45, 70 and 84 Levels. Pelton turbines have been installed to recover the potential energy and minimise the water temperature increase due to the Joule-Thomson effect.

Ice produced on surface is fed to the ice-dam located on 84 Level. Part of the water leaving this dam is pumped to two air coolers located on 84 Level and fed by gravity to open-circuit air coolers located on 89, 94, 99, 104 and 109 Levels. Pressure-reducing valves (PRVs) are installed on these levels to reduce the water pressure before entering the coolers. Part of the water, downstream of the PRVs, cascades into a secondary cooling dam located on 109 Level. Water for mining activities will originate from this dam.

Some of the ice from the surface plant is fed to a second ice-dam that is located on 110 Level. The water entering this dam will originate from the 109 Level dam and 84 Level ice-dam (a pelton turbine is installed on the feed from 84 Level dam). The water leaving the 110 Level dam is fed by gravity to 113, 116 and 120 Levels to closed-circuit air coolers. PRVs are installed to reduce the pressure before entering the coolers.

The warm water downstream of the closed-circuit air coolers (113, 116 and 120 Levels) will cascade into a warm water dam located on 120 Level. The water is pumped from this dam to a warm water dam located on 109 Level.

The water downstream of the open-circuit air coolers (89, 94, 99, 104 and 109 Levels) will cascade into the 109 Level warm water dam. Water will be pumped from this dam to the warm water dam located on 84 Level. It should be noted that fissure water and water from mining activities will report to 84, 109 and 120 Level warm water dams. Water from 84 Level dam will be pumped to a warm water dam located on 45 Level.

The water will be pumped back to a surface dam from the 45 Level warm water dam. The warm water from this dam is cooled in a pre-cooling tower on surface before being pumped to the surface refrigeration machines.

4.2 Design criteria

The mine's Supervisory Control and Data Acquisition (SCADA) system records specific data at the pressure-reducing valve (PRV) stations. The data for PRV stations located on 99 Level and 104 Level were provided by the mine for the period 19 to 26 March 2010. The data included water flow through the PRV station and discharge pressure. The pressure upstream of the PRV station on 99 Level was 42 bar while the pressure upstream of the PRV station on 104 Level was 52 bar (Robbins, 2010). The water circuit under consideration is shown in Figure 4.2.

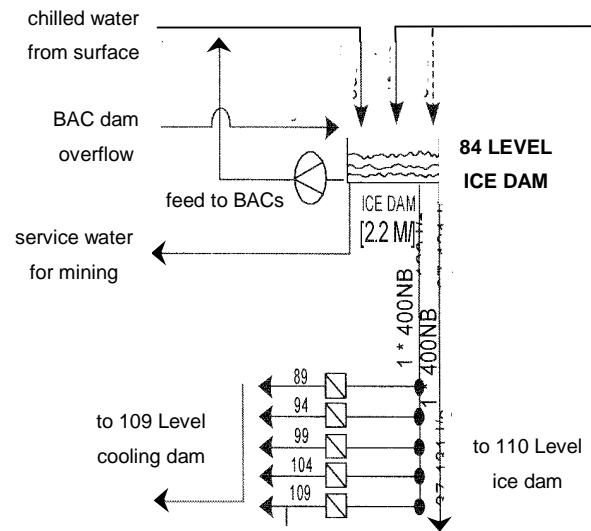


Figure 4.2 84 Level Ice dam (after du Toit, 2009)

4.2.1 Water flow and pressure data

The raw data for the pressure reducing stations were compared graphically. This included plots of water flow and pressure as a function of time for the 99 Level station and 104 Level station (APPENDIX A). It should be noted that there were significant variations in both water flow and pressure for the 99 Level station measurements. The flow varied between 0 and 36 l/s while the discharge pressure ranged from 0 to 17 bar.

However, the water flow and discharge pressure recorded at the 104 Level PRV station was relatively stable. The water flow and pressure remained fairly constant over certain time periods, with discrete changes in these parameters being observed. The flow varied between 9 and 140 l/s while the pressure ranged from 6 to 21 bar.

Due to the erratic flow and pressure data observed at the 99 Level valve station, the data was not used in further calculations. It would be possible to model both valves to recover energy, however the erratic data points introduced difficulty in identifying a suitable design flow and pressure. Therefore, only the 104 Level valve data was used in further calculations.

4.2.2 Regression of water flow and pressure data

The water flow through the 104 Level station, was notably higher during the week compared to the weekend. On the Saturday, the water flow remained at an average value of 40.3 l/s and the average discharge pressure of 14 bar. The average flow reduced to 15.3 l/s on Sunday at approximately 07:25; with a concurrent increase in pressure to 15.3 bar.

A subsequent increase in flow to 111.8 l/s and decrease in discharge pressure to 10.9 bar, was observed at 19:25 on Monday evening. From Tuesday to Friday, the average peak flow remained between 107.0 and 120.5 l/s; with an average pressure ranging between 9.8 and 10.9 bar. For about two hours each weekday, the flow reduced to a value between 11.1 and 24.9 l/s; while the pressure increased to 13.3 bar. The average water flow and average discharge pressure through the PRV station is presented in Table 4.2 and presented graphically in Figure 4.3 and Figure 4.4 respectively.

Table 4.2 Average water flow and pressure for 104 Level PRV station

Date	Day	Time		Average Water flow [l/s]	Average Discharge pressure [bar]
		Start	Finish		
19-Mar-10	Fri	0:00	18:00	99.5	10.6
		18:00	0:00	40.3	14.0
20-Mar-10	Sat	0:00	0:00	40.3	14.0
21-Mar-10	Sun	0:00	7:25	40.3	14.0
		7:25	0:00	15.3	15.3
22-Mar-10	Mon	0:00	19:25	15.3	15.3
		19:25	0:00	111.8	10.9
23-Mar-10	Tues	0:00	18:45	111.8	10.9
		18:45	21:50	13.1	13.2
		21:50	0:00	107.0	10.8
24-Mar-10	Wed	0:00	19:10	107.0	10.8
		19:10	21:20	11.1	13.3
		21:20	0:00	108.7	10.1
25-Mar-10	Thurs	0:00	18:55	108.7	10.1
		18:55	21:20	24.9	13.6
		21:20	0:00	120.5	9.8
26-Mar-10	Fri	0:00	15:00	120.5	9.8

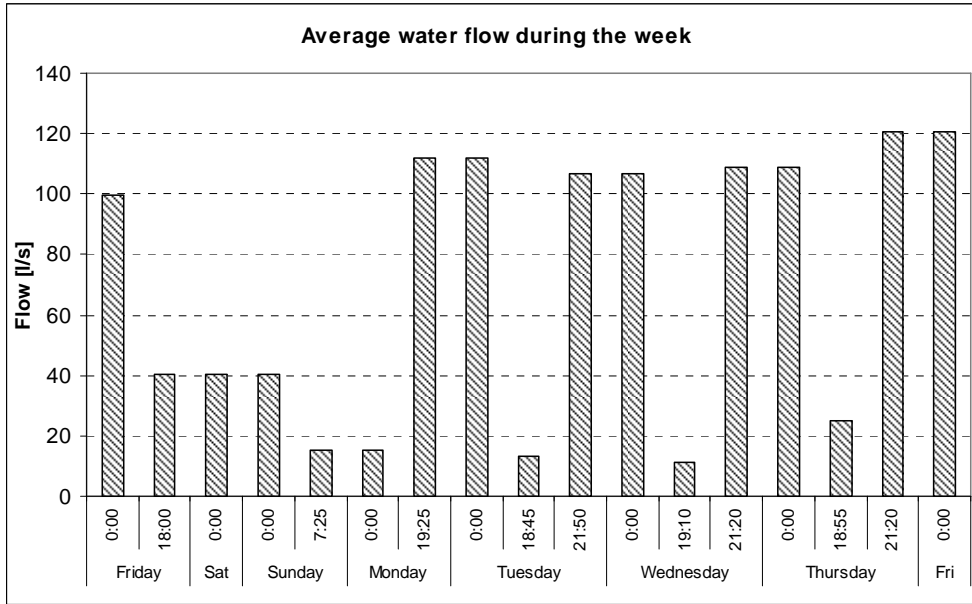


Figure 4.3 Average water flow through 104 Level PRV station (19 to 26 March 2010)

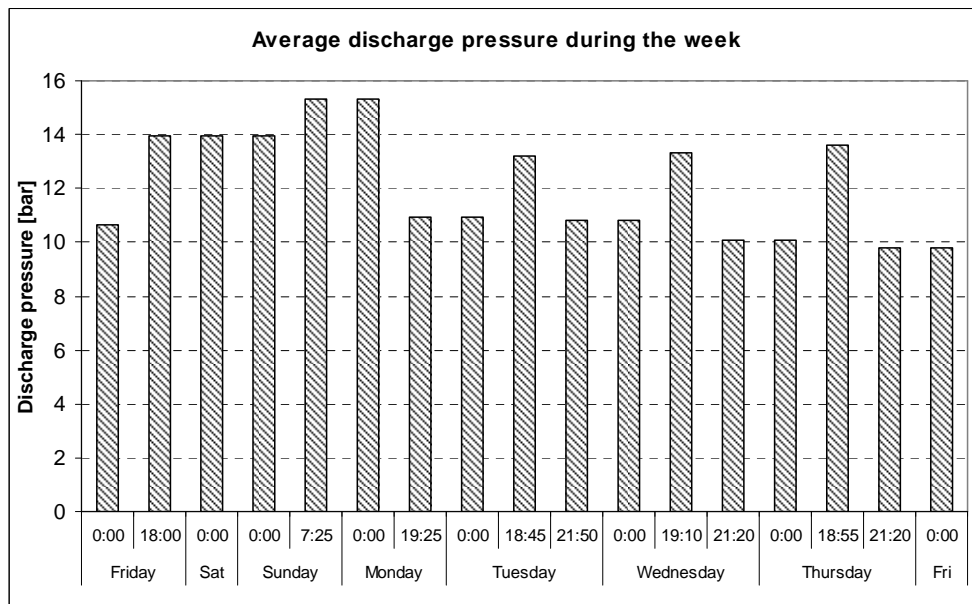


Figure 4.4 Average discharge pressure downstream of 104 Level PRV station (19 to 26 March 2010)

It should be noted that Monday, 22 March 2010 was a public holiday (Human Rights day) and lower water flows were observed. The water flow remained at 15.3 l/s until 19:25. This can be attributed to reduced mining activity on the

holiday, which required a lower consumption of service water and less air cooling (a reduced quantity of water was fed to the air cooler located downstream of the PRV station). This flow trend was considered representative of a Sunday.

During the week, the average peak water flows observed, vary between 99.5 and 120.5 l/s. For a period of two hours per day, the flow reduced to an average of 15.6 l/s. This trend was observed from Monday through Friday. The reduced water consumption (for the two hours) can be attributed to a change in working shifts (afternoon shift to night shift).

A typical week was then extracted from the data, based on the above observations. A weekday was characterised by an average water flow rate of 109.4 l/s for 22 hours and an average water flow of 15.6 l/s for the remaining two hours. On a Saturday the water flow would remain at an average of 40.3 l/s for 24 hours. At 07:30 on a Sunday, the water flow would drop to 15.6 l/s, and increase to a peak flow of 109.4 l/s at 19:30. The typical week is shown graphically in Figure 4.5.

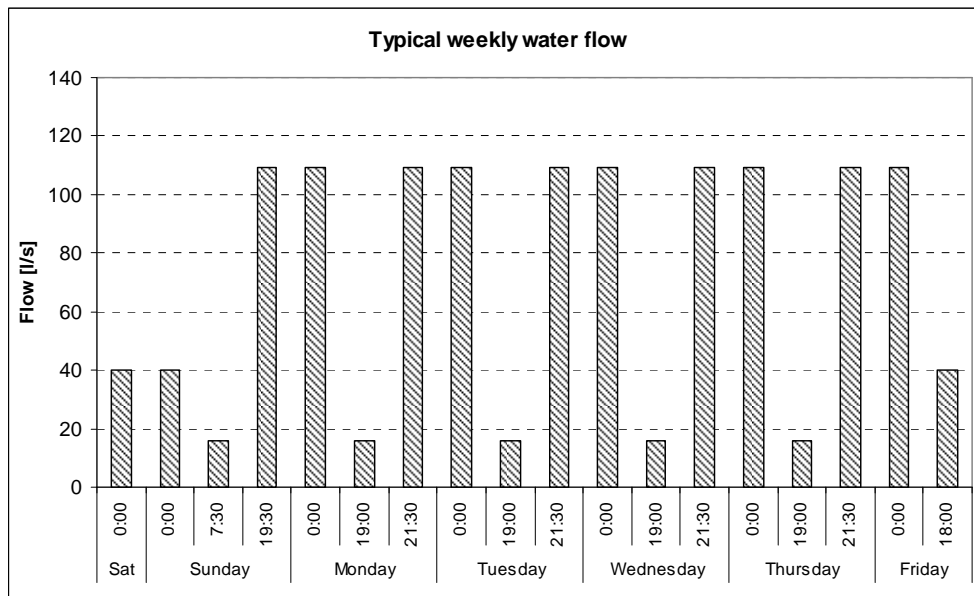


Figure 4.5 Average water flow through 104 Level PRV station (typical)⁸

⁸ The justification for the average water flows is presented in APPENDIX B.

The average water flow of 109.4 l/s was selected as the design value. The peak water flows (99.5 to 120.5 l/s) were observed during 102 hours of the week (61 %) and a significant amount of energy can be recovered during these periods.

The discharge pressures were influenced by the water flows. When the water flow increased, the pressure reduced; while a decrease in water flow resulted in an increase in pressure. This variation is shown in Figure 4.6.

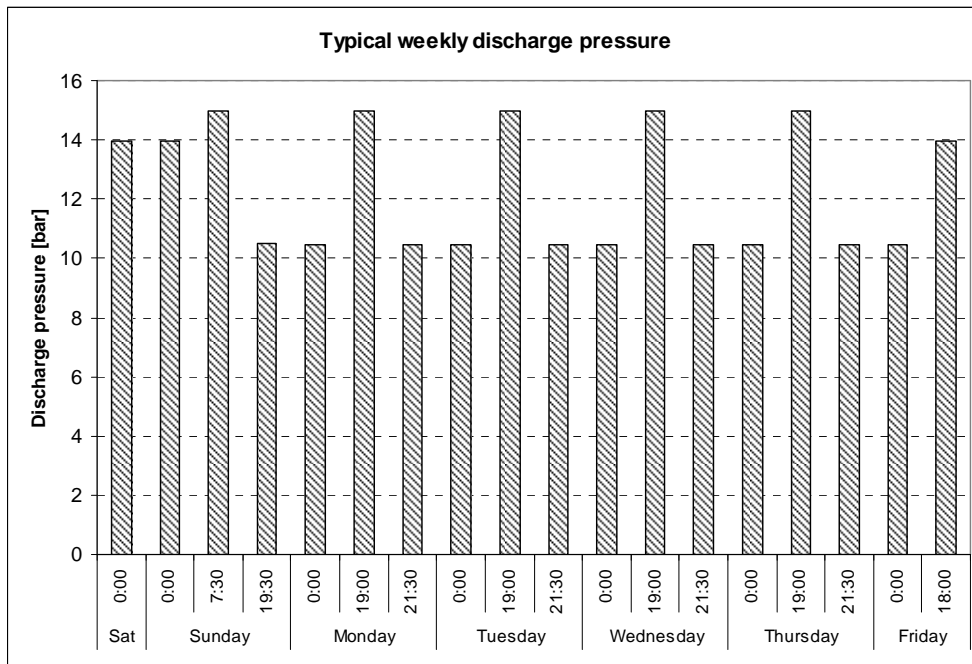


Figure 4.6 Average discharge pressure downstream of 104 Level PRV station (typical)

An average discharge pressure of 10.5 bar was selected since this corresponds to the average water flow of 109.4 l/s.

4.2.3 Water temperature

Chilled water and ice is fed to the 84 Level dam from surface. There will be energy losses in the ice conveying system between surface and the underground dams, which will include heat flow through pipe walls and dissipation of potential energy. Also, energy losses are expected in the water conveying system between surface and the 84 Level dam due to heat flow through the pipe walls and the dams as well as turbine inefficiencies and dissipation of potential energy. The net effect is an increase in the temperature of the water between surface and the 84 Level dam. The temperature in the ice dams and the level to which this is controlled is another important assumption.

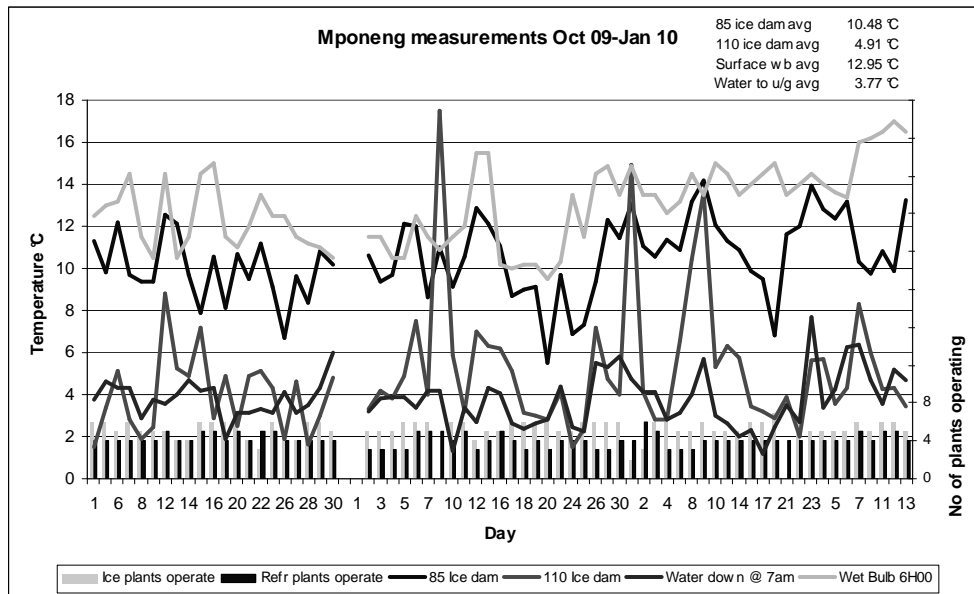


Figure 4.7 Air and water temperatures measured at Mponeng (du Toit, 2010)

Data from the mine (Figure 4.7) indicated that in 2009, the 84 Level ice dam was operating at around 10°C, however it was assumed that at the ice dam would operate at the more efficient value of 6.0°C.

The difference in elevation between 84 and 104 Levels is approximately 610 m. The friction in the pipe connecting these levels (from the dam to the PRV station) will increase the temperature of the water. It is assumed that the water temperature will increase by 0.1 °C to give an inlet water temperature of 10.1 °C.

4.2.4 Heat capacity

The heat capacity of water at constant pressure was obtained from the literature (Perry and Green, 1997) and is presented in Table 4.3. An average value of 4.194 kJ/kg.K was assumed.

Table 4.3 Variation of heat capacity with temperature

Temperature T [°C]	Heat capacity C_p [kJ/kg.K]
4.0	4.205
5.0	4.202
6.0	4.200
7.0	4.198
8.0	4.196
9.0	4.194
10.0	4.192
11.0	4.191
12.0	4.189
13.0	4.188
14.0	4.187
15.0	4.186

4.2.5 Specific volume and density

Values of specific volume V , were obtained from saturated steam tables in the literature (Smith et.al, 2001). The values are presented in Table 4.4 and an average value of $0.001 \text{ m}^3/\text{kg}$ has been assumed.

The density ρ , is the reciprocal of specific volume. Therefore, the density was assumed at a constant value of $1\ 000 \text{ kg/m}^3$.

Table 4.4 Variation of specific volume and density with temperature

Temperature T [°C]	Specific volume V [$\text{m}^3/\text{kg} \times 10^{-4}$]	Density ρ [kg/m^3]
4.0	10.0	1000
5.0	10.0	1000
6.0	10.0	1000
7.0	10.0	1000
8.0	10.0	1000
9.0	10.0	1000
10.0	10.0	1000
11.0	10.0	1000
12.0	10.0	1000
13.0	11.0	909
14.0	11.0	909
15.0	11.0	909

4.2.6 Viscosity

The values for the viscosity μ_F , were obtained from the literature (Perry and Green, 1997) and listed in Table 4.5. An average value of 1.34×10^{-6} Pa.s was assumed for the viscosity.

Table 4.5 Variation of viscosity with temperature

Temperature T [°C]	Viscosity μ_F [Pa.s x 10^{-6}]
4.0	1.57
5.0	1.52
6.0	1.47
7.0	1.43
8.0	1.39
9.0	1.35
10.0	1.31
11.0	1.27
12.0	1.24
13.0	1.20
14.0	1.17
15.0	1.14

4.2.7 Joule-Thomson coefficient

The Joule-Thomson coefficient μ_H , is the slope of a temperature-pressure plot at constant enthalpy. The coefficient can be expressed mathematically as

$$\mu_H = (\beta T - 1) V / C_P \quad (3.58)$$

The values for the volume expansivity β were obtained from the literature (Perry and Green, 1997) and listed in Table 4.6. An average value of -0.239 K per MPa was assumed for the Joule-Thomson coefficient at constant enthalpy. An average value of 0.006 K per MPa was assumed for the Joule-Thomson coefficient at constant entropy.

Table 4.6 Variation of volume expansivity and Joule-Thomson coefficient with temperature

Temperature T [°C]	Volume expansivity β [K ⁻¹ x 10 ⁴]	Joule-Thomson coefficient (constant enthalpy) μ_H [K / MPa]	Joule-Thomson coefficient (constant entropy) μ_S [K / MPa x 10 ⁻⁴]
4.0	0.003	-0.238	0.02
5.0	0.160	-0.237	1.06
6.0	0.312	-0.236	2.07
7.0	0.460	-0.235	3.07
8.0	0.604	-0.234	4.05
9.0	0.744	-0.233	5.01
10.0	0.880	-0.233	5.94
11.0	1.012	-0.232	6.86
12.0	1.141	-0.231	7.77
13.0	1.267	-0.253	9.52
14.0	1.389	-0.252	10.5
15.0	1.509	-0.251	11.4

4.2.8 Summary of design criteria

Water inlet pressure on 104 Level	52 bar
Water flow (average)	109.4 l/s
Water discharge pressure (average)	10.5 bar
Water inlet temperature	6.1 °C
Heat capacity of water	4.194 kJ/kg.K
Specific volume of water	0.001 m ³ /kg
Density of water	1 000 kg/m ³
Viscosity of water	1.34 x10 ⁻⁶ Pa.s
Joule-Thomson coefficient (μ_H)	-0.239 K per MPa
Joule-Thomson coefficient (μ_S)	0.006 K per MPa

4.3 System modelling

The pump-turbine system is shown in the process flow diagram (Figure 4.17, drawing FN-PT-10-001⁹). This gives a summary of the operating conditions of the pump-turbine system on 104 Level.

4.3.1 System curve

The system was modelled using the design criteria outlined above in conjunction with the mechanical energy balance. This is given by the formula,

$$P_1 / \rho_1 + \frac{1}{2} u_1^2 + g z_1 = P_2 / \rho_2 + \frac{1}{2} u_2^2 + g z_2 + W_s + g h_f \quad (3.71)$$

Point 1 refers to the entering water conditions, while point 2 refers to the pump outlet conditions.

The inlet water pressure P_1 was given as 52 bar, while the outlet pressure P_2 was calculated at 10.5 bar. The density of the water was assumed to be constant¹⁰ at the inlet and outlet; at a value of 1 000 kg/m³.

⁹ This refers to engineering drawings. "FN" is the author's initials, "PT" refers to pump-turbine, "10" is the year in which the drawing was compiled (2010) and "001" is a sequential number.

¹⁰ The fluid was assumed to be incompressible since no significant temperature difference was observed across the turbine.

The design water flow was 109.4 l/s. A nominal pipe diameter of 250 mm was selected for the inlet and outlet of the pump. This resulted in an average velocity of 2.2 m/s. Therefore the velocity terms on the left- and right-hand side of the energy balance were equal and cancelled each other out.

The elevation difference $\Delta z (z_1 - z_2)$, constituted the height between the pump suction and discharge centre-lines. This static height was 0.45 m.

The frictional losses h_f resulted from the pipes, pipe fittings and valves that were selected (Figure 4.24 and Figure 4.25). The total friction loss was calculated by summing the loss from each component (Section 3.7) and including it in the energy balance. The friction loss determined at a water flow of 109.4 l/s was 25.2 kPa which included a design factor of 10 %.

The mechanical energy balance was then reduced to

$$(P_1 - P_2) / \rho + g (z_1 - z_2) - g h_f = W_s \quad (4.1)$$

The shaft work W_s was the available pressure that could be recovered. The available pressure for energy recovery at the design flow of 109.4 l/s was 4 127 kPa. Since the frictional losses from pipe roughness, valves and fittings increase at higher flow rates, the water flow was varied and a system curve was generated (Figure 4.8).

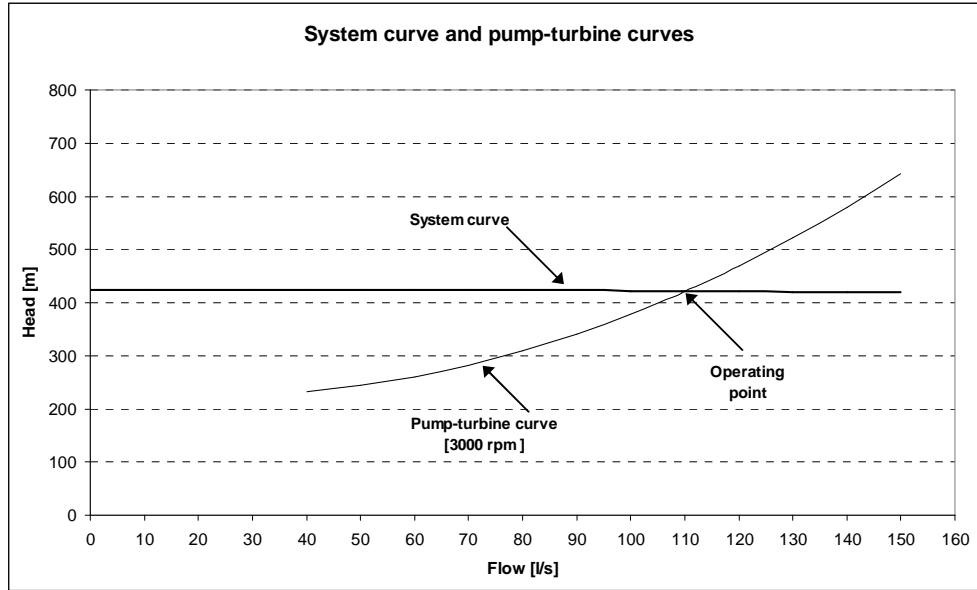


Figure 4.8 System curve and pump-turbine curve

The calculation of a point on the system curve is presented in APPENDIX D.

4.3.2 Pump-turbine model

A pump-turbine was selected at the design flow rate of 109.4 l/s. The inlet pressure to the system was 52 bar and the discharge pressure was 10.5 bar. Friction losses arising from piping, valves and fitting resulted in 4 127 kPa being available for energy recovery. The pump-turbine curve for this duty was provided by Sulzer. A multi-stage pump having four stages was proposed.

The pump-turbine system was modelled using a design proposed by van Antwerpen and Greyvenstein (2005). The design included the regression of turbine curves for pumps operating in reverse. Head/flow/speed and efficiency/flow/head relations were derived from first principles. The relation for the pump head was

$$h = s (a_1 q^2 - a_2 q N + a_3 N^2) \quad (4.2)$$

where,

- h – pump head
- q – water flow
- N – pump speed
- a_i – regression constants
- s – number of stages

The pump efficiency was described by a fourth-order polynomial

$$\eta = y_1 \phi^4 + y_2 \phi^3 + y_3 \phi^2 + y_4 \phi + y_5 \quad (4.3)$$

where,

- η – pump efficiency
- ϕ – Ratio of water flow to pump speed (q / N)
- y_i – regression constants

The pump-turbine curves for the head and efficiency were regressed using these models. A graph was plotted and the data was fitted to a second-order polynomial (Figure 4.9) for a single stage ($s = 1$). The coefficients of the polynomial were used to determine the regression constants a_1 to a_3 . The pump manufacturer specified a speed of 3 000 rpm.

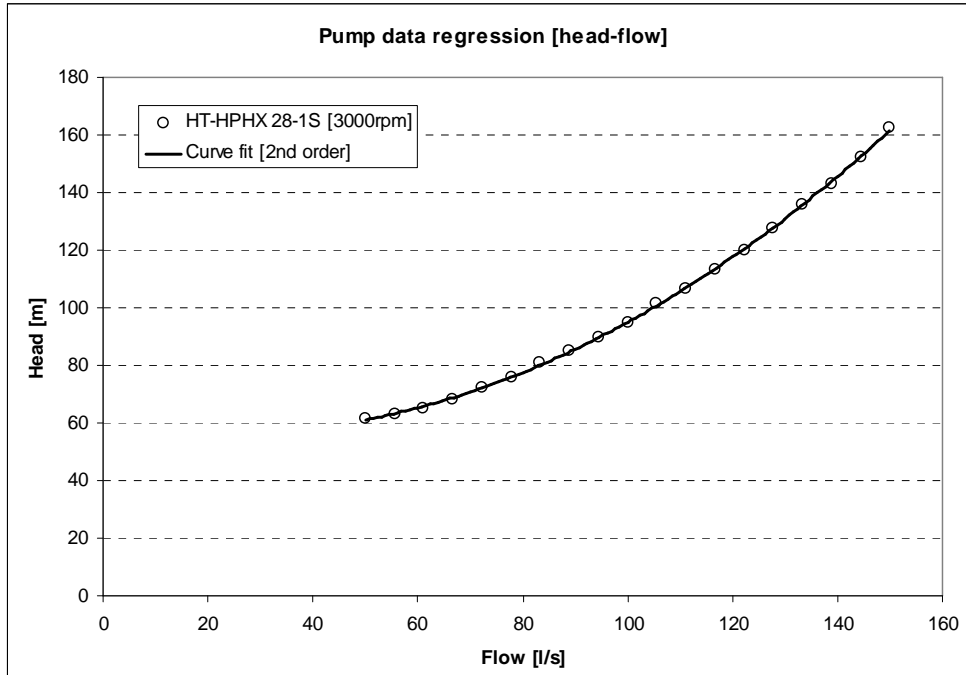


Figure 4.9 Pump-turbine head curve regression

From Figure 4.9, the pump-turbine head curve can be mathematically expressed as

$$H = s (6.50 \times 10^{-3} q^2 - 1.01 \times 10^{-4} q N + 6.67 \times 10^{-6} N^2)$$

The correlation coefficient (R^2) of 0.9998 indicated an acceptable data fit to the second-order polynomial.

A similar procedure was followed for the pump-turbine efficiency. The data was fitted to a fourth-order polynomial (Figure 4.10).

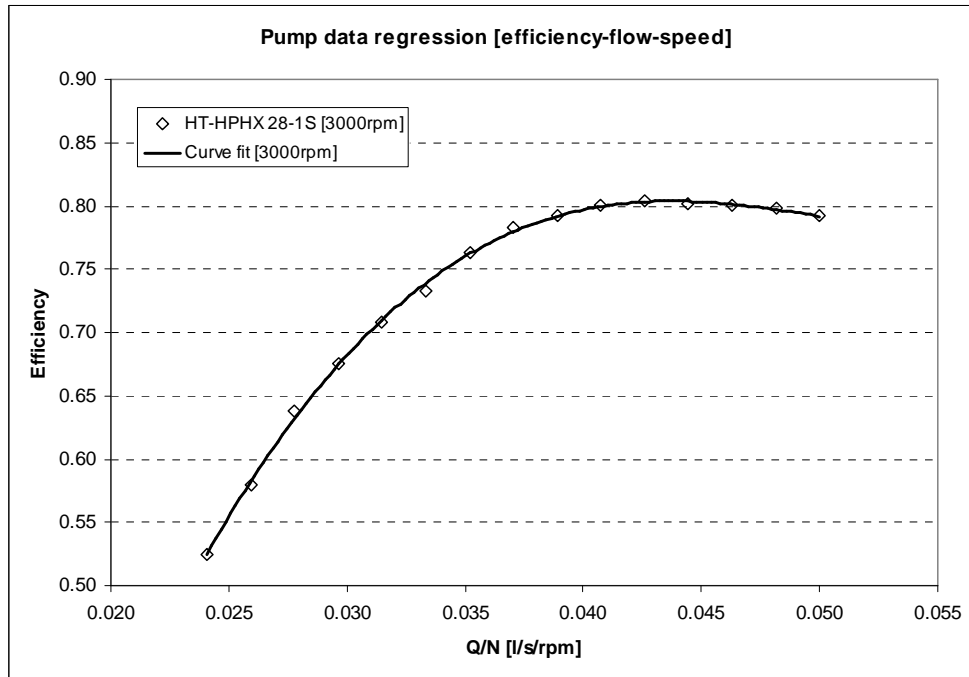


Figure 4.10 Pump-turbine efficiency curve regression

From Figure 4.10, the pump-turbine efficiency curve was mathematically expressed as

$$\eta = 1.55 \times 10^5 \phi^4 - 9.21 \times 10^3 \phi^3 - 1.00 \times 10^3 \phi^2 + 88.5 \phi - 0.949$$

The correlation coefficient (R^2) for the efficiency curve was 0.9991.

4.3.3 System alternatives: variable and constant speed operation

Van Antwerpen and Greyvenstein (2005) also proposed two modes of operation for the pump-turbine system, namely, variable speed and constant speed (Figure 4.11). The regression models derived in the previous section were used to design the variable and constant speed systems.

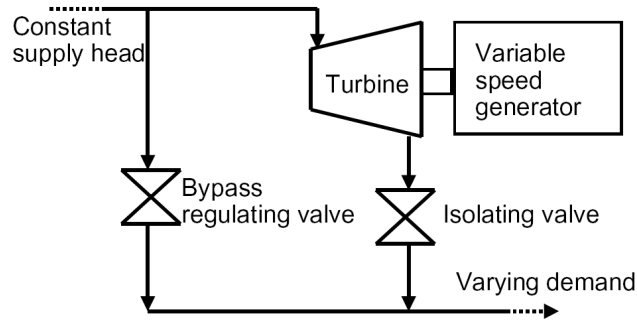


Figure 4.11 Schematic layout of a variable turbine speed pressure reducing system (van Antwerpen and Greyvenstein, 2005)

In the variable speed model, the pump-turbine can accommodate a range of flows by adjusting the shaft speed. The system curve was drawn together with the pump-turbine curve at varying speeds (Figure 4.12).

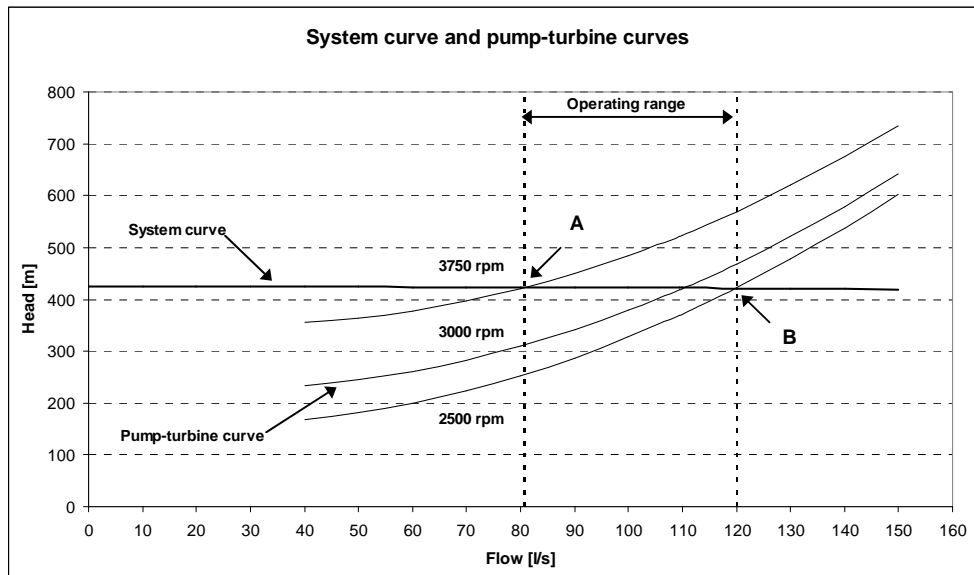


Figure 4.12 System and pump-turbine curves (variable speed)

The system head was compared to the pump-turbine head and used to determine the speed at which the pump would operate at varying water flow rates. This was achieved by solving equation (4.2) implicitly for the speed. The computations revealed that the pump-turbine shaft speed would operate in the range, 2 500 to 4 100 rpm. The corresponding operating water flow range from the system curve was 40 to 130 l/s.

The pump-turbine efficiency placed a constraint on the range of operating water flow and shaft speed. The efficiency was calculated using equation (4.3) at the determined flow rate/speed pairs (Figure 4.13). This reduced the operating flow range to between 52 and 120 l/s.

A further constraint on the water flow range was the pump-turbine runaway speed of 3 900 rpm¹¹. The upper limit for the pump-turbine shaft speed was therefore selected at 5 % below the runaway speed, namely, 3 750 rpm. Consequently, the pump-turbine would operate between 2 500 and 3 750 rpm. The corresponding water flow range was 80.7 to 120 l/s.

It should be noted that an increase in water flow through the pump-turbine results in a decrease in the operating speed. This observation is consistent with the variable speed pump-turbine model proposed by van Antwerpen and Greyvenstein (2005). When the flow is 80.7 l/s the operating speed will be 3 750 rpm (point A, Figure 4.12). At point B, the operating speed has decreased to 2 500 rpm and the flow has increased to 120 l/s.

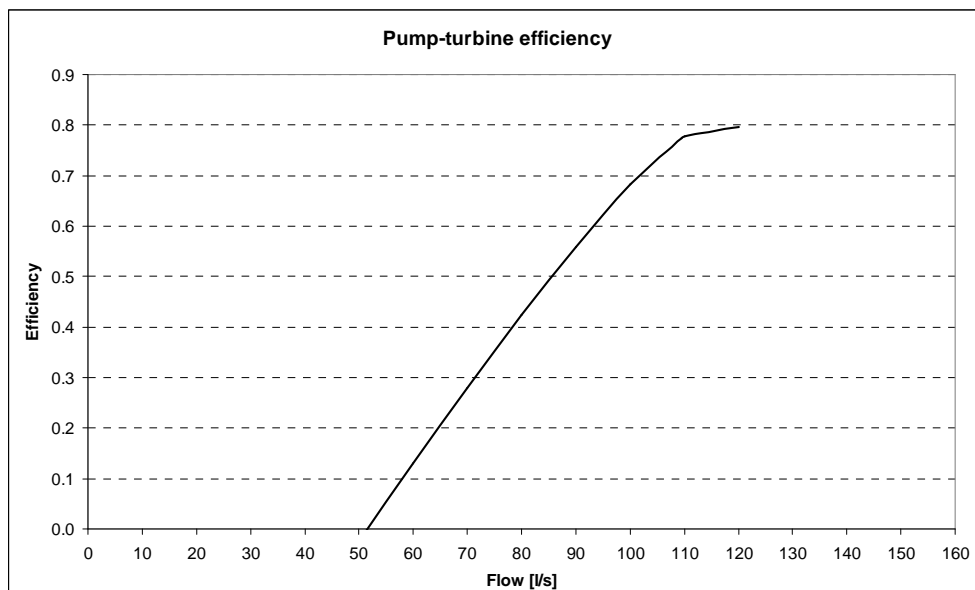


Figure 4.13 Pump-turbine efficiency curve (variable speed)

¹¹ The pump-turbine manufacturer stated that the runaway speed for this pump-turbine would be 130 % of the normal operating speed of 3 000 rpm (Tasker, 2011).

It has been shown that the (system) average water flow varies between 11.1 and 120.5 l/s. The pump-turbine operating range (80.7 to 120 l/s), could not adequately cope with the system water flow range. This necessitated a bypass line in parallel with the pump-turbine system to cater for water flows outside pump-turbine flow range. Two pressure-reducing valves would be installed in series in the bypass line to reduce the pressure from 52 bar to 10.5 bar.

This defined three modes of operation for the system (Table 4.7).

Table 4.7 Modes of operation for the pump-turbine system at variable speed

	Mode I	Mode II	Mode III
Water flow range	0 – 80.7 l/s	80.7 – 120 l/s	> 120 l/s
System configuration	Turbine off Bypass open	Turbine on Bypass closed	Turbine on Bypass open

At low water flows (Mode I), the turbine would not operate, but pressure reduction is achieved using the pressure-reducing valves. Mode II describes the turbine operation, where energy will be recovered. The bypass also caters for higher flow demands (Mode III), when the water flow increases above 120 l/s.

Depending on the mode of operation (Table 4.7), the overall efficiency will be determined by the operation of the pressure-reducing valves and the pump-turbine. When operating in Mode I, all the water will flow through the bypass and the system efficiency will be zero (no energy will be recovered). When the flow increases above 80.7 l/s, the system will then operate in Mode II and energy will be recovered by the pump-turbine. The system efficiency will be the same as the pump-turbine efficiency and determined using the regressed equation for the efficiency [equation (4.3)].

When the system operates in Mode III, energy will be recovered by the pump-turbine and energy will be dissipated across the pressure-reducing valves in the bypass. The following relation can be used to determine the system efficiency, η_{SYS}

$$\eta_{SYS} = \eta (q / q_{SYS}) \quad (4.4)$$

The maximum water flow through the pump-turbine q is 120 l/s and the corresponding efficiency η is 80 %. The total flow entering the system will be q_{SYS} .

The second alternative for the pump-turbine system is operation at constant shaft speed. In Figure 4.11, the variable speed generator becomes a constant speed generator; while the isolating valve becomes a pressure regulating valve (pp 65).

A shaft speed of 3 000 rpm (50 Hz) was selected since this corresponds to the frequency of electrical power supplied by Eskom. This mitigated the need for complex power electronics when connecting the system to the electrical power grid (Section 4.3.5).

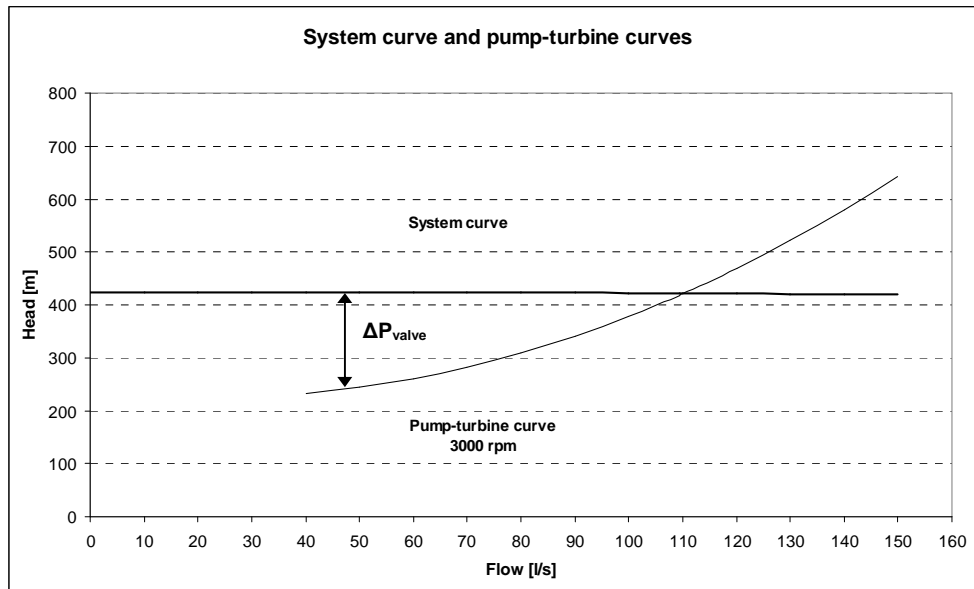


Figure 4.14 System and pump-turbine curves (constant speed)

The operating water flow range for the pump-turbine system is 40 to 110 l/s (Figure 4.15). A minimum flow of 40 l/s is required to prevent cavitation in the pump-turbine. The upper limit for the flow range (110 l/s) was determined by the intersection of the pump-turbine and system head curves. The pump-turbine can not operate above 110 l/s since the system head is lower than the required pump-turbine head.

An efficiency of 77.2 % is observed at the maximum water flow of 110 l/s. However, the system efficiency below 110 l/s, was lower due to the presence of the pressure-reducing valve in series.

A pressure-reducing valve is required in series with the pump-turbine since at water flows below the operating point; the pump-turbine does not use the full system head.

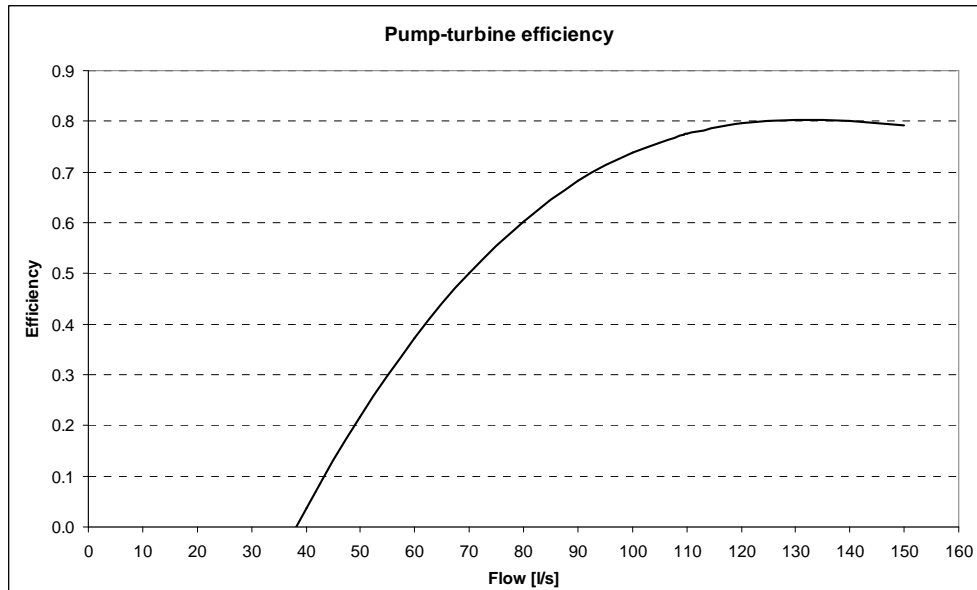


Figure 4.15 Pump-turbine efficiency curve (constant speed)

Three modes of operation for the system were also defined for the constant speed alternative (Table 4.8). A bypass line will also be installed to cater for water flows outside the pump-turbine operating range. The bypass pressure reducing valves would be the same as for the variable speed alternative.

The pump-turbine curve and system curve intersected at 110 l/s and defined the upper limit for Mode II operation. The minimum flow was 40 l/s (Figure 4.15).

Table 4.8 Modes of operation for the pump-turbine system at constant speed

	Mode I	Mode II	Mode III
Water flow range	0 – 40 l/s	40 – 110 l/s	> 110 l/s
System configuration	Turbine off Bypass open	Turbine on Bypass closed	Turbine on Bypass open

The system efficiency is influenced by the pump-turbine and pressure-reducing valves. In Mode I, no energy will be recovered and the efficiency will be zero. When in Mode II, the system efficiency will depend on the pump-turbine efficiency and energy dissipated by the valve installed in series. The relationship used was

$$\eta_{SYS} = \eta (h / h_{SYS}) \quad (4.5)$$

In the above equation, the system efficiency η_{SYS} was determined using the pump-turbine efficiency η and head h at corresponding water flows. Equation (4.3) was used when the system operated in Mode II only.

When the flow increased above 110 l/s, the bypass allowed additional water flow. The system efficiency for Mode III of operation, involved the solution of equation (4.5).

The system efficiency for variable and constant speed alternatives is shown graphically below.

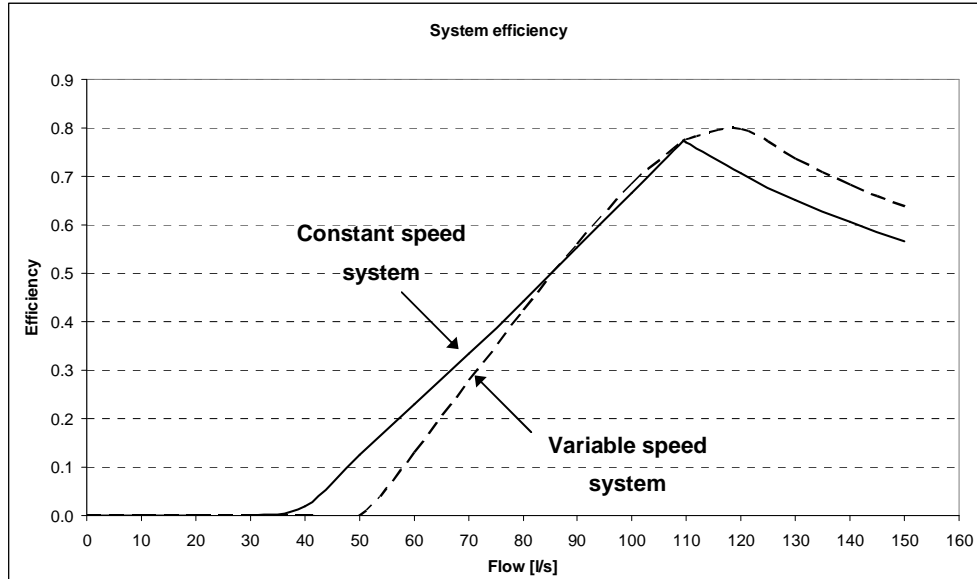


Figure 4.16 System efficiency for variable and constant speed alternatives

The constant speed system would recover energy over a wider water flow range. The variable speed system shows a steeper rise to peak efficiency with higher efficiencies observed above 120 l/s. The constant speed system had a maximum efficiency of 77.2 % at 110 l/s, while the variable speed system had a peak efficiency of 80 % at 120 l/s.

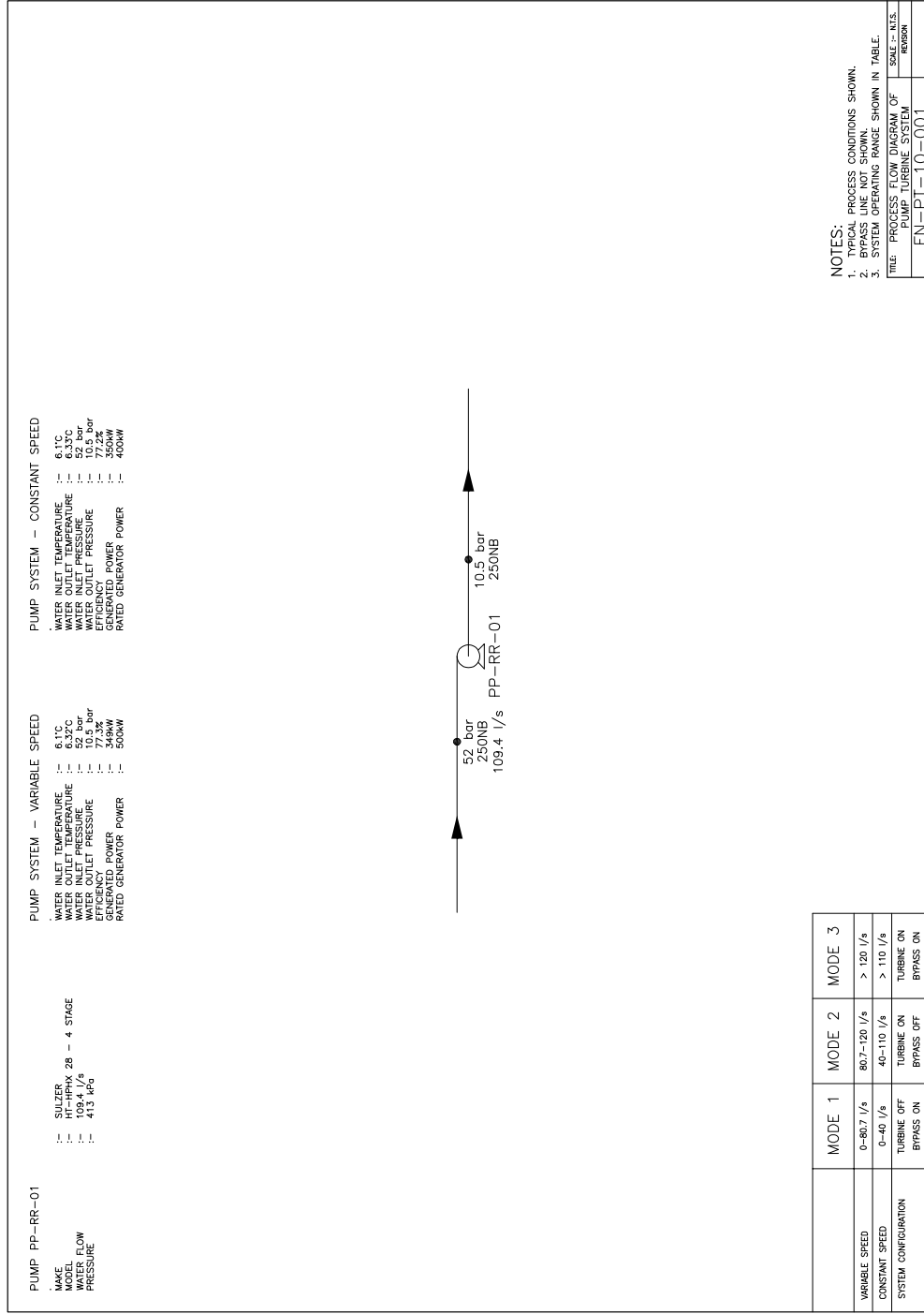


Figure 4.17 Process flow diagram (FN-PT-10-001)

4.3.4 Energy recovery and discharge water temperature

The water pressure entering the 104 Level PRV station was given as 52 bar. This pressure resulted from the gain in potential energy between the 84 Level dam and the 104 Level PRV station. The required discharge pressure was 10.5 bar. The water temperature entering the PRV station was 10.1 °C.

The simplified mechanical energy balance used for the computing the system curve was

$$W_s = (P_1 - P_2) / \rho + g (z_1 - z_2) - g h_f \quad (4.1)$$

The first two terms on the right-hand side of the above equation are constants, while the third term is a function of flow. At higher flows, the friction term increased and the net effect was reduced energy available for recovery.

The integrated form of the fundamental property relation $dH = T dS + V dP$ for an adiabatic, isentropic process was

$$(\Delta H)_s = V \Delta P \quad (3.63a)$$

and the path of the expansion process on a Mollier diagram:

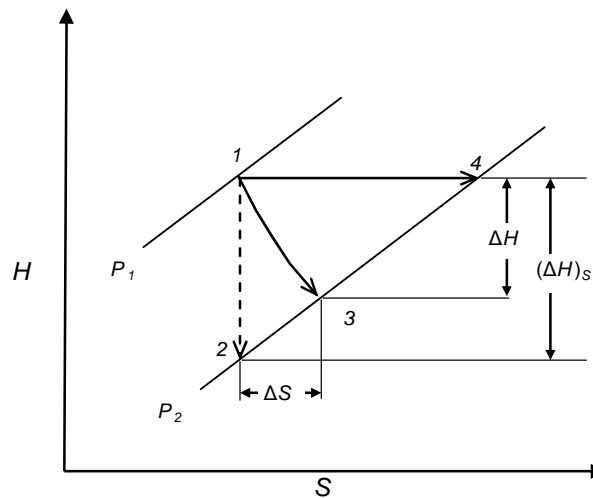


Figure 3.4 Expansion process of a fluid (after Smith, et. al., 2001)

The “equivalent pressure term” $\Delta P'$ is defined here to include the pressure, potential energy and friction terms. Since the friction term increases at higher water flow rates, $\Delta P'$ will not remain constant but decrease slightly at higher

water flows (the friction term is negative). The form was the same as defined previously as

$$(\Delta H')_S = V \Delta P' \quad (3.64)$$

and

$$(W_s)_S = (\Delta H')_S \quad (3.65)$$

The value of $\Delta P'$ used in the above equation was the value previously calculated for generating the system curve. This value was 4 127 kPa at the design water flow of 109.4 l/s. The enthalpy difference, at constant entropy, was 4.13 kJ/kg while the maximum shaft power was 452 kW at the design condition.

The pump-turbine efficiency was given by the pump manufacturer (APPENDIX C). After computing the isentropic enthalpy difference $(\Delta H')_S$, the actual enthalpy difference across the turbine $\Delta H'$ was calculated using

$$\eta = \Delta H' / (\Delta H')_S \quad (3.66a)$$

The enthalpy difference $\Delta H'$, was 3.19 kJ/kg and the hydraulic power was 349 kW at a predicted efficiency of 77.3 %.

The discharge water temperatures were then calculated using the Joule-Thomson coefficients at constant entropy μ_S and constant enthalpy μ_H . The temperature entering the turbine was 10.1 °C and is entropic process, path 1-2, resulted in the water temperature reducing to 10.08 °C. However, the temperature increased to 11.09 °C when the isenthalpic process, path 1-4, was followed.

The water discharge temperature when the pump-turbine was present resulted in a temperature greater than the isentropic process temperature and less than the isenthalpic process temperature. This temperature was 10.32 °C.

4.3.5 Electrical design

The hydraulic power produced by a turbine system will be converted to electrical power using an electrical drive. An induction machine was selected since it is easy to maintain and common in industry. This eliminated the commutator-brush system of the dc machine which is subject to mechanical breakdown.

For the variable speed alternative, the model predicted a hydraulic power generated at the peak flow of 120 l/s (Mode II operation) of 394 kW at a pump-turbine efficiency of 79.7 %. A 15 % safety margin was added to yield an expected generated power of 454 kW. Therefore, a standard WEG induction generator at a rated power of 500 kW was selected.

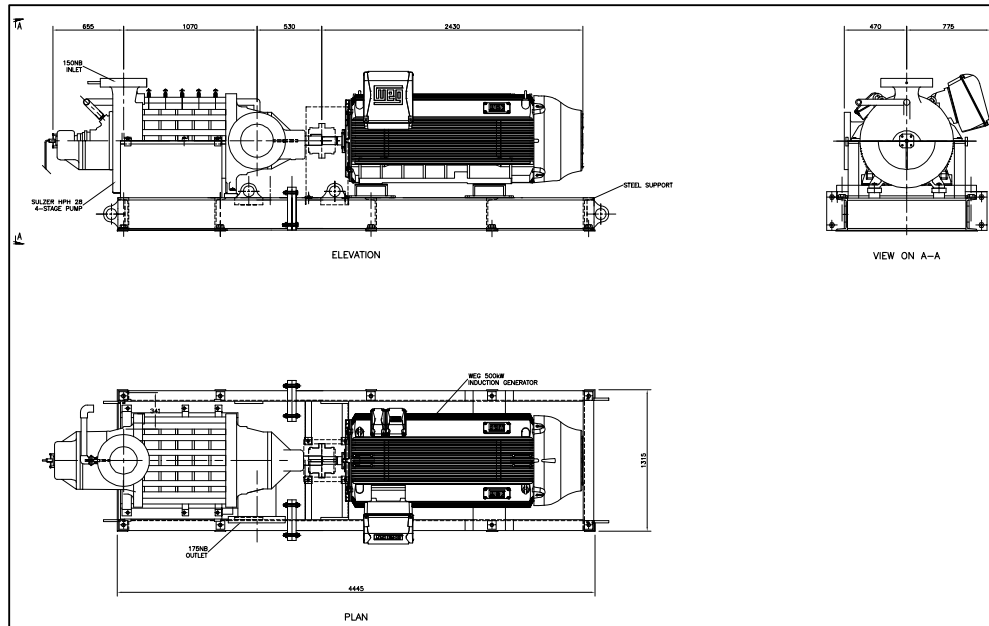


Figure 4.18 General arrangement of pump-turbine & generator – variable speed (FN-PT-10-004)

The pump-turbine at constant speed is expected to generate 353 kW of power at the peak flow of 110 l/s and efficiency of 77.3 % (maximum water flow for Mode II operation). When the safety margin of 15 % was added, the power generated will be 406 kW. Therefore, a WEG induction generator rated at 400 kW was selected.

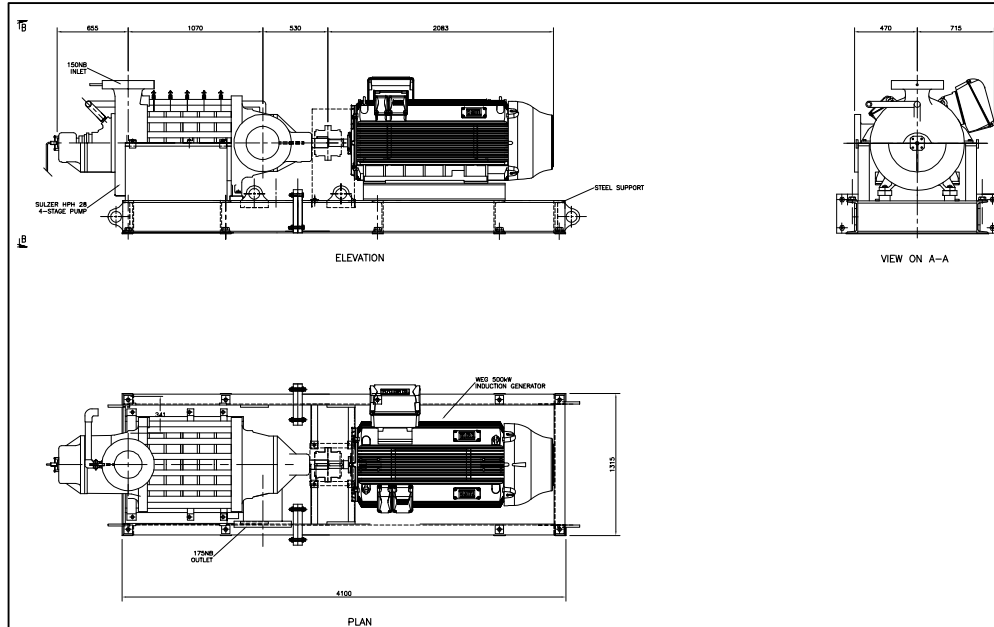


Figure 4.19 General arrangement of pump-turbine & generator – constant speed (FN-PT-10-005)

It should be noted that the electrical losses within the induction generator were assumed at 96 %¹².

The power generated by the pump-turbine will be fed back into the electrical power grid at a substation in the vicinity of the pump-turbine system. The stand-alone system was not preferred since a local source that could utilise the power was not available (i.e. a pump or fan).

The constant speed system will generate power at a shaft speed of 3 000 rpm or 50 Hz. This corresponded to the Eskom supply frequency and will therefore be connected using an electrical cable (240 mm², 4 core, low voltage, PVC insulated) and WEG 400 kW switchgear. The switchgear would be installed in a spare panel within the substation and cables would be routed from the electrical drive to the substation. A loss factor of 5 %¹³ was assumed between the pump-turbine system and the electrical system.

¹² This value was taken from the datasheet provided by the manufacturer (APPENDIX C).

¹³ Eskom loss factors for transmission (0-300 km) and distribution (≥ 500 V and < 66 kV) are 1.0096 and 1.0758 respectively. The average of these values is 1.043.

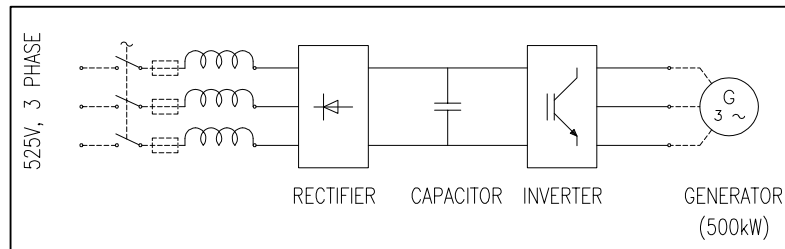


Figure 4.20 Single line diagram – variable speed (FN-PT-10-006)

The variable speed system will operate between 2 500 rpm and 3 750 rpm (42 to 63 Hz). This system will therefore require a WEG 500 kW variable frequency drive (VFD) in addition to cabling (300 mm², 4 core, low voltage, PVC insulated) and a WEG VFD panel. The variable frequency drive panel will convert the incoming variable frequencies to the supply frequency of 50 Hz.

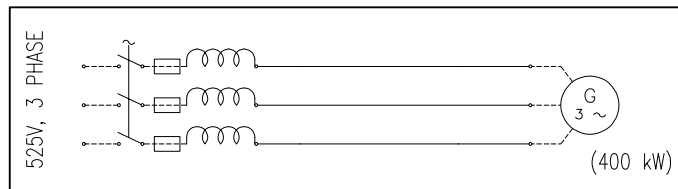


Figure 4.21 Single line diagram – constant speed (FN-PT-10-007)

The power expected to be fed back into the grid by the variable speed alternative, for the typical week is shown in Figure 4.22. At the average maximum water flow of 109.4 l/s, the electrical power generated will be 318.5 kW. Since the lower limit for the operating range in Mode II was 52 l/s, no energy is expected to be recovered at a flow of 40.3 l/s.

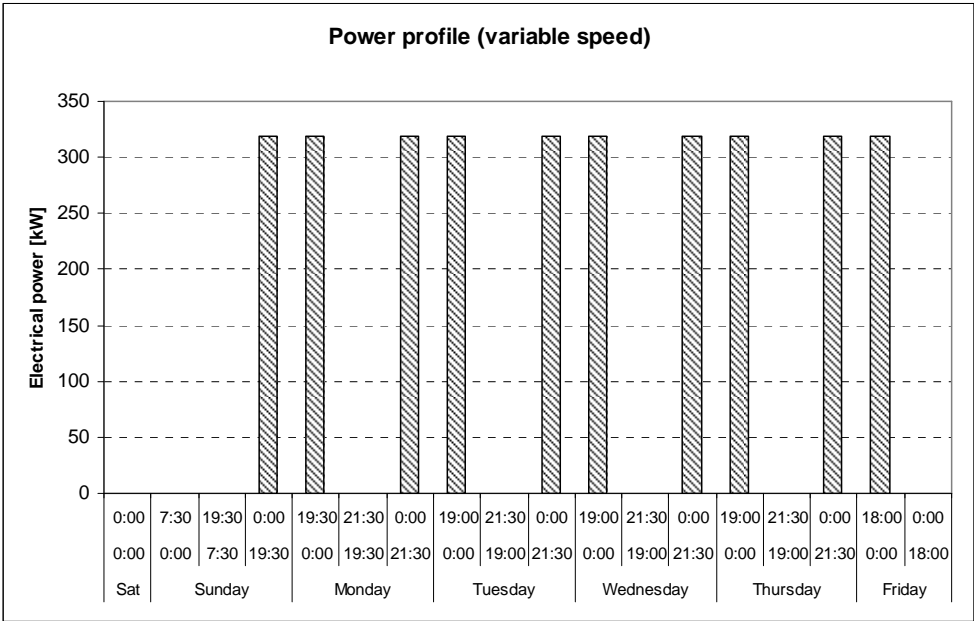


Figure 4.22 Power profile for a typical week (variable speed alternative)

For the constant speed alternative (Figure 4.23), the power generated at the water flow of 109.4 l/s will be marginally higher at 319.1 kW; and at a flow of 40.3 l/s, 5.7 kW is expected to be recovered and fed back to the power grid.

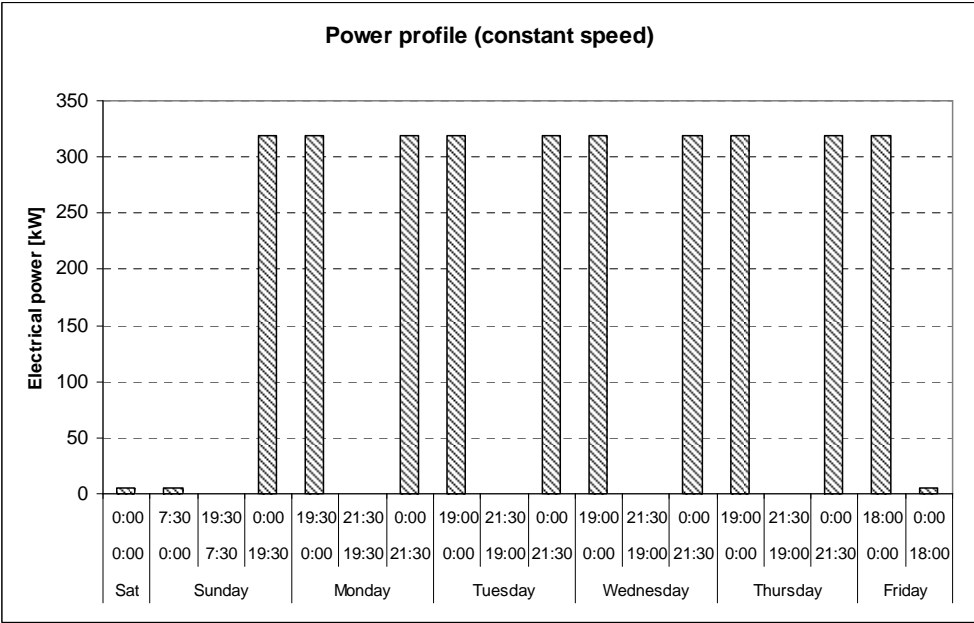
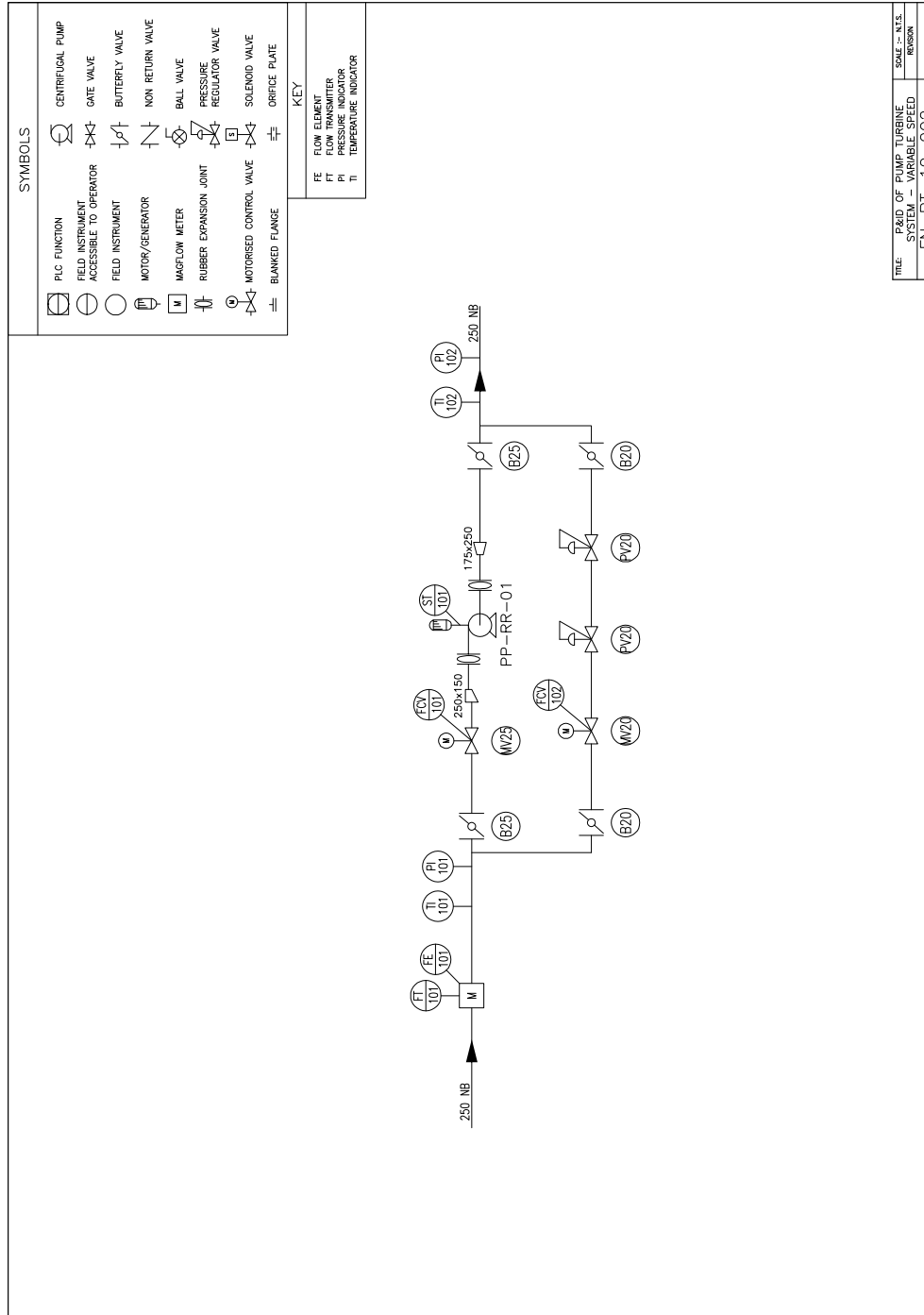


Figure 4.23 Power profile for a typical week (constant speed alternative)

4.3.6 System operation and control

The pump-turbine system consists of various components to enable generation of power and minimise the temperature increase of the water. Three modes of operation have been defined in Section 4.3.3. Mode II describes the water flow range in which the pump-turbine will operate. The bypass line with the pressure-reducing valve is necessary for Mode I operation (low flow condition) and Mode III operation (high flow condition). An Allen-Bradley programmable logic controller (PLC) will be installed to monitor the system operation and provide feedback on status of the system (normal, fault, failure). Tag numbers for valves and instrumentation are indicated in the piping and instrumentation diagram (Figure 4.24).



TITLE: P&ID OF PUMP TURBINE SYSTEM - VARIABLE SPEED
 FN-PT-10-002
 SCALE: N.T.S.
 REVISION

Figure 4.24 Piping and instrumentation diagram – variable speed (FN-PT-10-002)

A magnetic flow meter FE-101 will measure the water flow entering the system.
 Two motorised control valves (FCV-101 and FCV-102) will be installed

downstream of the flow meter. When FCV-101 is open, water will flow to the pump and when FCV-102 is open, water will flow through the bypass line. Isolating manual valves (B25 and B20) are installed for maintenance purposes. Pressure indicators (PI-101 and PI-102) are installed to measure the inlet and outlet water pressures. Temperature indicators (TI-101 and TI-102) are installed to measure the inlet and outlet water temperatures. In the event of a power failure, FCV-101 will fail closed and FCV-102 will fail open.

In variable speed mode the pump-turbine will operate at varying shaft speeds, ranging from 2 500 to 3 750 rpm (42 to 63 Hz). When the water flow is below 80.7 l/s, valve FCV-102 must open to allow the water to flow through the bypass line. FCV-102 must remain closed (Mode I operation).

When the water flow exceeds 80.7 l/s, a signal must be sent to valve FCV-102 to close and a signal must be sent to FCV-101 to open. This will allow the water to flow through the pump-turbine. No water will flow through the bypass line (Mode II operation).

When the water flow increases above 120 l/s, a signal will be sent to FCV-102 to open while FCV-101 will remain open. This will allow the additional water above 120 l/s to flow through the bypass line (Mode III operation); while the maximum water flow of 120 l/s will flow through the pump-turbine (FCV-101 will be open and the pump speed will be 2 500 rpm).

A speed transmitter ST-101 will measure the pump-turbine shaft speed. When the water flow is at 80.7 l/s, the pump-turbine will operate at a shaft speed of 3 750 rpm. When the water flow increases, the pump speed will reduce. The maximum water flow through the pump system will be 120 l/s and the corresponding pump speed will be 2 500 rpm. The speed of the pump-turbine will adjust according to the system curve (Figure 4.12). In the event of the pump-turbine shaft speed reaching the runaway speed of 3 900 rpm, valve FCV-101 must close and FCV-102 must open to allow the water to flow through the bypass line.

In constant speed alternative (Figure 4.25), the pump will operate at a fixed speed of 3 000 rpm (50 Hz). When the water flow is below 40 l/s, valve FCV-102 must open to allow the water to flow through the bypass line. FCV-101 must remain closed (Mode I operation).

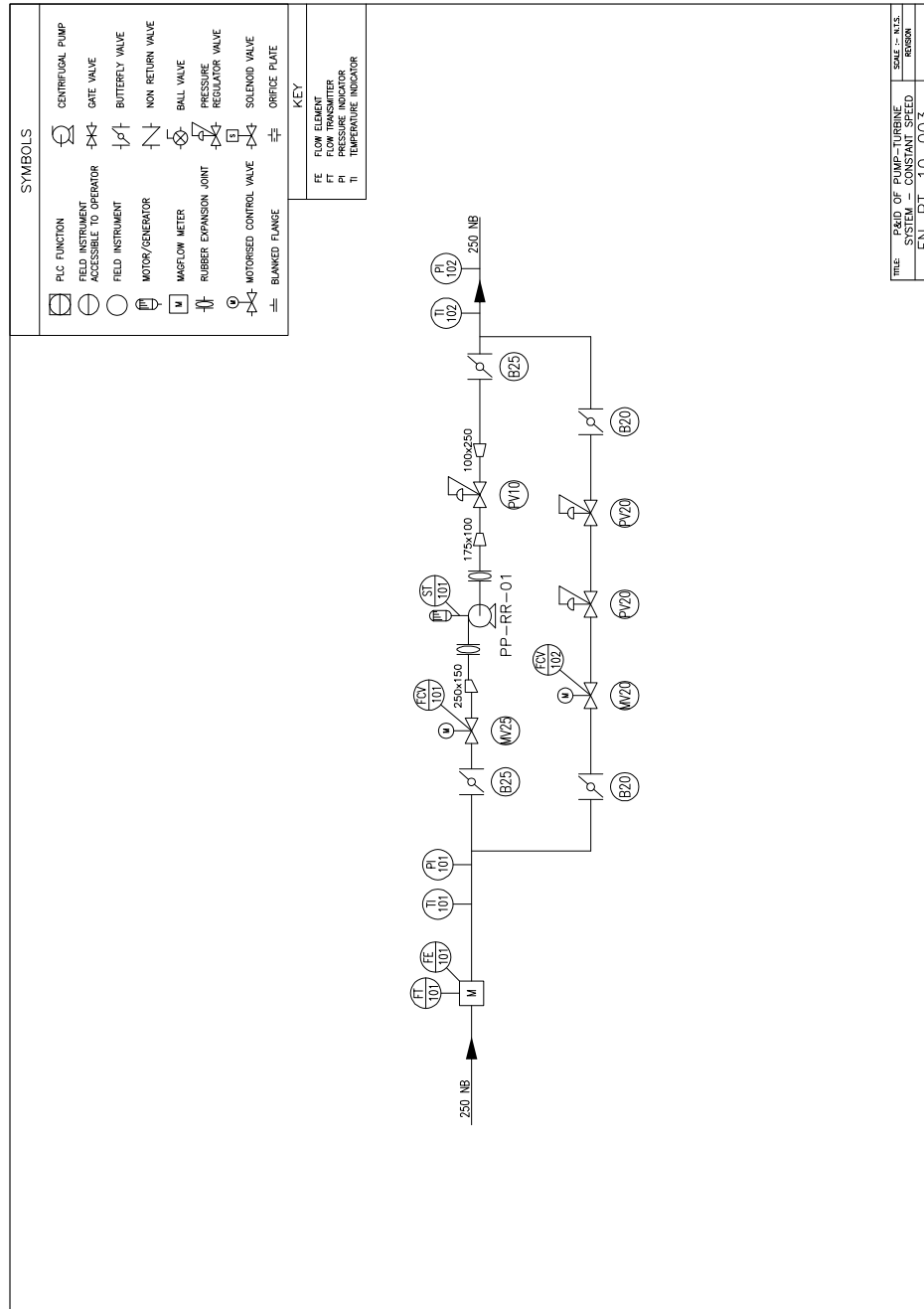


Figure 4.25 Piping and instrumentation diagram – constant speed (FN-PT-10-003)

When the water flow increases above 40 l/s a signal will be sent to FCV-102 to close, and FCV-101 to open. The pump-turbine will operate at a water flow rate between 40 and 109 l/s (Mode II operation).

When the water flow increases above 109 l/s, a signal will be sent to FCV-102 to open while FCV-101 will also remain open. This will allow the additional water above 109 l/s to flow through the bypass line (Mode III operation); while the maximum water flow of 109 l/s will flow through the pump-turbine.

The pressure-sustaining valve installed in series with the pump-turbine (100 NB) will ensure that the shaft speed remains at 3 000 rpm. This will be achieved by “absorbing” part of the system head (Figure 4.14)

4.4 Capital expenditure

The capital cost of the pump-turbine system operating at constant speed has been estimated at R 3 776 900 (base date: January 2011). The capital cost for the variable speed alternative is slightly higher at R 4 726 300.

All items must be purchased at the start of the project.

4.5 Financial analysis

The power generated was converted to electrical power income, using the power profile for the week (Figure 4.22 and Figure 4.23) and Eskom’s Megaflex rates for different periods of the day (APPENDIX E). The rates for the year 2012 are presented in the table below.

Table 4.9 Eskom Megaflex tariffs (2012)

Summer (Sept – May)	Peak	Standard	Off-peak
Price [cents per kWh]	77.3	53.1	41.6
Winter (Jun – Aug)	Peak	Standard	Off-peak
Price [cents per kWh]	248.1	82.6	55.6

It should be noted that the periods during which power was generated by the pump-turbine system did not correspond entirely within the Eskom tariff periods. It was therefore necessary to allocate the power generated during the week into the Eskom defined rate periods to obtain an acceptable estimate of the power income. As an example, Figure 4.26 illustrates the power generated by the constant speed alternative on the Friday, with the corresponding Eskom tariffs for the summer months (low demand season).

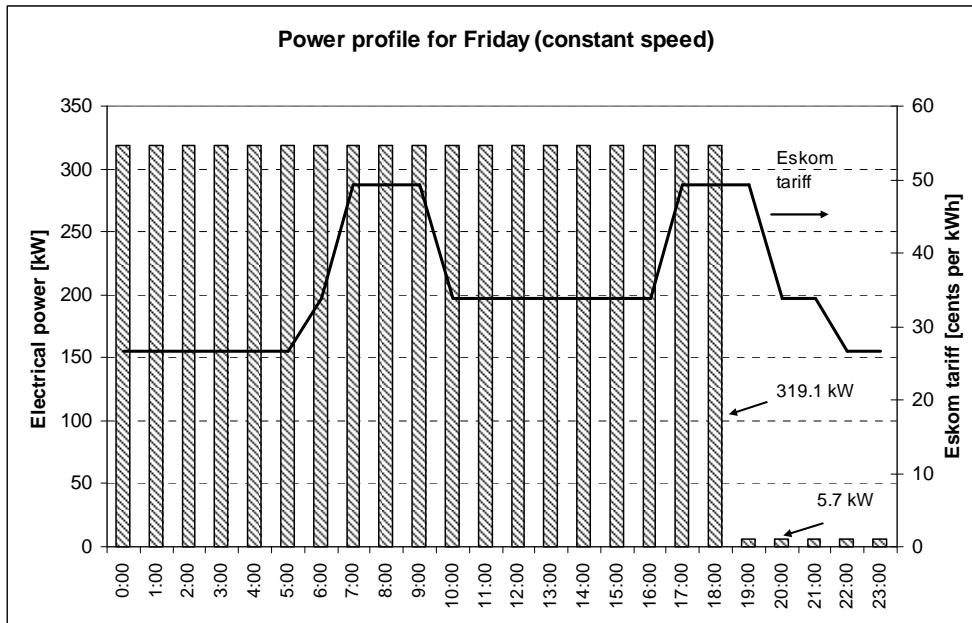


Figure 4.26 Power generated and Eskom tariffs for a Friday at constant speed

For the typical week, the variable speed alternative generated 6 146 kWh during the peak periods, 14 814 kWh during standard periods and 13 395 kWh during off-peak periods. The electrical power income generated for the summer and winter months for a week, are presented in Table 4.10.

Table 4.10 Electrical power income for a week in 2012

Summer (Sept – May)	Peak	Standard	Off-peak	Total
Electrical power income [R]	4 801	7 952	5 635	18 388
Winter (Jun – Aug)	Peak	Standard	Off-peak	Total
Electrical power income [R]	15 407	12 370	7 521	35 298

It should be noted that the electrical power income listed in the above table would be for the year 2011. Annual increases to these tariffs have been approved by the National Energy Regulator of South Africa (NERSA). These tariffs will increase by 25.8 % in 2011 and increase by a further 25.9 % in 2012. Years 2013 and 2014 will have 25 % increases in cost (Eskom, 2010). This has the implication of higher electrical power income being generated in later years (APPENDIX G).

A business case has been compiled for the pump-turbine system. Predicted cash-flows for each year have been calculated using the above Eskom proposed tariffs and presented in APPENDIX G. The projected cash flows over a ten-year horizon are presented in Figure 4.27.

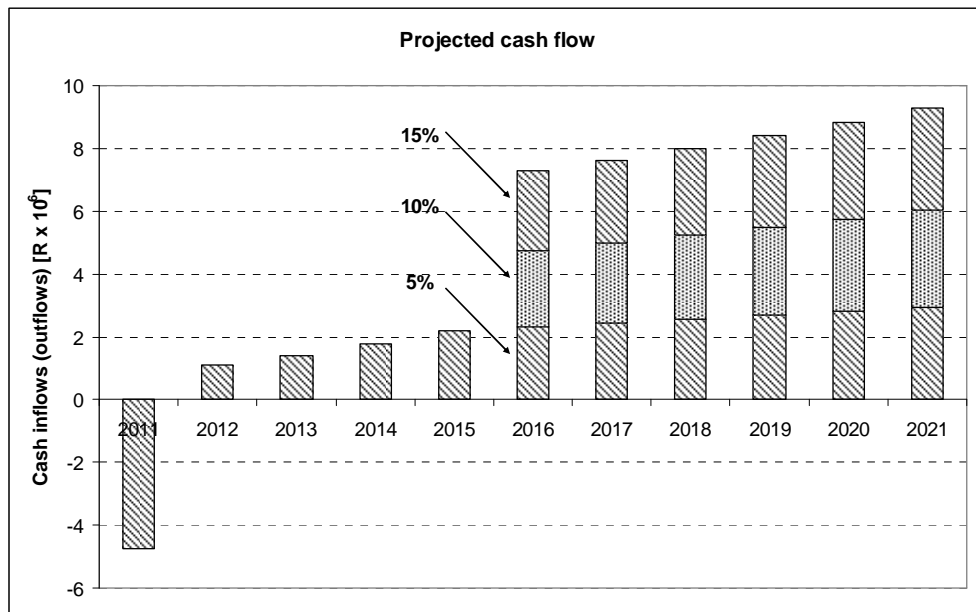


Figure 4.27 Projected cash inflows and outflows for the pump-turbine system (variable speed)

Eskom have also stated that the tariff will increase annually by 6 % from 2016 (Eskom, 2010). However, the proposed increase can change in the interim. A sensitivity analysis was therefore carried out for tariff increases of 5, 10 and 15 %. The cash inflow and outflows for the constant speed alternative is presented below.

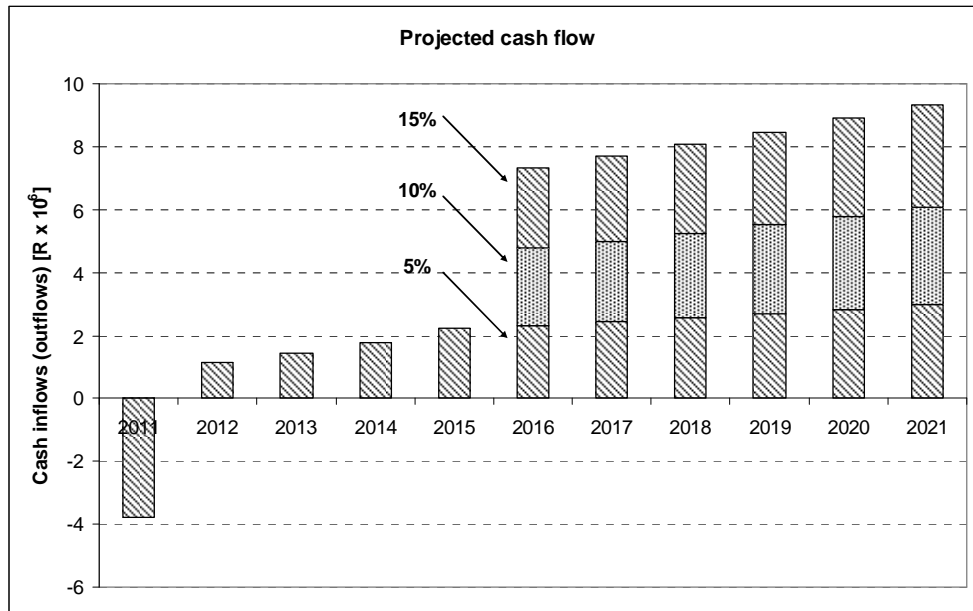


Figure 4.28 Projected cash inflows and outflows for the pump-turbine system (constant speed)

4.5.1 Net present value and internal rate of return

The feasibility of the project was ascertained using the Net present value (NPV) method. This economic model considers the time-value of money by “discounting” the future cash flows to present day. The cash-flows are discounted to present day by using the formula

$$NPV = (\text{future cash-flows}) \times (1 + \text{discount rate})^{-n} \quad (4.6)$$

A discount rate of 10 % was used and over a ten year period (n), the NPV for the pump-turbine system was R 11 564 500 for the variable speed alternative. The NPV for the constant speed alternative was slightly higher at R 11 644 600.

The Internal rate of return (IRR) is the “hurdle” rate at which the discounted future cash-flows are equivalent to the capital investment of the project. This implies a zero value for the NPV in equation (4.6) above.

The IRR for the variable speed alternative was 34.4 % while the constant speed alternative had an IRR of 42.9 %.

It should be noted that the NPV and IRR calculated above are based on an annual tariff increase of 5 % from 2016. The table below summarises increases of 10 and 15 %.

Table 4.11 Net present values and Internal rates of return

Tariff increase from 2016	5 %	10 %	15 %
Variable speed alternative			
Net present value [kR]	11 565	11 877	12 189
Internal rate of return [%]	34.4	35.0	35.5
Constant speed alternative			
Net present value [kR]	11 645	11 959	12,273
Internal rate of return [%]	42.9	43.5	44.1

4.5.2 Payback period

The NPV and IRR consider future cash-flows and the time-value of money. The payback period is the length of time for the future cash-flows to equal the capital expenditure.

The payback period for the pump-turbine system was calculated at 3.8 years for the variable speed alternative and 2.3 years for the constant speed alternative.

4.6 Project management

The project will take approximately 38 weeks to from project kick-off to commissioning and hand-over. This includes all civil, mechanical and electrical works. The items with the longest lead times are the pump-turbine set and VSD and switchgear (16 and 22 weeks respectively). The project schedule is included in APPENDIX H.

4.7 Conclusion

The data for the pressure reducing valve station on 104 Level was regressed to obtain a design water flow and pressure. A suitable pump was thereafter selected. Design criteria were defined and models proposed in the literature were employed to predict the performance of the pump-turbine system. The technical and economic feasibility of two alternative systems were subsequently examined. The constant speed alternative was shown to be the better option. A schedule was also provided for construction of the system.

5 CONCLUSION AND RECOMMENDATIONS

5.1 Summary of the project

A study has been carried out to ascertain the feasibility of replacing a pressure-reducing valve with a turbine. This was achieved by using data received from AngloGold Ashanti Mponeng mine. The data included water flows and pressure data recorded at a pressure-reducing station located on 104 Level. A statistical analysis and data regression was carried out and a typical operating week was obtained. The average water flow through the station was 109.4 l/s with a corresponding discharge pressure of 10.5 bar.

A multi-stage pump was selected at the design water flow and pressure. The pump would operate in reverse i.e. the high pressure water will enter the pump via the “discharge” nozzle and exit via the “suction” nozzle. Turbine curves for the pump were provided by Sulzer and the pump selected was HPH 28-1S. The pump-turbine curves for the head and efficiency was regressed using models proposed by van Antwerpen and Greyvenstein (2005). The regressed models were used to define two alternative systems; namely a variable shaft speed system and a constant shaft speed system.

An operating water flow range was defined for each alternative system. The quantity of energy expected to be recovered was calculated and would be fed back to the electrical power grid. At the design water flow, the variable speed system potentially generated 318.5 kW; while 319.1 kW would be generated at constant speed. The discharge water temperature for both systems would be 10.32 °C.

Capital costs were compiled from budget quotations received from potential suppliers and historical costs¹⁴. The variable speed system requires R 4 726 300 capital investment while the constant speed system costs R 3 776 900.

¹⁴ BBE Cost Database, 2010.

A financial analysis for the variable speed system revealed an NPV of R 11 565 000; IRR of 34.4 % and payback of 3.8 years. The constant speed system has an NPV of R 11 645 000; IRR of 42.9 % and payback of 2.3 years.

Both systems are technically and economically feasible. However, the constant speed system would be the better alternative.

5.2 Recommendations for further work

It is recommended to progress beyond the current project scope into a construction and testing phase.

The work would include the verification of the design calculations and predicted results by experimental data. This can be achieved by procurement and construction of the constant speed system and equipping the experimental site with suitable data-logging systems.

The pump system will be installed in parallel to the existing pressure-reducing station located on 104 Level. This is to ensure continuity of the chilled water supply in the event that the experimental facility becomes unavailable due to any number of factors.

5.3 Closure

The objective of the project was to evaluate the economic feasibility of replacing a pressure reducing valve with a pressure reducing turbine. Towards that end, an energy recovery system was designed using a standard pump that would operate in reverse. It has been shown that the system would recover energy in a manner that is both technically and economically feasible.

REFERENCES

ABERDARE POWER CABLES, (2009) "Cable facts and figures handbook",
Aberdare Cables (Pty) Ltd, Gauteng.

ANONYMOUS, (Oct 2010), Eskom – Looking ahead (chief executive breakfast presentation), Eskom, South Africa, Internet: <http://www.eskom.co.za/tariffs.php>,
27 Nov 2010.

ANONYMOUS, Selected historical exchange rates and other interest rates, South African Reserve Bank, Internet:
<http://www.resbank.co.za/Research/Rates/Pages/Rates-Home.aspx>,
4 April 2011.

ARRIAGA M., (2010), Pump as turbine – A pico-hydro alternative in Lao People's Democratic Republic, Renewable Energy, Vol.35, pp 1109-1115.

BLUHM, S.J., HEMP, R., FUNNELL, R., SHEER, T.J., BUTTERWORTH, M.D., RAWLINS, A., (Apr 2000), Deepmine Task 6.5.3, Efficiency of chilled water distribution systems, Bluhm Burton Engineering, Johannesburg, South Africa.

BLUHM, S.J., VON GLEHN, F.H., SMIT, H., (Feb 2003), Important basics of mine ventilation and cooling planning, Journal of the Mine Ventilation Society of South Africa, Conference Proceedings, CSIR Pretoria.

BUSE, F., (1981), Using centrifugal pumps as hydraulic turbines, Chemical Engineering, pp 113-117.

CONRADIE, D., (Apr 2010), Tariffs and charges 2010/2011,
Internet: <http://www.eskom.co.za/live/content.php>, 27 Nov 2010.

CREAMER, M., (Jun 25, 2010), South Deep will prove to be one the best investments ever made – Gold Fields, Mining Weekly, Creamer Media, Johannesburg.

DERAKHSHAN, S., NOURBAKHS, A., (2008), Theoretical, numerical and experimental investigation of centrifugal pumps in reverse operation, Experimental Thermal and Fluid Science, Vol. 32, pp 1620-1627.

DOUGLAS, J.F., GASIOREK, J.M., SWAFFIELD, J.A., (1995), Fluid Mechanics, Third edition, Longman Group Limited, England.

DU TOIT, L., (2009), Mponeng simplified CW reticulation system, AngloGold Ashanti Mponeng, North-west province, South Africa.

DU TOIT, L., (2010), Mponeng dam temperatures, AngloGold Ashanti Mponeng, North-west province, South Africa.

FERGUSON, D.W.B., BLUHM, S.J., (Nov 1984), Performance testing of an energy recovery turbine at a three-stage spray chamber, Journal of the Mine Ventilation Society of South Africa, Vol. 37, pp 121-125.

FUNNELL, R.C., GUNDERSEN, R.E., BLUHM, S.J., VON GLEHN, F.H., (March 2006), The synergistic benefits and limitations of hydro-mine power for mine cooling, South African Institute of Mining and Metallurgy Conference, Johannesburg.

GEANKOPLIS, C.J., (1993), Transport Processes and Unit Operations, Third Edition, Prentice-Hall, New Jersey.

GOPAL, A.K., HARPER, G.S., (Mar 1999), Deepmine Task 13.4.1, "Energy recovery device", CSIR Miningtek, Johannesburg, South Africa.

GOPALAKRISHNAN, S., (1986), Power recovery turbines for the process industry, Proceedings of the Third Pump Users Symposium, pp 3-11.

GRAY, C.B., (1989), Electrical Machines and Drive Systems, Longman Scientific and Technical, England.

HOFFMAN, D., (Jul 1994), The installation of a 3-Chamber pipe-feeder system – its effect on the design of the water reticulation system, Journal of the Mine Ventilation Society of South Africa, Vol. 47, pp 142-144.

LAUX, C.H., (1982), Reverse-running standard pumps as energy recovery turbines, Sulzer Technical Review, Vol. 2, pp 23-27.

LUYBEN, W.L., (1989), Process modelling, Simulation, and Control for Chemical Engineers, Second Edition, McGraw-Hill, New York

MANKBADI R.R., MIKHAIL, S.A., (1984), A turbine-pump system for low-head hydropower, Energy Conversion and Management, Vol.25, No. 3, pp 339-344.

MARAIS, J., (Feb 6, 2011), Oppenheimers reposition, Sunday Times, Independent Newspapers, Gauteng, South Africa.

MASSEY, B.S., (1970) Mechanics of fluids, Second edition, Van Nostrand Reinhold Company, Canada.

McPHERSON, M.J., (1993), Subsurface Ventilation and Environmental Engineering, Chapman and Hall, London.

O'DONNELL, M.A., (Feb 19, 2010), The energy behind the world's deepest gold mine, Mining Weekly, Creamer Media, Johannesburg.

ORCHARD, B., KLOS, S., (2009), Pumps as turbines for water industry, World Pumps, pp 22-23.

PATEL, M.R., (2006), Wind and Solar Power Systems, Second edition, CRC Press, Florida.

PERRY, R.H., GREEN, D.W., (1997), Perry's Chemical Engineers Handbook, Seventh Edition, McGraw-Hill, New York.

PETERS, M.S., TIMMERHAUS, K.D., WEST, R.D., (2003), Plant Design and economics for chemical engineers, Fifth Edition, McGraw-Hill, New York.

RAJA, W.A., PIAZZA, R.W., (1981), Reverse running centrifugal pumps as hydraulic power recovery turbines for seawater reverse osmosis systems, Desalination, Vol. 38, pp 123-134.

RAMOS, H., BORGA, A., (1999), Pumps as turbines: an unconventional solution to energy production, Urban Water, Vol. 1, pp 261-263.

RAMSDEN, R., (Sept 1983), The temperature rise of chilled water flowing through pipes, Journal of the Mine Ventilation Society of South Africa, Vol. 36, pp 85-93.

RAMSDEN, R., BLUHM, S.J., (Sept 1985) Energy recovery turbines for use with underground air coolers, Proceedings of the Second US Mine Ventilation Symposium, Reno, Nevada, USA, pp 571-80.

RICHMOND, S.B., (1964) Statistical Analysis, Second edition, The Ronald Press Company, New York

ROBBINS, A., (Mar 26, 2010), PRV Station data, AngloGold Ashanti Mponeng, North-west province, South Africa.

SAYERS, A.T., (1946), "Hydraulic and Compressible Flow Turbomachines", Library of Congress Cataloging-in-Publication Data, Britain.

SCHOLL, H.G., (2000), A pump-turbine combination for sea water, World Pumps, pp 24-25.

SMITH, J.M., Van Ness, H.C., Abbott, M.M., (2001), Introduction to Chemical Engineering Thermodynamics, Sixth edition, McGraw-Hill, New York.

TASKER, M, (2011), Runaway speed, Sulzer, Gauteng, South Africa.

TORBIN, R.N., (1989), Alternate methods of energy recovery for the mining industry, IEEE Transactions on Industry Applications, Vol. 25, No. 5, pp 811-818.

VAN ANTWERPEN, H.J., GREYVENSTEIN, G.P., (2005), Use of turbines for simultaneous pressure regulation and recovery in secondary cooling water systems in deep mines, Energy Conversion and Management, Vol. 46, pp 563-575.

VAN DER MERWE, M.L., (Mar 1986), Power recovery from chilled water at the Buffelsfontein gold mine Southern shaft, Journal of the Mine Ventilation Society of South Africa, Vol. 39, pp 37-45.

WALTERS, D.M, PRETORIUS, A.R.W., (1994), How a three chamber pipe feeder system operates, Journal of the Mine Ventilation Society of South Africa, Vol. 47, pp 144-146.

WHILLIER, A., (Apr 1977), Recovery of energy from water going down mine shafts, Journal of South African Institute of Mining and Metallurgy, Vol. 77 pp 183-186.

WILLIAMS, A.A., (1996) Pumps as turbines for low cost micro hydro power, World Renewable Energy Congress, Denver, Colorado, USA, pp 1227-1234.

BIBLIOGRAPHY

ANONYMOUS, (1998), Pump-turbine research project completed, World Pumps, pp 12.

CREAMER, M., (Apr 21, 2010), Gold Fields spotlights unrivalled riches of one-of-a-kind South Deep gold mine, Mining Weekly, Creamer Media, Johannesburg.

CREAMER, M., (Feb 9, 2009), World's new deepest mine 'safe, cheap' – AngloGold, Mining Weekly, Creamer Media, Johannesburg.

FRASER, P., LE ROUX, D., (May 2008), Energy savings by recovering the pressure head in mines: A review of the theoretical and practical issues associated with the design, installation, operation and maintenance of the 3 Chamber pump systems (3CPS) and turbine energy recovery systems, Proceedings of the Mine Ventilation Conference, CSIR Pretoria.

HEGERMAN, C., (Mar 1997), Optimising the cooling of the Vaal Reefs No.11 shaft underground environment and a description of refrigeration and energy recover equipment used, Journal of the Mine Ventilation Society, Vol. 50, pp 18-24.

KRAMERS, A.P., (Mar 2002), Deepmine Task 6.4.2: Assessment of three-pipe chamber feeder (3CPF) technology, CSIR Miningtek, Johannesburg, South Africa.

LAUX, C.H., (1980), Reversible multistage pumps as energy recovery turbines in oil supply systems, Sulzer Technical Review, Vol. 2, pp 61-75.

MOHAN, N., UNDELAND, T.M., ROBBINS, W.P., (1995), Power Electronics: Converters, Applications and Design, John Wiley and Sons, United States of America.

NAUTIYAL, H., VARUN, KUMAR, A., (2010), Reverse running pumps analytical, experimental and computational study: a review, Renewable and Sustainable Energy Reviews, Vol. 14, pp 2059-2067.

O'DONNELL, M.A., (Jun 25, 2010), New-order mining rights approved for gold mine expansion project, Mining Weekly, Creamer Media, Johannesburg.

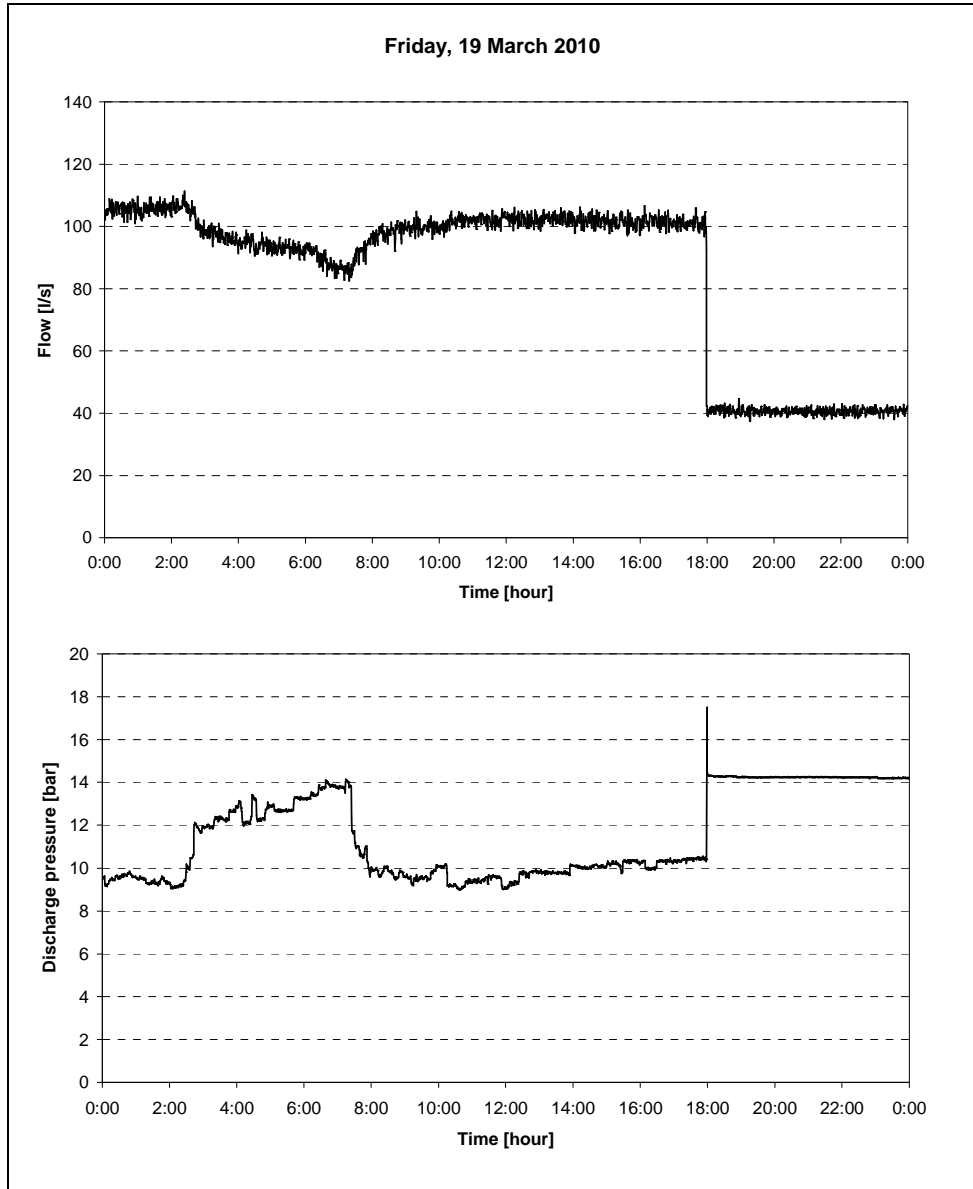
SHAFER, L.L., (1982), Pumps as power turbines, Mechanical Engineering, pp 40-43.

STEPANOFF, A.J., (1957), Centrifugal and Axial Flow Pumps, Second edition, John Wiley and Sons, United States of America.

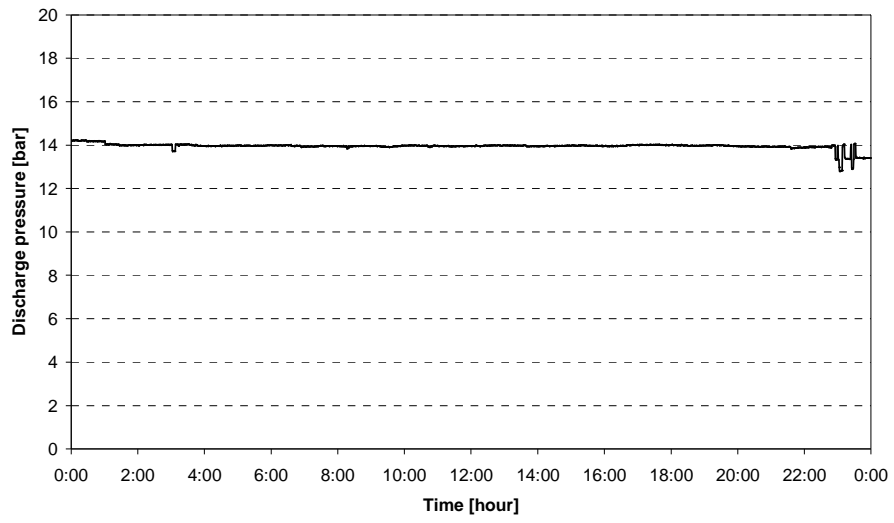
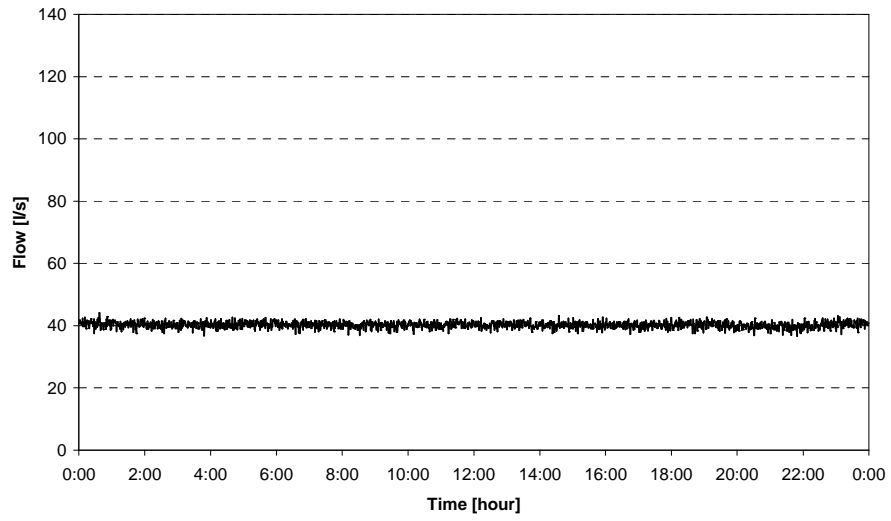
WILLIAMS, A.A., SMITH, N.P.A., BIRD, C., HOWARD, M., (1998), Pumps as Turbines and Induction Motors as Generators for Energy Recovery in Water Supply Systems, Journal of the Chartered Institution of Water and Environmental Management, Vol. 12, pp 175-178.

APPENDIX A RAW DATA

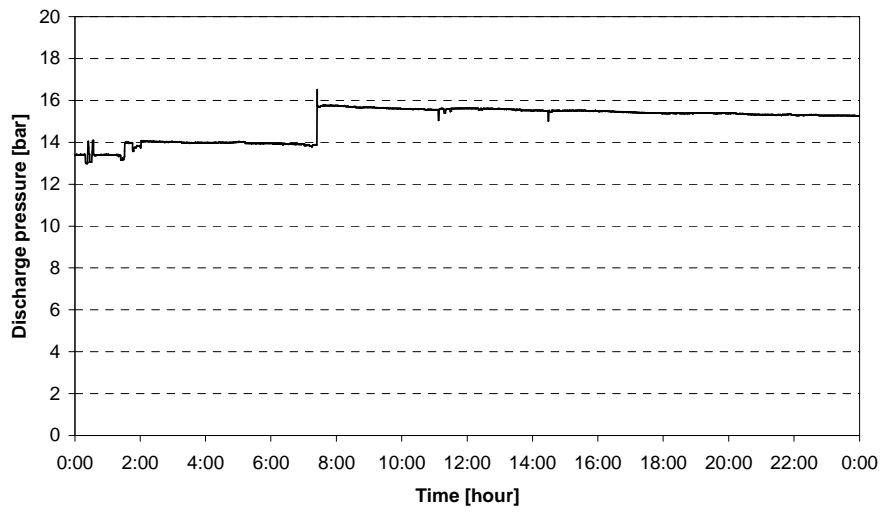
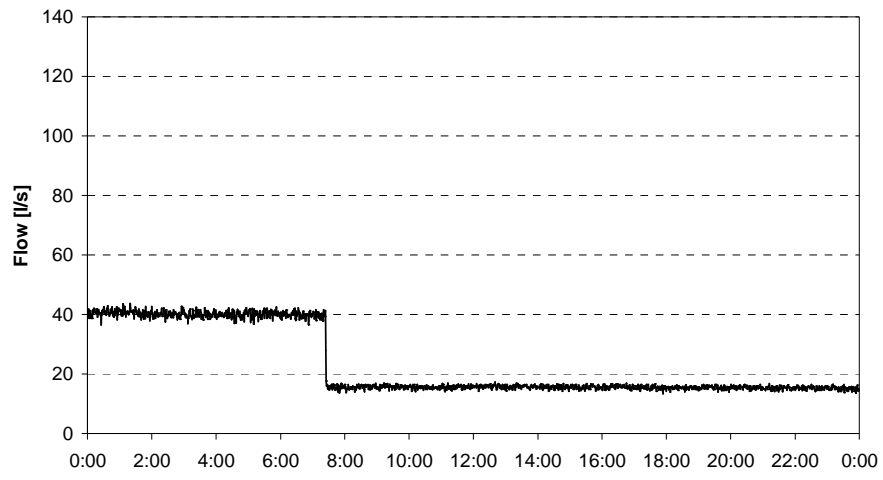
A.1 104 Level PRV data



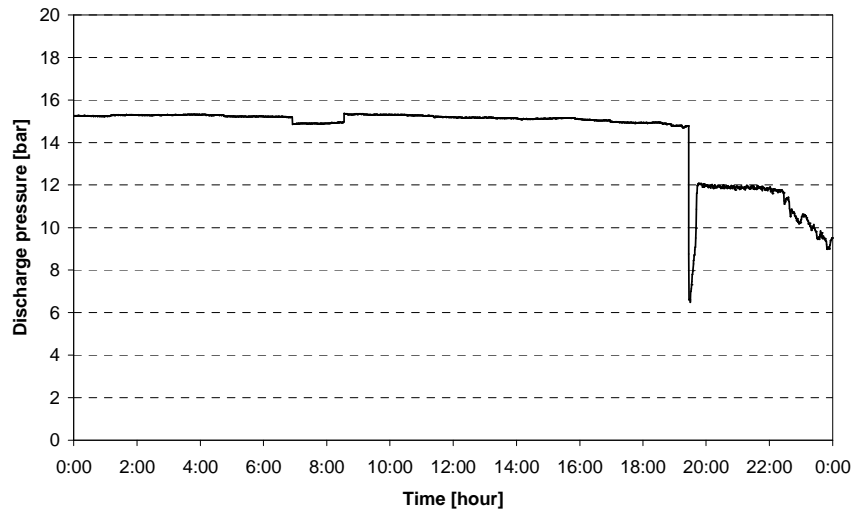
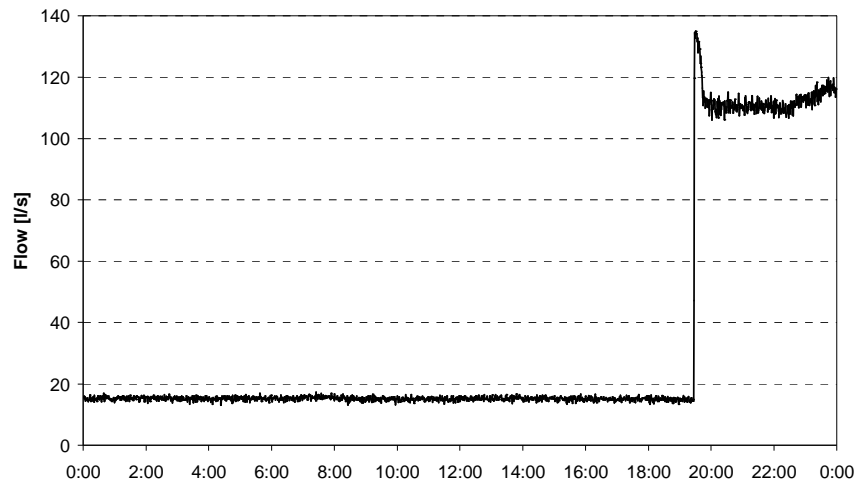
Saturday, 20 March 2010



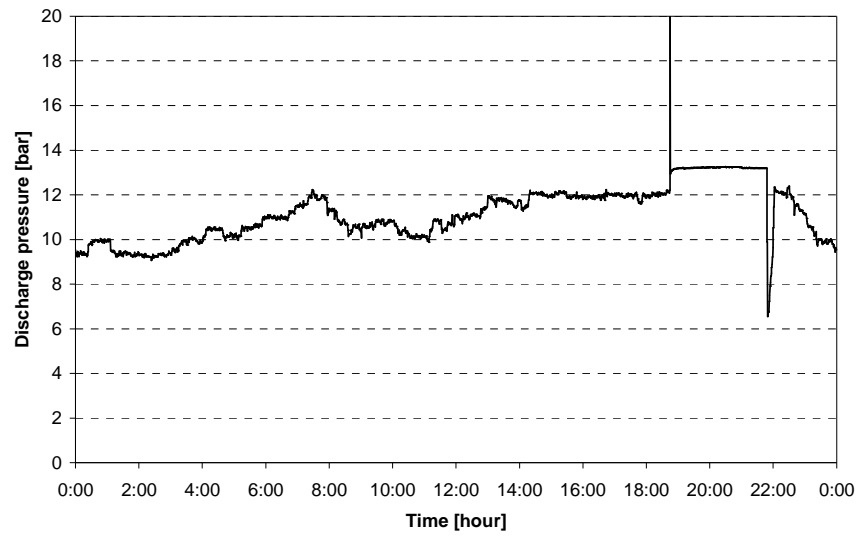
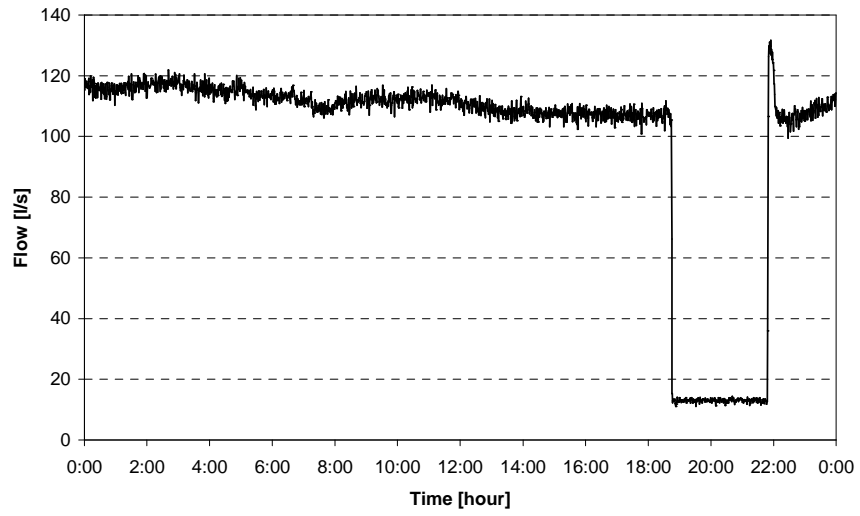
Sunday, 21 March 2010



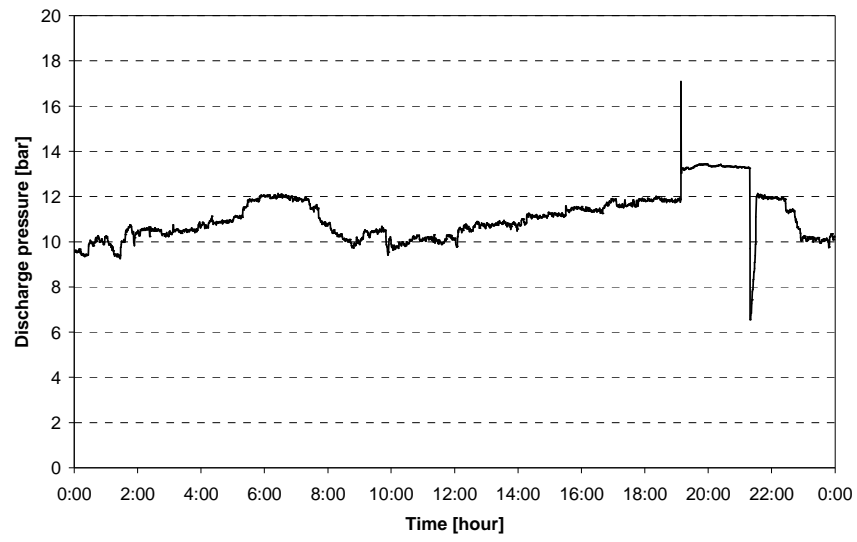
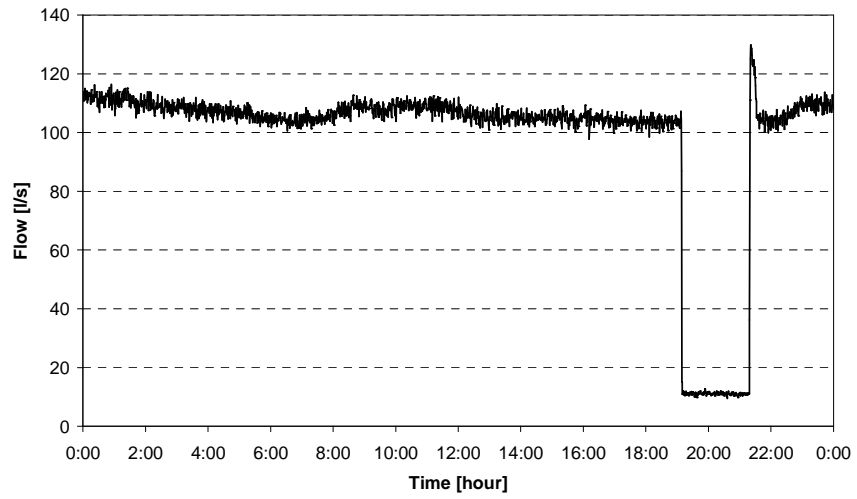
Monday, 22 March 2010



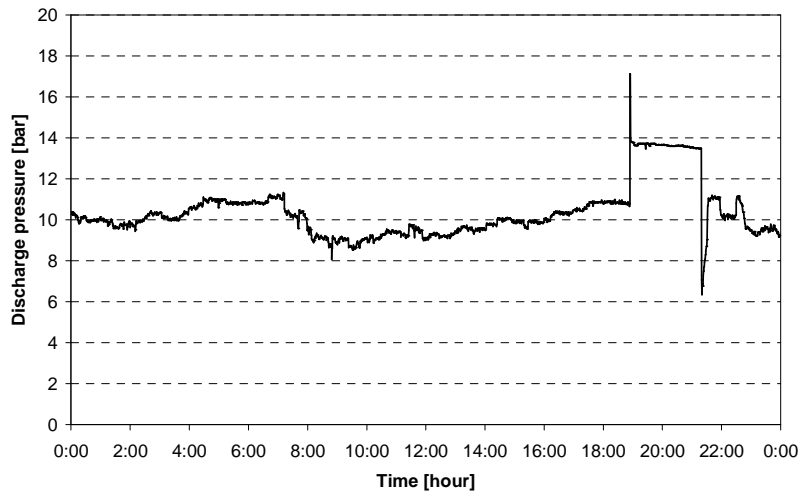
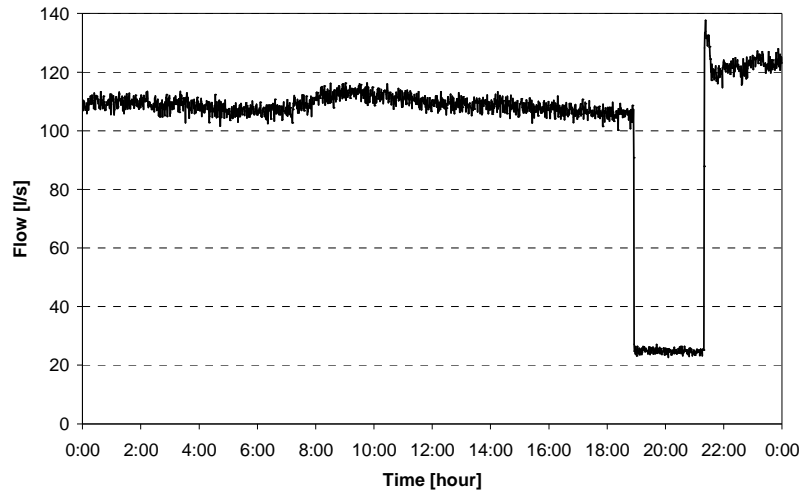
Tuesday, 23 March 2010



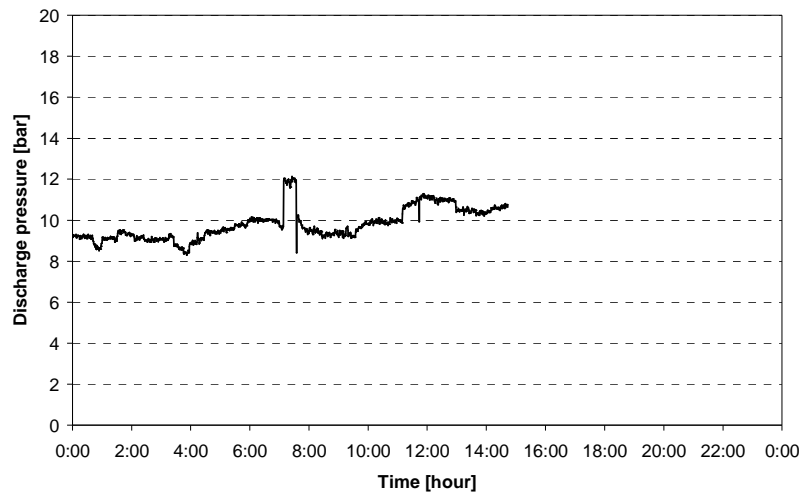
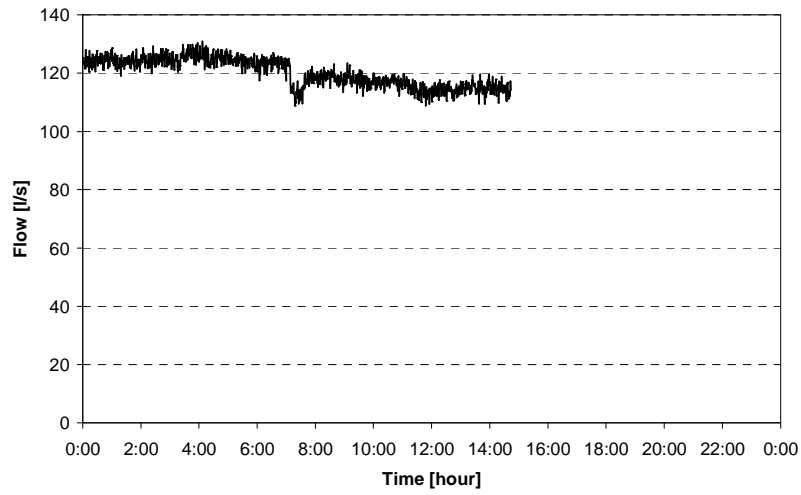
Wednesday, 24 March 2010



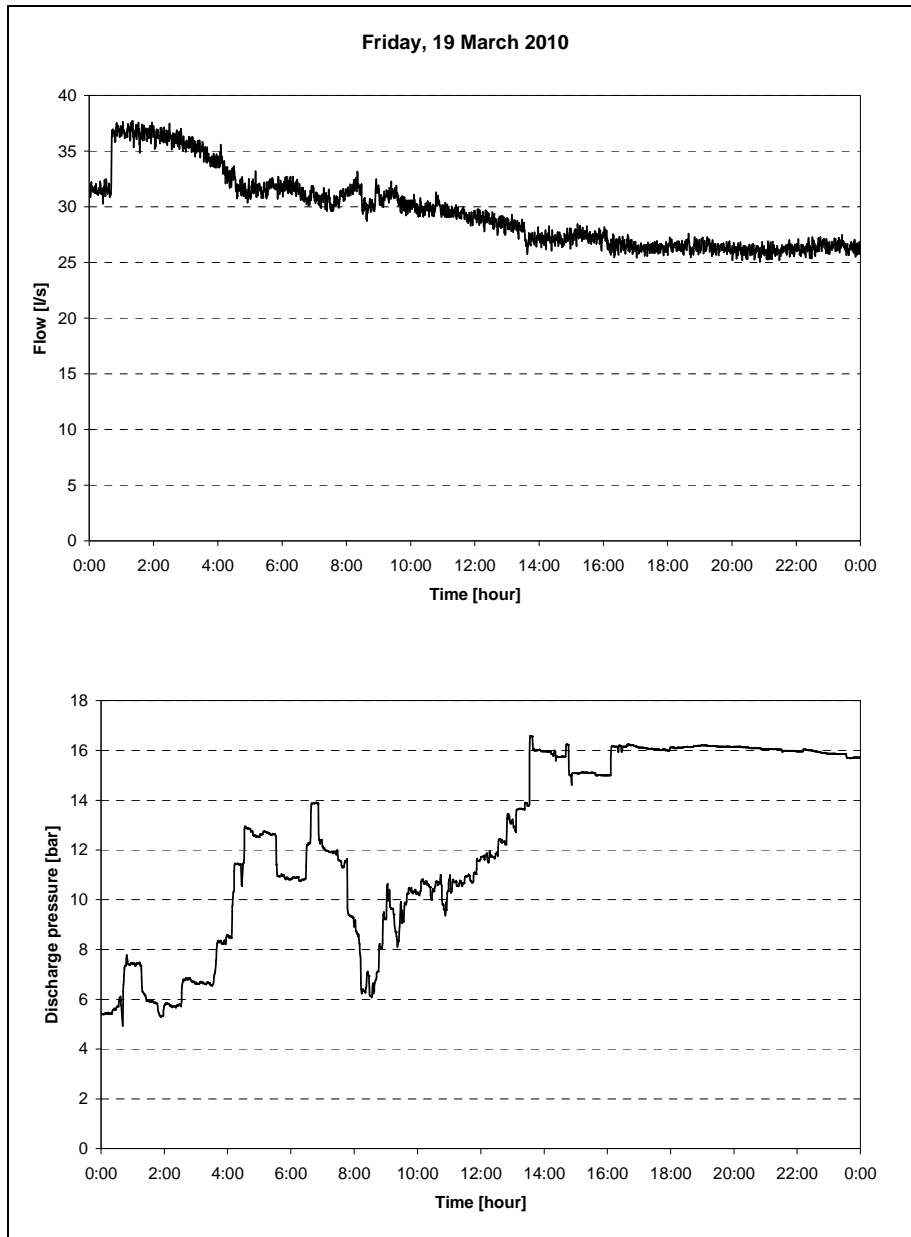
Thursday, 25 March 2010



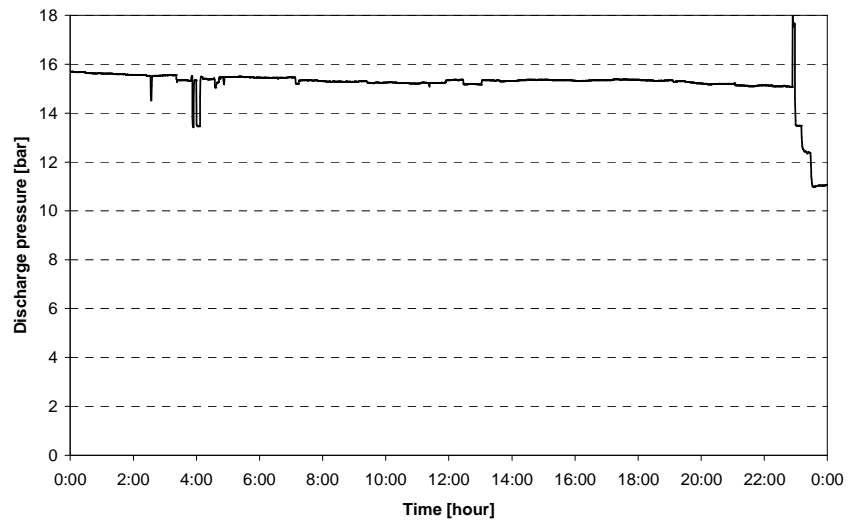
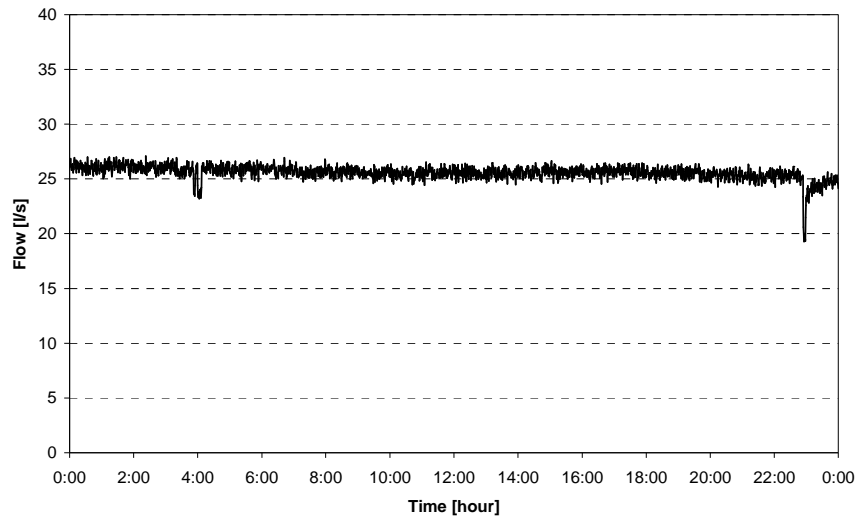
Friday, 26 March 2010



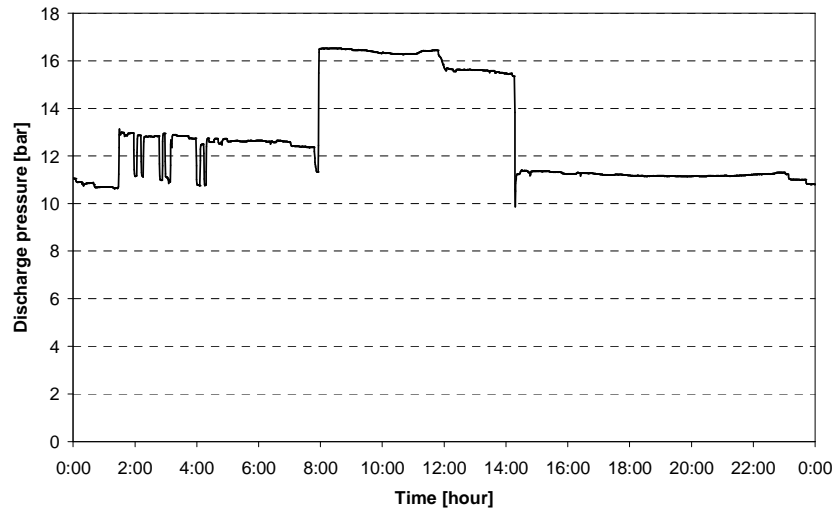
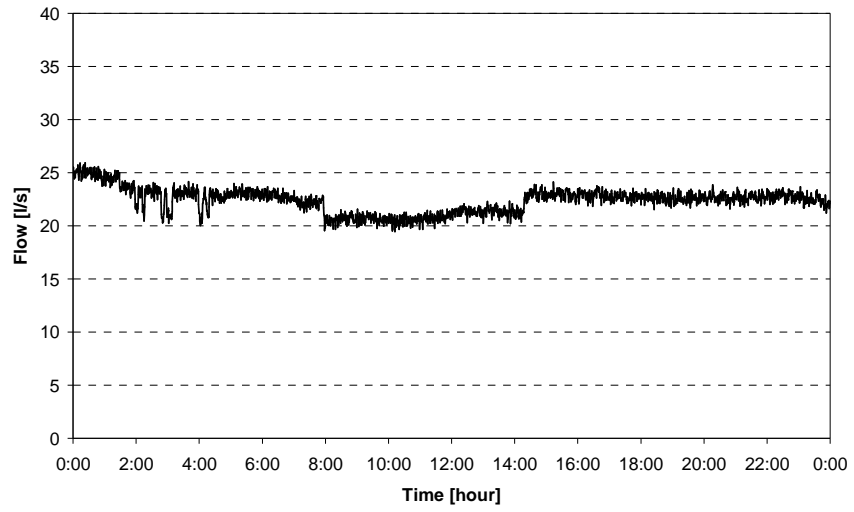
A.2 99 Level PRV data



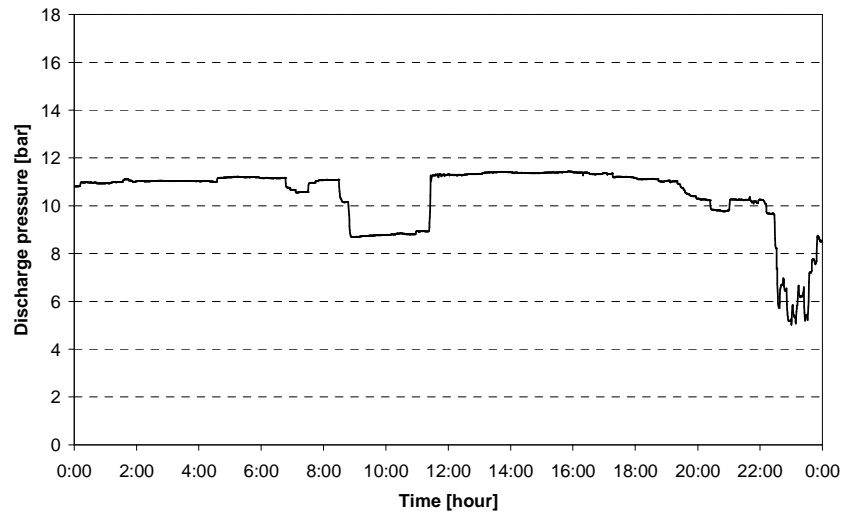
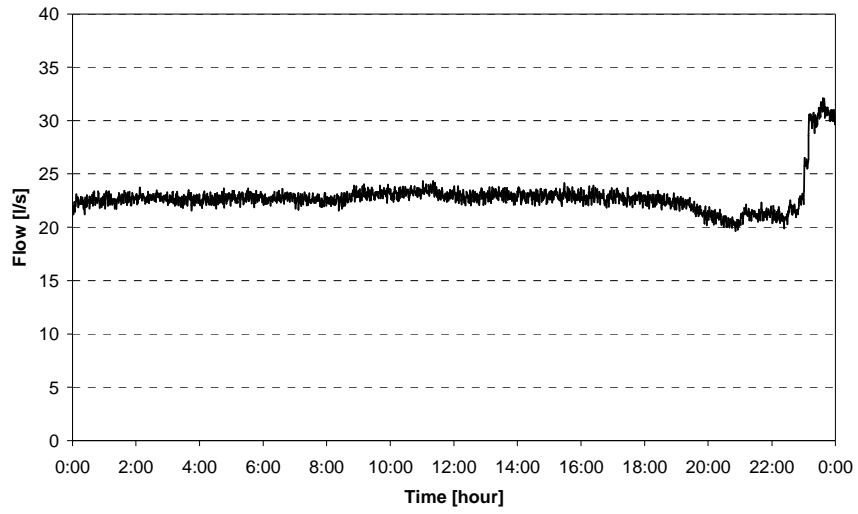
Saturday, 20 March 2010



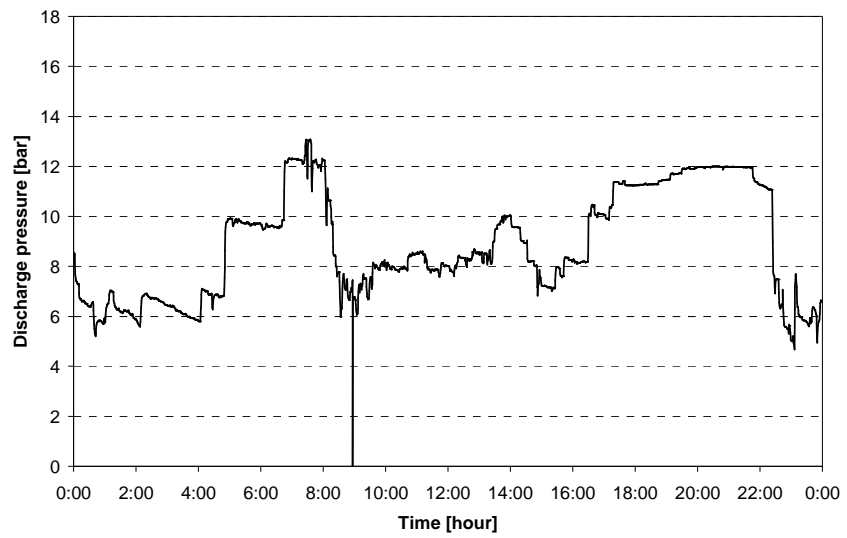
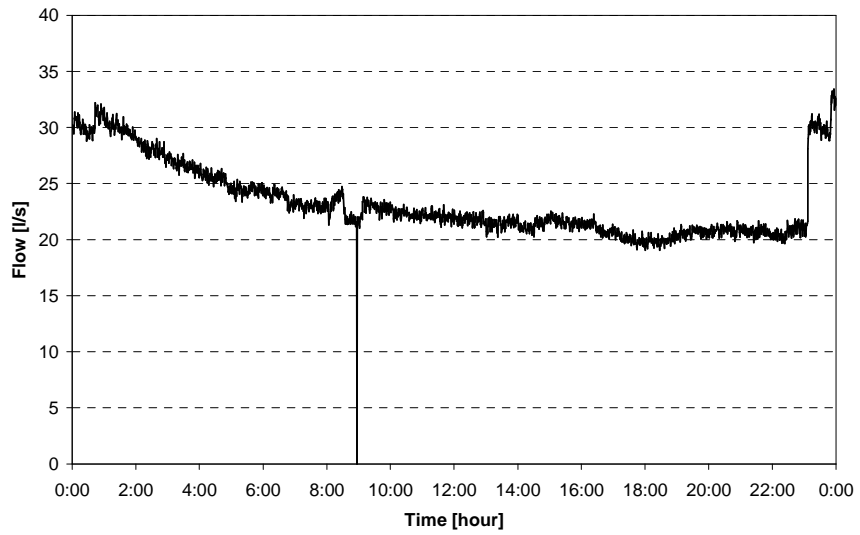
Sunday, 21 March 2010



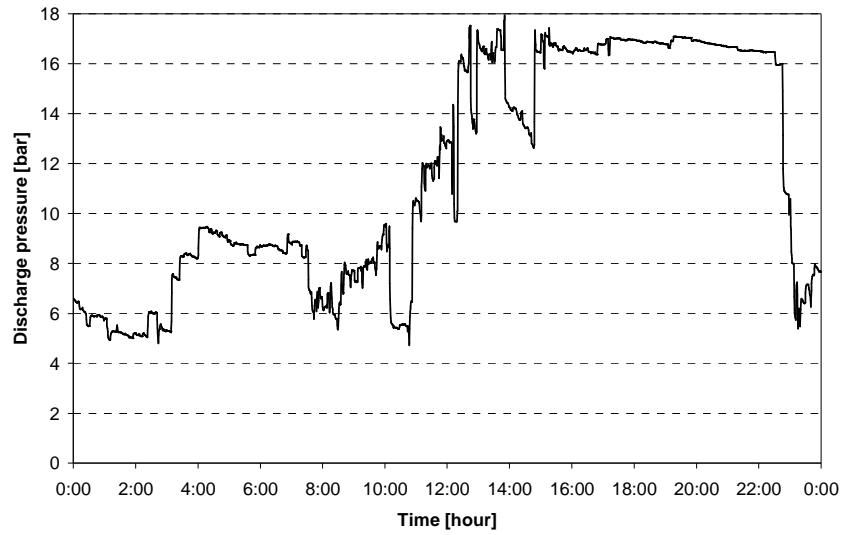
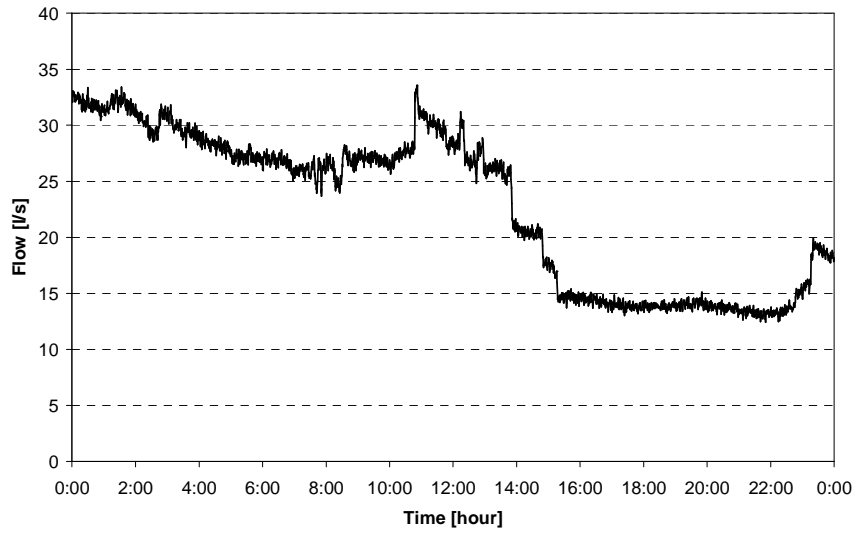
Monday, 22 March 2010



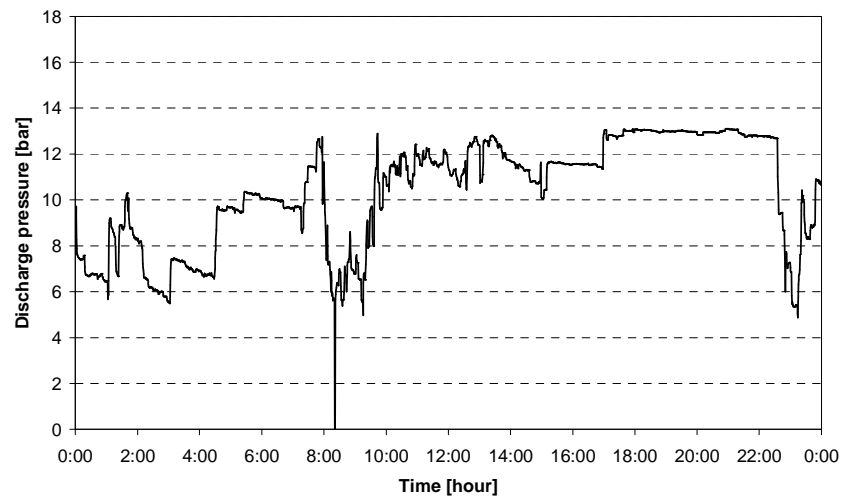
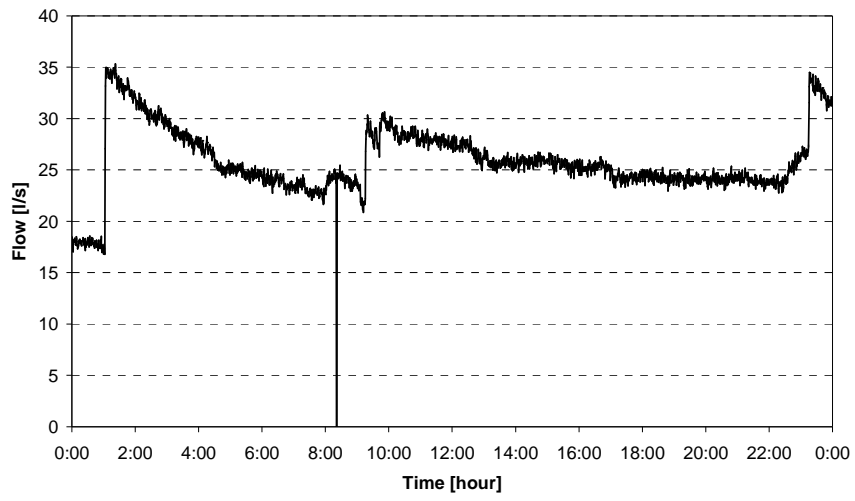
Tuesday, 23 March 2010



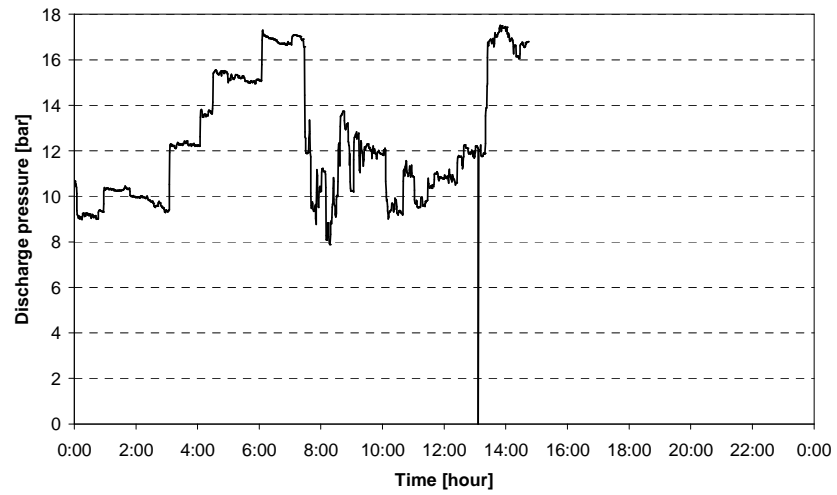
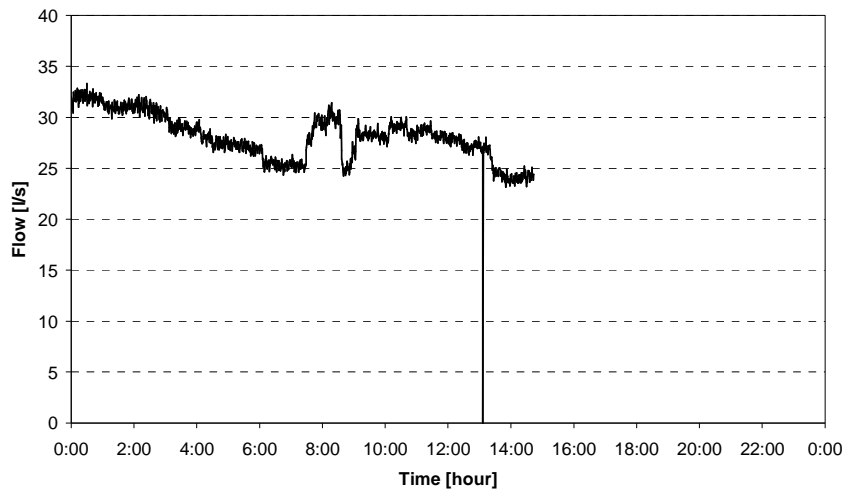
Wednesday, 24 March 2010



Thursday, 25 March 2010



Friday, 26 March 2010



APPENDIX B REGRESSION OF WATER FLOW DATA

The purpose of regressing the data is to identify a weekly trend. This was achieved using descriptive statistics. Statistical theory will be presented below, followed by calculations and a justification of the values selected.

B.1 Statistical analysis¹⁵

The *average* value (\bar{x}) of a data range, is the sum of the observations in the data range divided by the number of observations (n) in the range. Mathematically,

$$(\bar{x}) = \sum x / n \quad (\text{B.1})$$

The average value in isolation is of little significance. The *standard deviation* (s) gives an indication of how wide the data varies from the average; and is calculated using

$$s = [\sum (x - \bar{x})^2 / (n - 1)]^{1/2} \quad (\text{B.2})$$

In a data range, the *median* divides the data such that half of the observations are larger and half are smaller. The *mode* of the range is the value in the data range with highest number of occurrences.

The above parameters provide information on the tendency of data to centre about a particular value. As an example, when the median and mode of the data range are equal, the data is symmetrical about that value.

B.2 104 Level station data

The water flow through the 104 Level pressure-reducing valve station shows three distinct ranges; and the flows have been classified as peak, intermediate and low. A histogram of the raw data shows these ranges below.

¹⁵ Richmond, S.B., 1964

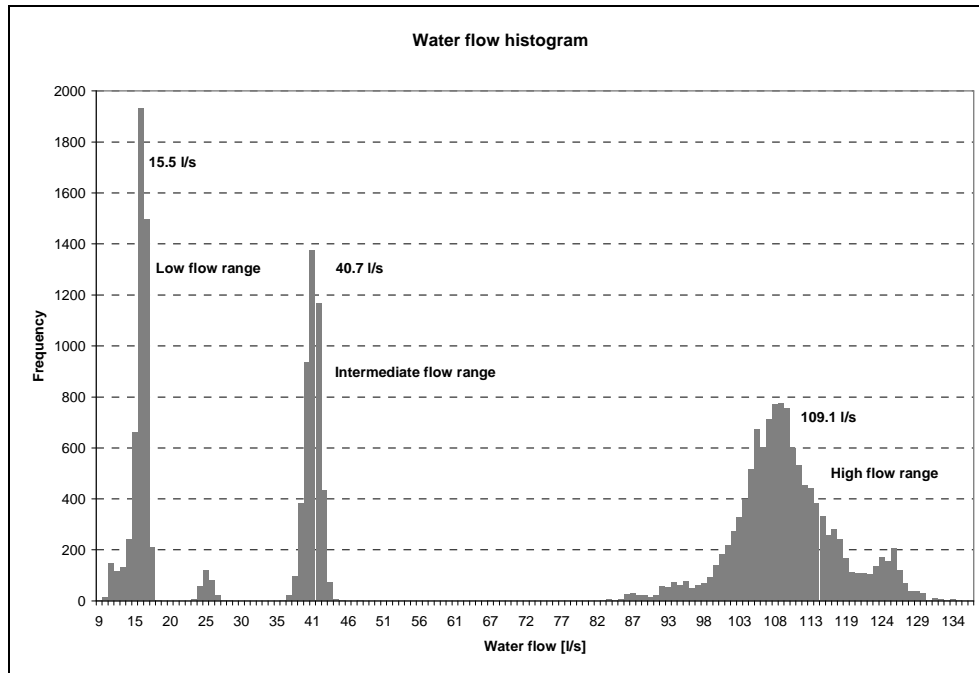


Figure B1 Histogram for water flow through the 104 Level station

The value indicated in each flow range (Figure B1) is the mode. Table B1 lists the statistical parameters that were calculated from the data for the week.

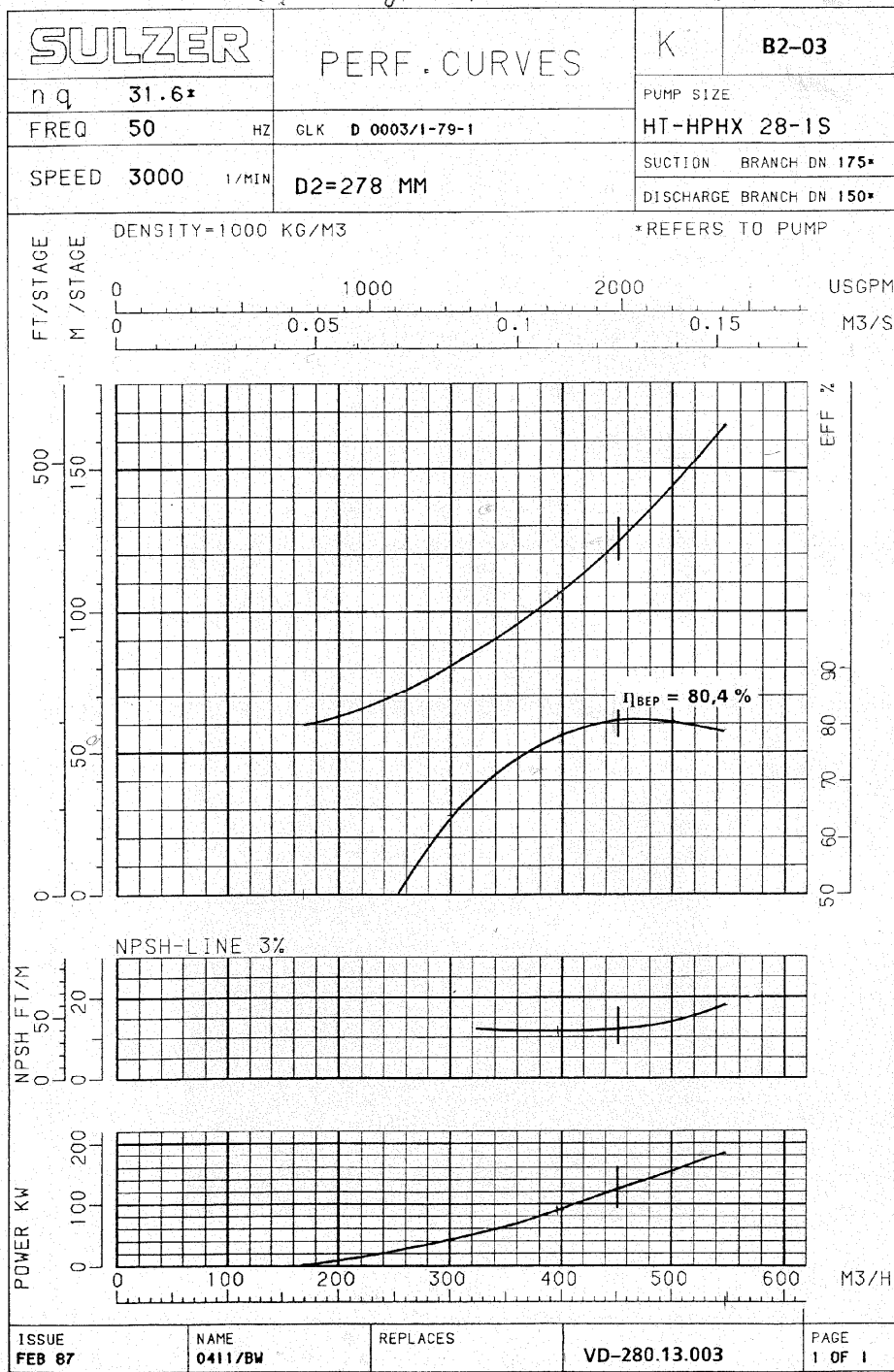
Table B1 Statistical analysis of water flow data

Water flow [l/s]	Low	Intermediate	Peak
Sample size (<i>n</i>)	4 491	5 267	12 197
Average (\bar{x})	15.6	40.3	109.4
Standard deviation (<i>s</i>)	3.1	1.1	7.7
Median	15.3	40.3	108.8
Mode	15.5	40.7	109.1

The average value was used in the calculations since central tendency about this value is observed (a marginal difference is noted between the average, median and mode).

APPENDIX C MANUFACTURER'S DATA

C.1 Pump-turbine curves (Sulzer)



C.2 Induction generator performance curves (Zest energy)

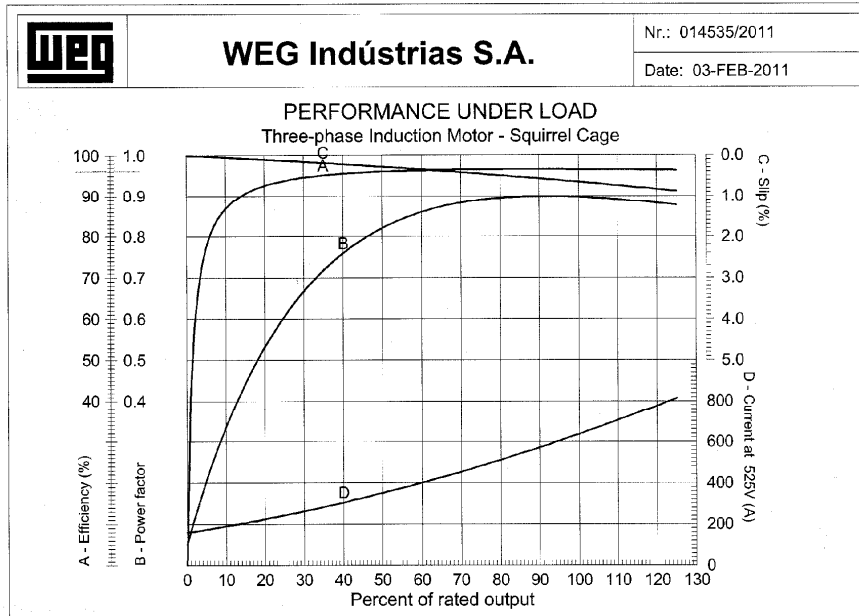


Figure C1 500 kW induction generator for variable speed alternative

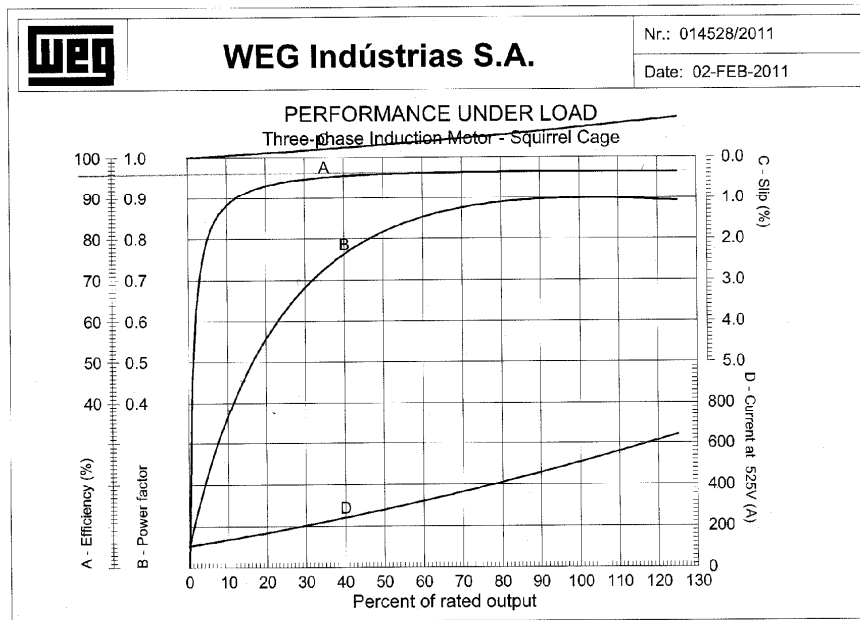


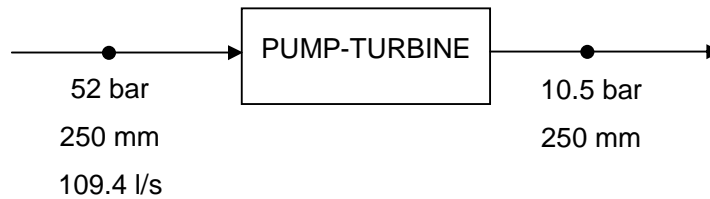
Figure C2 400 kW induction generator for constant speed alternative

APPENDIX D SAMPLE CALCULATIONS

D.1 System Curve

The system curve (Figure 3.6, pp 40) was generated determining the available shaft work, at a range of water flows. A flow of 110 l/s and discharge pressure of 10.5 bar will be used to illustrate the methodology.

The system under consideration is



The mechanical energy balance has been derived as

$$(P_1 - P_2) / \rho + g (z_1 - z_2) - g h_f = W_s \quad (4.1)$$

and multiplying the equation by density ρ gives

$$(P_1 - P_2) + \rho g (z_1 - z_2) - \rho g h_f = \rho W_s$$

The available work $W_s = 4\,150 + 4.41 - 27.8 =$ **4 127 kPa**

- Pressure term: $P_1 - P_2 = (52 - 10.5) \text{ bar} \times 100 \text{ kPa} / \text{bar} =$ 4 150 kPa
- Potential energy term: $\rho g (z_1 - z_2) = 1\,000 \times 9.79 \times 0.45 = 4\,406 \text{ Pa} = 4.41 \text{ kPa}$

$$\rho = 1\,000 \text{ kg/m}^3$$

$$g = 9.79 \text{ m/s}^2$$

$$z_1 - z_2 = 0.45 \text{ m}$$

(elevation difference between suction and discharge centre-lines)

- Friction loss term: $\rho g h_f =$ sum of friction losses (pipe, pipe fittings and valves)

$$= 3 \times (0.597) + 5.76 + 3.11 + 6.76 + 5.28 + 1.76$$

$$= 25.2 \text{ kPa}$$

A design factor of 10 % was added to the total friction loss to give 27.8 kPa

From the P&ID (FN-PT-10-002) the following fittings are present:

	Loss coefficient	Pressure loss
Butterfly valves (3-off)	$K_L = 0.24$	$K_L \rho u^2 / 2$
Anti-vibration joint (1-off)	$K_L = 0.3$	$K_L \rho u^2 / 2$
Anti-vibration joint (1-off)	$K_L = 0.3$	$K_L \rho u^2 / 2$
Reducer (1-off)	$K_L = 0.55(1 - A_2/A_1)$	$K_L \rho u_2^2 / 2$
Diffuser (1-off)	$K_L = (1 - A_1/A_2)$	$K_L \rho u_1^2 / 2$

For a *butterfly valve*, $K_L \rho u^2 / 2 = 0.24 \times 1\,000 \times 2.23^2 / 2 = 597 \text{ Pa} = 0.597 \text{ kPa}$

$$D = 250 \text{ mm} \quad A = \pi / 4 \times D^2 = \pi / 4 \times 0.25^2 = 0.049 \text{ m}^2$$

$$u = q / A = 109.4 / 0.049 / 1\,000 = 2.23 \text{ m/s}$$

Similarly, the pressure losses for the anti-vibration joints are 5.76 kPa (150 mm) and 3.11 kPa (175 mm).

For the *reducer*, $K_L \rho u_2^2 / 2 = 0.55 (1 - A_2/A_1) \rho u_2^2 / 2 = 0.55(1 - 0.018/0.049) 1\,000 \times 6.20^2 / 2$

$$= 6758 \text{ Pa} = 6.76 \text{ kPa}$$

$$D_1 = 250 \text{ mm} \quad A = \pi / 4 \times D^2 = \pi / 4 \times 0.25^2 = 0.049 \text{ m}^2$$

$$D_2 = 150 \text{ mm} \quad A = \pi / 4 \times D^2 = \pi / 4 \times 0.15^2 = 0.018 \text{ m}^2$$

$$u = q / A = 109.4 / 0.018 / 1\,000 \quad (\text{velocity at the smaller area is used})$$

$$= 6.20 \text{ m/s}$$

Similarly, the pressure loss for the diffuser is 5.28 kPa.

The *pipe friction* was $4f(L/D) \rho u^2 / 2$

$$= 4 \times 0.0037 \times (12 / 0.25) 1\,000 \times 2.23^2 / 2$$

$$= 1757 \text{ Pa}$$

$$= 1.76 \text{ kPa}$$

The friction factor was solved implicitly using the Colebrook equation

$$\begin{aligned} 1 / f^{1/2} &= -4 \log [\varepsilon / 3.7 D + 1.256 / (\text{Re } f^{1/2})] \\ &= -4 \log [0.07 / 3.7 (0.25) + 1.256 / (4.16 \times 10^8 f^{1/2})] \end{aligned}$$

Therefore,

$$f = 0.0037$$

$$\varepsilon = 0.07 \text{ mm} \quad (1.5 \text{ times the roughness of a new steel pipe} - 0.046 \text{ mm})$$

$$\begin{aligned} \text{Re} &= Lu \rho / \mu_F && \text{(characteristic length } L \text{ will be the pipe diameter } D) \\ &= 0.25 \times 2.23 \times 1000 / \\ &1.34 \times 10^{-6} \\ &= 4.16 \times 10^8 \end{aligned}$$

D.2 Pump-turbine curves

The pump-turbine curve provided by the manufacturer was regressed to give (Section 4.3.2)

$$h = s (6.50 \times 10^{-3} q^2 - 1.01 \times 10^{-4} q N + 6.67 \times 10^{-6} N^2)$$

For the variable speed alternative, the speed N was solved implicitly, at a given water flow q and corresponding system head h . At the design flow of 109.4 l/s, the system head was 421.8 m. Substituting into the above equation ($s = 4$ stages) yields

$$421.8 = 4 \{ 6.50 \times 10^{-3} (109.4)^2 - 1.01 \times 10^{-4} (109.4) N + 6.67 \times 10^{-6} N^2 \}$$

Hence, $N = 3014$ rpm

At constant speed, $N = 3000$ rpm. Both water flow and speed are known, and are inserted on the right-hand side in the above equation. At 109.4 l/s

$$H = 4 \{ 6.50 \times 10^{-3} (109.4)^2 - 1.01 \times 10^{-4} (109.4) (3000) + 6.67 \times 10^{-6} (3000)^2 \}$$

And $H = 420.1$ m. The pressure drop across the valve would be the difference between the system and pump-turbine head.

D.3 System Efficiency

The pump-turbine efficiency curve provided by the manufacturer was regressed to give (Section 4.3.2)

$$\eta = 1.55 \times 10^5 \phi^4 - 9.21 \times 10^3 \phi^3 - 1.00 \times 10^3 \phi^2 + 88.5 \phi - 0.949$$

where ϕ is the flow to speed ratio, q/N . At the design flow, $\phi = 109.4 / 3\ 014 = 0.036$ l/s per rpm. Therefore, the pump-turbine efficiency is

$$\eta = 1.55 \times 10^5 (0.036)^4 - 9.21 \times 10^3 (0.036)^3 - 1.00 \times 10^3 (0.036)^2 + 88.5 (0.036) - 0.949$$

and $\eta = 0.773$ or 77.3 %.

The system efficiency is defined by the mode of operation. In Mode I, the water flows through the bypass and no energy is recovered, therefore the system efficiency is zero. In Mode II, the system efficiency would be equivalent to the pump-turbine efficiency when operating at variable speed. At water flows above the flow at which peak efficiency is observed, the system efficiency reduces according to

$$\eta_{SYS} = \eta (q / q_{SYS}) \quad (4.4)$$

At a water flow of 130 l/s,

$$\eta_{SYS} = 0.797 (120 / 130)$$

and $\eta_{SYS} = 0.736$ or 73.6 %.

At constant speed (3 000 rpm), the series pressure-reducing valve will reduce the system efficiency when the pump-turbine operates (Mode II) according to

$$\eta_{SYS} = \eta (h / h_{SYS}) \quad (4.5)$$

The peak flow for Mode II was 110 l/s and the efficiency was 77.2 %. At a flow of 90 l/s,

$$\eta_{SYS} = 0.772 (342.5 / 422.7)$$

therefore $\eta_{SYS} = 0.553$ or 55.3 %.

At a flow above 110 l/s (Mode III operation), equation (4.5) is used,

$$\eta_{SYS} = 0.772 (110 / 130)$$

and

$$\eta_{SYS} = 0.652 \text{ or } 65.2 \%$$

D.4 Energy recovered

The energy recovered by the pump-turbine was calculated. A flow of 109.4 l/s and discharge pressure of 10.5 bar will be used to illustrate the methodology.

$$\Delta P' = 4\,127 \text{ kPa} \quad (\text{equivalent pressure term from system curve calculation})$$

For the variable speed alternative,

Enthalpy difference (isentropic)

$$\begin{aligned} (\Delta H')_S &= V \Delta P' \\ &= 0.001 \times 4127 \\ &= 4.127 \text{ kJ/kg} \end{aligned}$$

Maximum shaft power

$$\begin{aligned} (W_S)_S &= q (\Delta H')_S \\ &= 109.4 \times 4.127 \\ &= 451 \text{ kW} \end{aligned}$$

Enthalpy difference (actual)

$$\begin{aligned} \Delta H' &= \eta (\Delta H')_S \\ &= 0.773 \times 4.127 \\ &= 3.19 \text{ kJ/kg} \end{aligned}$$

Actual pump-turbine power

$$\begin{aligned} W_S &= \eta (W_S)_S \\ &= 0.773 \times 452 \\ &= 349 \text{ kW} \end{aligned}$$

The pump-turbine efficiency is used above to calculate the energy recovered (not system efficiency η_{SYS}).

D.5 Energy fed into the power grid

The energy recovered by the pump-turbine at a flow of 109.4 l/s was 349 kW for the variable speed alternative. The generator efficiency was assumed at 96 % and the electrical system loss was 5 %.

$$\begin{aligned} \text{Power at electrical drive} &= 0.96 \times 349 \text{ kW} \\ &= 335 \text{ kW} \end{aligned}$$

$$\begin{aligned}
 \text{Power fed into grid} &= (1 - 0.05) \times 335 \text{ kW} \\
 &= 319 \text{ kW}
 \end{aligned}$$

When the system operation changes from Mode II to Mode III, the water entering the system will flow through the bypass, while the pump-turbine still operates. Therefore, in Mode III energy will be generated and fed into the grid.

D.6 Discharge water temperatures

The pump-turbine outlet water temperature was calculated. A flow of 109.4 l/s and discharge pressure of 10.5 bar will be used to illustrate the methodology.

- Isenthalpic discharge water temperature: using the Joule-Thomson coefficient at constant enthalpy ,

$$\mu_H = (\partial T / \partial P)_H \approx \Delta T / \Delta P' = (T_1 - T_4) / \Delta P'$$

Rearranging results in

$$\begin{aligned}
 T_4 &= T_1 - \mu_H \Delta P' \\
 &= 10.1 - (-0.2388) \times 4.127 \\
 &= 11.09 \text{ }^\circ\text{C}
 \end{aligned}$$

- Isentropic discharge water temperature: using the Joule-Thomson coefficient at constant entropy,

$$\mu_S = (\partial T / \partial P)_S \approx \Delta T / \Delta P' = (T_1 - T_2) / \Delta P'$$

Rearranging results in

$$\begin{aligned}
 T_2 &= T_1 - \mu_S \Delta P' \\
 &= 10.1 - (0.006) \times 4.127 \\
 &= 10.08 \text{ }^\circ\text{C}
 \end{aligned}$$

- Actual pump-turbine discharge water temperature: the enthalpy change across the pump-turbine,

$$\Delta H' = C_P (T_4 - T_3)$$

$$\text{and } \Delta H' = \eta_{SYS} (\Delta H')_S$$

$$= \eta_{SYS} V \Delta P'$$

Rearranging results in

$$\begin{aligned}T_3 &= T_4 - \eta_S V \Delta P' / C_P \\ &= 10.1 - 0.773 (0.001) 4.127 / 4.194 \\ &= 10.32 \text{ }^\circ\text{C}\end{aligned}$$

The system efficiency was used to calculate discharge temperature since it considers the presence of the series pressure reducing valve (constant speed alternative) and bypass pressure reducing valve (both alternatives).

D.7 Electrical cable sizing

The cables that were selected for the pump-turbine system was based on a calculation outlined in a handbook published by Aberdare Cables.

The full-load current I_{FL} was calculated using the following relation:

$$I_{FL} = P * 1000 / (3^{1/2} * V * \cos \phi)$$

where, P is the power in kW, V is the supply voltage and $\cos \phi$ is the power factor (0.9).

Therefore, for the variable speed alternative,

$$I_{FL} = 394 * 1000 / (3^{1/2} * 525 * 0.9) = 482 \text{ Amps}$$

From Table 6.2, pp 38, the current rating close to the above full load amps is 509 Amps for a cable size of 300 mm². This cable can carry 509 Amps continuously when installed under standard conditions in air.

The voltage drop is calculated using the voltage drop factor (0.189 mV/A/m, from Table 6.2) and the starting current. Since the pump-turbine will be direct on line, the full load amps are multiplied by a factor of 6. A distance of 25 m was assumed between the induction generator and the substation.

Hence

$$\text{Volt drop} = 0.189 \text{ mV/A/m} \times 6 \times 482 \times 25 \text{ m} / 1000 = 13.7 \text{ volts}$$

$$\text{The percentage voltage drop was } 13.7 / 525 \times 100 = 2.6 \%$$

The 300 mm², 4 core, SWA low voltage cable selected is acceptable (the maximum voltage drop allowed by SABS 0142-1978 is 5 %).

Similarly for the constant speed alternative, the cable selected was 240 mm², 4 core, SWA low voltage (the percentage voltage drop calculated was 2.6 %).

D.8 Electrical power income

The financial analysis involves in the calculation of the electrical power income. This will be illustrated below for the variable speed alternative.

Eskom has defined time periods during the week that have different tariff charges, namely, peak, standard and off-peak (Table D2). The calculation of the final values is illustrated in APPENDIX E.

Table D2: Eskom Megaflex tariffs (2012)

Summer (Sept – May)	Peak	Standard	Off-peak
Price [cents per kWh]	77.3	53.1	41.6
Winter (Jun – Aug)	Peak	Standard	Off-peak
Price [cents per kWh]	248.1	82.6	55.6

Depending on the period during which power is generated, the power income would be different.

Table D3 Power generated during Eskom defined periods

Hours	318.5 kW			0 kW			0 kW
	Peak	Standard	Off-peak	Peak	Std	Off-peak	
Mon	4.5	9.5	8.0	–	–	–	2.0
Tues	4.0	9.5	8.0	–	–	–	2.5
Wed	4.0	9.5	8.0	–	–	–	2.5
Thurs	4.0	9.5	8.0	–	–		2.5
Fri	3.0	9.0	6.0	2.0	2.0	2.0	–
Sat	–	–	–	–	7.0	17	–
Sunday	–	–	4.5	–	–	7.5	12

Multiplication of the power with the operating hours gives kilowatt-hours (Table D4).

Table D4 Energy generated during Eskom defined periods

kWh	Peak	Standard	Off-peak
Monday	1 433	3 026	2 548
Tuesday	1 274	3 026	2 548
Wednesday	1 274	3 026	2 548
Thursday	1 274	3 026	2 548
Friday	956	2 867	1 911
Saturday	0	0	0
Sunday	0	0	1 433
Total	6 211	14 970	13 536

Finally, the electrical power income is determined by multiplying the respective Megaflex cost (Table D2) by the energy generated. The income is listed in the table below.

Table D5 Electrical power income for a week (2012)

Summer (Sept – May)	Peak	Standard	Off-peak	Total
Electrical power income [R]	4 801	7 952	5 635	18 388
Winter (Jun – Aug)	Peak	Standard	Off-peak	Total
Electrical power income [R]	15 407	12 370	7 521	35 298

D.9 Present value calculation

The compound interest concept was used to “convert” the costs listed in the Literature review to an equivalent present day value (2011). The formula used was (Peters, et. al., 2003)

$$FV = PV(1 + i)^n$$

where FV is the future amount, that includes the present amount or principle (PV), *i* is the interest rate based on length of one interest period; while *n* is the number of time units or interest periods. The energy saving of R 70 500 in 1977, will be “converted” to an equivalent value in 2011.

Annual interest rates were obtained from published data (by the South African Reserve Bank) from 1977 and 2011. Average annual interest rates were used. (When a change in the rate occurred during the year, the average rate was obtained by summing the interest rates scaled by the fraction of months the rate prevailed out of 12 months).

The average interest rate *i*, calculated from 1977 to 2011, is 15.4 %, while the number of interest periods is 34 years. Substituting in the above equation yields

$$FV = 70\,500 (1 + 0.154)^{34}$$

$$FV = 9\,232\,500$$

The other costs have also been “converted” present day value by adopting this approach. Table D6 summarises the values.

Table D6 Summary of present value costs

Year	<i>PV</i> [R]	<i>i</i> [%]	<i>n</i> [years]	<i>FV</i> [R]
1977	70 500	15.4	34	9 232 500
1977	60	15.4	34	7 900
1984	200	15.9	27	11 300
1986	45 000	15.5	25	1 717 300
1989	99 770	15.6	22	2 534 500
1996	6 440	14.4	15	50 100
2000	2 000 000	12.6	11	7 610 200

The costs shown for 1989 and 1996 were \$ 38 000 and \$ 1 500 respectively. These values were converted to Rand using the average annual exchange rate. The average rand-dollar exchange rate in 1989 was R 2.60 per \$; while in 1996, the average exchange rate was R 4.30 per \$ (from data published by the South African Reserve Bank).

APPENDIX E ESKOM TARIFFS

Eskom publishes the tariff charges to its urban, residential and rural customers. A year is split into a high demand season and a low demand season. The winter months, June to August would fall under the high demand season and have higher tariffs. The remainder of the year (September to May) would be classified as low demand season having lower tariff charges.

The seasons are further divided into three regions, namely peak, standard and off-peak. These define different charges for weekdays and weekends; as well as different times of the day. The regions are described in Figure E1 below.

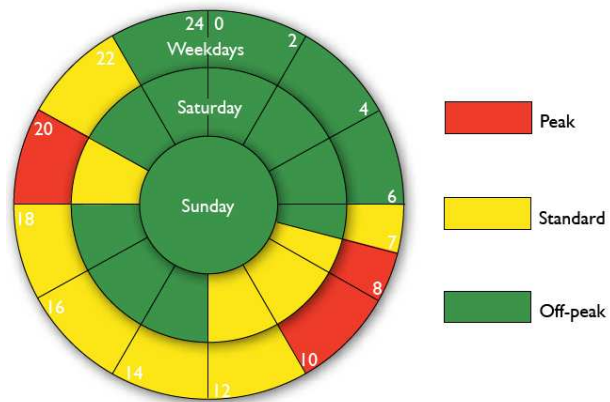


Figure E1 Eskom's defined time of use periods (Conradie, 2010)

Furthermore, distance also influences the cost through a transmission network charge. This depends on the distance from a central point in Johannesburg and described in Figure E2. For a distance under 300 km, there is no additional charge. Between 300 and 600 km a surcharge of 1% is added. A further 300 km would increase the cost by a further percent. Where the radial distance exceeds 900 km, the transmission network charge would be increased by 3%.

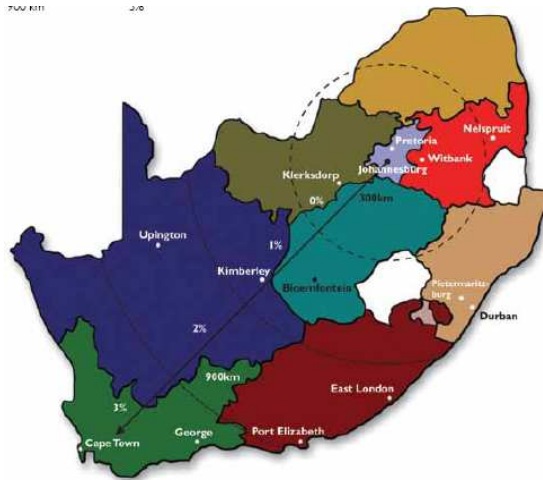


Figure E2 Transmission zones and applicable percentages (Conradie, 2010)

Mponeng is charged Megaflex rates and the calculation of the cost will be illustrated below. The remaining charges are shown graphically for a weekday and Saturday in Figure E3 and Figure E4 respectively. The off-peak rate would apply for the entire of Sunday.

The Active energy charge during the high demand season and a peak period is 142.38 c/kWh. The transmission zone is less than 300 km and the voltage is between 500 volts and 66 kilovolts. Adding the environmental levy of 2 c/kWh gives 144.38 c/kWh.

A reactive energy charge of 5.89 c/kvarh is levied. This value is divided by the power factor (0.96) to convert it to 6.14 c/kWh. It should be noted that during the low demand season, there is no charge for reactive energy. A rate-rebalancing levy of 3.09 c/kWh is also included.

Distribution network charges would include a network access charge (R 6.72 per kVA/month); a network demand charge (R 12.73 per kVA/month) and a transmission network charge (R 3.35 per kVA/month). The network demand charge is the highest actual demand during peak and standard periods for given month. Assuming the distribution network charges to be 25% higher than the continuous rate, the total charge would be 4.12 c/kWh.

Capital charges would include a service charge (R 1 638.73 per account/day) and an administration charge (R 52.33 per day). Assuming 25 MW of continuous absorbed power, the total charge would be 0.27 c/kWh.

Combining the above, the peak cost during the high demand season would be 158 c/kWh.

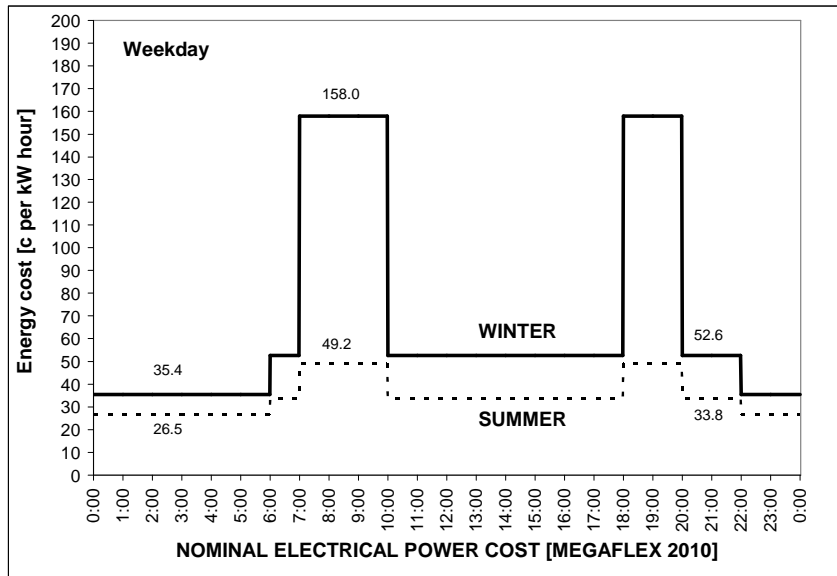


Figure E3 Nominal Megaflex tariff for a weekday

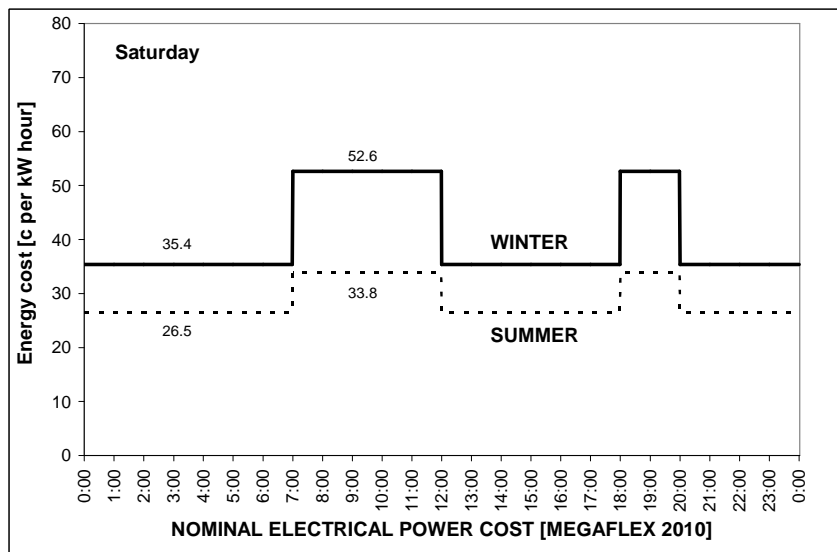


Figure E4 Nominal Megaflex tariff for a Saturday

The Eskom published rates are also included.

APPENDIX G FINANCIAL CALCULATIONS

G.1 Variable speed alternative

BUSINESS CASE		2010	2011	Year 0	Year 1	Year 2	Year 3	Year 4	Year 5	Year 6	Year 7	Year 8	Year 9	Year 10
		2010	2011	2011	2012	2013	2014	2015	2016	2017	2018	2019	2020	2021
Eskom Megaflex [cents per kWh (average)]														
Winter (June to August)														
Peak		158.0	197.2		248.1	312.3	390.4	488.0	512.4	538.0	564.9	593.1	622.8	653.9
Standard		52.6	65.7		82.6	104.0	130.0	162.6	170.7	179.2	188.2	197.6	207.5	217.8
Off-peak		35.4	44.2		55.6	70.0	87.4	109.3	114.8	120.5	126.5	132.9	139.5	146.5
Summer (September to May)														
Peak		49.2	61.4		77.3	97.3	121.7	152.1	159.7	167.7	176.0	184.8	194.1	203.8
Standard		33.8	42.2		53.1	66.9	83.6	104.5	109.7	115.2	121.0	127.0	133.4	140.0
Off-peak		26.5	33.1		41.6	52.4	65.5	81.9	86.0	90.3	94.8	99.5	104.5	109.7
Annual increase %		24.8	25.8		25.9	25.0	25.0	5.0	5.0	5.0	5.0	5.0	5.0	
								10.0	10.0	10.0	10.0	10.0	10.0	
								15.0	15.0	15.0	15.0	15.0	15.0	
VARIABLE SPEED ALTERNATIVE														
Power generated (kW)														
Maximum		318.5	318.5		318.5	318.5	318.5	318.5	318.5	318.5	318.5	318.5	318.5	318.5
Minimum		0.0	0.0		0.0	0.0	0.0	0.0	0.0	0.0	0.0	0.0	0.0	0.0
Energy generated (kWh)														
One week														
Peak		6,211	6,211		6,211	6,211	6,211	6,211	6,211	6,211	6,211	6,211	6,211	6,211
Standard		14,970	14,970		14,970	14,970	14,970	14,970	14,970	14,970	14,970	14,970	14,970	14,970
Off-peak		13,536	13,536		13,536	13,536	13,536	13,536	13,536	13,536	13,536	13,536	13,536	13,536
Electrical power income (R)														
Winter (June to August) - one week														
Peak		9,813	12,247		15,407	19,397	24,246	30,308	31,823	33,414	35,085	36,839	38,681	40,615
Standard		7,879	9,833		12,370	15,573	19,467	24,333	25,550	26,828	28,169	29,577	31,056	32,609
Off-peak		4,791	5,979		7,521	9,470	11,837	14,796	15,536	16,313	17,128	17,985	18,884	19,828
Summer (September to May) - one week														
Peak		3,058	3,816		4,801	6,044	7,556	9,444	9,917	10,413	10,933	11,480	12,054	12,656
Standard		5,065	6,321		7,952	10,012	12,515	15,644	16,426	17,247	18,110	19,015	19,966	20,964
Off-peak		1,270	1,979		5,635	7,095	8,869	11,086	11,640	12,222	12,833	13,475	14,148	14,856
Winter (June to August)	14 weeks	314,759	392,819		494,166	622,156	777,694	972,118	1,020,724	1,071,760	1,125,348	1,181,616	1,240,696	1,302,731
Summer (September to May)	34 weeks	319,381	411,956		625,211	787,141	983,926	1,229,908	1,291,403	1,355,974	1,423,772	1,494,961	1,569,709	1,648,194
Capital cost (R)				(4,726,300)										
Summary		634,140	804,775	(4,726,300)	1,119,378	1,409,297	1,761,621	2,202,026	2,312,127	2,427,734	2,549,120	2,676,576	2,810,405	2,950,926
				(4,726,300)	1,119,378	1,409,297	1,761,621	2,202,026	2,422,229	2,543,340	2,670,507	2,804,032	2,944,234	3,091,446
				(4,726,300)	1,119,378	1,409,297	1,761,621	2,202,026	2,532,330	2,658,946	2,791,894	2,931,489	3,078,063	3,231,966
Discount rate	10%													
Net present value of electrical power income (R)	11,564,542	11,876,669	12,188,796											
Internal rate of return (%)	34.4%	35.0%	35.5%											
Payback (years)	3.8													
Net surplus (loss)	6,838,242	7,150,369	7,462,496											

G.2 Constant speed alternative

BUSINESS CASE		2010	2011	Year 0 2011	Year 1 2012	Year 2 2013	Year 3 2014	Year 4 2015	Year 5 2016	Year 6 2017	Year 7 2018	Year 8 2019	Year 9 2020	Year 10 2021
Eskom Megaflex [cents per kWh (average)]														
Winter (June to August)														
Peak		158.0	197.2		248.1	312.3	390.4	488.0	512.4	538.0	564.9	593.1	622.8	653.9
Standard		52.6	65.7		82.6	104.0	130.0	162.6	170.7	179.2	188.2	197.6	207.5	217.8
Off-peak		35.4	44.2		55.6	70.0	87.4	109.3	114.8	120.5	126.5	132.9	139.5	146.5
Summer (September to May)														
Peak		49.2	61.4		77.3	97.3	121.7	152.1	159.7	167.7	176.0	184.8	194.1	203.8
Standard		33.8	42.2		53.1	66.9	83.6	104.5	109.7	115.2	121.0	127.0	133.4	140.0
Off-peak		26.5	33.1		41.6	52.4	65.5	81.9	86.0	90.3	94.8	99.5	104.5	109.7
Annual increase %		24.8	25.8		25.9	25.0	25.0	5.0	5.0	5.0	5.0	5.0	5.0	5.0
								10.0	10.0	10.0	10.0	10.0	10.0	10.0
								15.0	15.0	15.0	15.0	15.0	15.0	15.0
CONSTANT SPEED ALTERNATIVE														
Power generated (kW)														
Maximum		319.1	319.1		319.1	319.1	319.1	319.1	319.1	319.1	319.1	319.1	319.1	319.1
Minimum		5.7	5.7		5.7	5.7	5.7	5.7	5.7	5.7	5.7	5.7	5.7	5.7
Energy generated (kWh)														
One week														
Peak		6,235	6,235		6,235	6,235	6,235	6,235	6,235	6,235	6,235	6,235	6,235	6,235
Standard		15,051	15,051		15,051	15,051	15,051	15,051	15,051	15,051	15,051	15,051	15,051	15,051
Off-peak		13,714	13,714		13,714	13,714	13,714	13,714	13,714	13,714	13,714	13,714	13,714	13,714
Electrical power income (R)														
Winter (June to August) - one week														
Peak		9,851	12,294		15,466	19,471	24,339	30,424	31,945	33,542	35,219	36,980	38,829	40,771
Standard		7,922	9,886		12,437	15,658	19,572	24,465	25,688	26,973	28,322	29,738	31,224	32,786
Off-peak		4,854	6,057		7,620	9,594	11,992	14,990	15,740	16,527	17,353	18,220	19,132	20,088
Summer (September to May) - one week														
Peak		3,070	3,831		4,819	6,068	7,585	9,481	9,955	10,452	10,975	11,524	12,100	12,705
Standard		5,093	6,356		7,995	10,066	12,583	15,728	16,515	17,341	18,208	19,118	20,074	21,078
Off-peak		1,287	2,005		5,709	7,188	8,985	11,231	11,792	12,382	13,001	13,651	14,334	15,051
Winter (June to August)	14 weeks	316,763	395,320		497,313	626,117	782,646	978,307	1,027,223	1,078,584	1,132,513	1,189,139	1,248,596	1,311,025
Summer (September to May)	34 weeks	321,279	414,500		629,814	792,936	991,170	1,238,962	1,300,910	1,365,956	1,434,254	1,505,966	1,581,265	1,660,328
Capital cost (R)				(3,776,900)										
Summary		638,042	809,820	(3,776,900)	1,127,127	1,419,052	1,773,816	2,217,270	2,328,133	2,444,540	2,566,767	2,695,105	2,829,860	2,971,353
				(3,776,900)	1,127,127	1,419,052	1,773,816	2,217,270	2,438,996	2,560,946	2,688,994	2,823,443	2,964,615	3,112,846
				(3,776,900)	1,127,127	1,419,052	1,773,816	2,217,270	2,549,860	2,677,353	2,811,221	2,951,782	3,099,371	3,254,339
Discount rate	10%													
Net present value of electrical power income (R)	11,644,597	11,958,885	12,273,173											
Internal rate of return (%)	42.9%	43.5%	44.1%											
Payback (years)	2.3													
Net surplus (loss)	7,867,697	8,181,985	8,496,273											

APPENDIX H PROJECT SCHEDULE

